Functional Analysis of the Dynein Light Chain Genes, *Dnali1* and *Tcte3*

Dissertation

zur Erlangung des Doktorgrades

der Mathematisch-Naturwissenschaftlichen Fakultäten

der Georg-August-Universität zu Göttingen

vorgelegt von

Sajid Rashid

aus Rawalpindi, Pakistan

Göttingen 2005

D7

Referent: **Prof. Dr. W. Engel**

Korreferentin: **PD Dr. S. Hoyer-Fender**

Tag der mündlichen Prüfungen:

INDEX

ABBREVIATIONS

ABI	Applied Biosystem Instrument
APS	Ammonium peroxydisulfate
ATP	Adenosintriphosphate
BCP	1-bromo-3-chloropropane
bp	base pair
BSA	Bovine serum albumin
°C	Degree Celsius
CASA	Computer Assisted Semen Analysis
cDNA	complementary DNA
dATP	Desoxyriboadenosintriphosphate
dH20	destilled water
DAPI	Diamidino-2-phenylindole dihydrochloride
dCTP	Desoxyribocytosintriphosphate
DMSO	Dimethyl sulfoxide
DEPC	Diethylpyrocarbonate
DNA	Deoxyribonucleic acid
Dnase	Deoxyribonuclease
dNTP	deoxynucleotidetriphosphate
dpc	day post coitus
dT	deoxythymidinate
DTT	Dithiothreitol
CE	Cys-rich-EGF-like
EDTA	Ethylene diamine tetraacetic acid
ES	Embryonic stem
FCS	Fetal calf serum
FITC	Fluorescein isothiocyanate
GST	Glutathione S-transferase
g	gravity
Gfp	Green fluorescence protein
gm	gram
HEPES	N-(-hydroxymethyl)piperazin,N'-3-propansulfoneacid
hr(s)	hour(s)

IPTG	Isopropyl-ß-thiogalactopyranoside
IVF	In vitro fertilization
kb	kilobase
LB	Luria-Bertrani
LIF	Recombinant leukaemia inhibitory factor
LPS	lipopolysaccharides
M	molarity
Mb	Mega base pair
MOPS	3-[N-Morpholino]-Propanesulfate
mRNA	messenger Ribonucleic acid
mg	milligram
ml	milliliter
µl	microliter
µm	micrometer
min	minute
NaAc	Sodium acetate
NBT	Nitro-blue tetrazolium
NCBI	National Center for Biotechnology Information
Neo	*Neomycin*
ng	nanogram
nm	nanometer
NTP	Nucleotidetriphospate
OD	Optimal density
ORF	Open Reading Frame
Pa	Pascal
PAGE	Polyacrylamide Gel Electrophoresis
PCR	Polymerase chain reaction
PH	Prepondirance of hydrogen ions
Pmol	pmol
PBS	Phosphatebuffersaline
PBT	Phosphatebuffersaline + Tween
PMSF	Phenylmethylsulfonyl fuoride
RNA	Ribonucleic acid
Rnase	Ribonuclease

Rnasin	Ribonuclease inhibitor
rpm	revolution per minute
RT	Room temperature
RT-PCR	Reverse transcriptase-PCR
SDS	Sodium Dodecylsulfate
SDS-PAGE	SDS-Polyacrylamide Gel Electrophoresis
sec	second
SV 40	Simian Virus 40
Taq	*Thermus aquaticus*
TBE	Tris-Borate-EDTA-Electrophoresis buffer
TE	Tris-EDTA buffer
TEMED	Tetramethylethylene diamine
Tris	Trihydroxymethylaminomethane
U	Unit
UV	Ultra violet
V	Voltage
w/v	weight/volume
X-Gal	5-bromo-4-chloro-3-indolyl-ß-galactosidase
ZP	Zona Pellucida

Symbol of amino acids

A	Ala	Alanine
B	Asx	Asparagine or Aspartic acid
C	Cys	Cysteine
D	Asp	Aspartic acid
E	Glu	Glutamic acid
F	Phe	Phenylalanine
G	Gly	Glycine
H	His	Histidine
I	Ile	Isoleucine
K	Lys	Lysine
L	Leu	Leucine
M	Met	Methionine
N	Asn	Asparagine
P	Pro	Proline
Q	Gln	Glutamine
R	Arg	Arginine
S	Ser	Serine
T	Thr	Threonine
V	Val	Valine
W	Trp	Tryptophan
Y	Tyr	Tyrosine
Z	Glx	Glutamine or Glutamic acid

Symbols of nucleic acid

A	Adenosine
C	Cytidine
G	Guanosine
T	Thymidine
U	Uridine

1. INTRODUCTION

1.1 Dynein motors

Dyneins are the multi-component complexes that are involved in a number of fundamental cellular processes including, mitotic spindle formation and orientation, assembly and motility of cilia and flagella, vesicle transport, formation and localization of the Golgi complex, nuclear migration and generation of left-right asymmetry in the developing embryo (for review: Karki and Holzbaur, 1999; King, 2000).

Dynein motors consist of 1-3 heavy (HCs), intermediate (ICs) and light chains (LC) (Figure 1.1), which differ in their molecular weight and function (Gibbons, 1995; King, 2000). Dynein heavy chains harbour the motor domain and generate the force for sliding of microtubules, while intermediate and light chains are involved in the assembly and regulation of the whole complex. Intermediate chains from outer arm, inner arm I1 and cytoplasmic dyneins have been implicated in attaching the motor to specific cellular cargoes (King et al., 1991; Yang and Sale, 1998). Light intermediate chains have a potential role in regulating the motor function through control of dynein membrane interactions (Niclas et al., 1996). In mammals, more than ten genes encoding dynein heavy chains have been identified (Tanaka et al., 1995; Neesen et al., 1997), while the number of intermediate and light chain genes in mammals is not precisely known.

Cytoplasmic and axonemal dyneins contain a wide isoform variety, as multiple distinct motor activities are apparently required to accomplish their functions. Axonemal dyneins contain multiple heavy chains with different intrinsic motor activities and are present in the core structure of cilia and flagella, the axoneme (Figure 1.1). The axonemal ultrastructure is mainly composed of one central complex and nine outer-doublet microtubules with attached inner and outer dynein arms, radial spokes and nexin links (Figure 1.2). The dynein arms on one doublet microtubule generate force against the adjacent microtubule, causing them to slide by means of ATP-dependent reactions (Witman, 1992). Inner and outer dynein arms line the length of microtubules in the axoneme (Porter and Johnson, 1989; Mitchell, 1994).

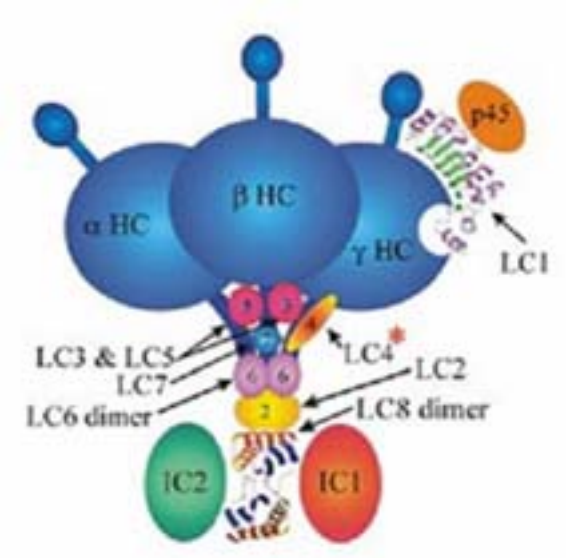

Figure 1.1. Structure and composition of an axonemal outer dynein arm complex of the green alga *Chlamydomona*s indicating location of various polypeptide components. A series of light chains (LCs; LC1, 3, 4 and 5) interact directly with the heavy chain (HC) and appear to be involved in the regulation of motor activity. The basal complex associated with the amino-terminal domain of HC comprises a series of intermediate chains (ICs) and members of the LC8, Tctex1/Tctex2 and LC7/roadblock families (adopted from Dibella et al., 2001).

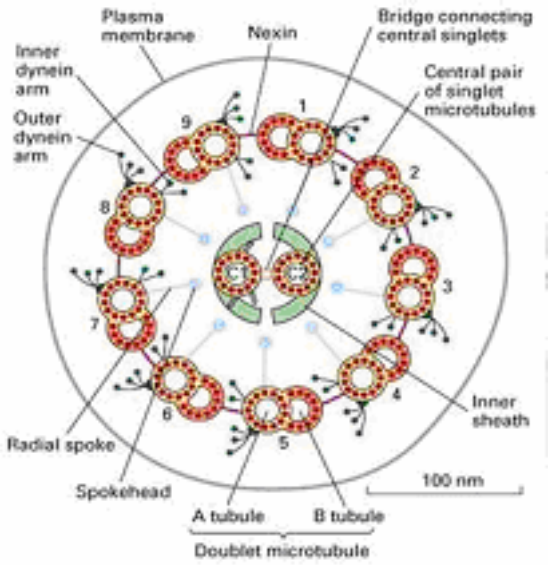

Figure 1.2. Schematic diagram of the flagellar axoneme in cross-section. The inner and outer dynein arms are multi-subunit ATPases that generate relative sliding movements between the outer doublet microtubules. The radial spokes and central pair microtubules with their associated projections coordinate the dynein-induced sliding to generate a variety of waveforms (adopted from Karp et al., 2002).

Cytoplasmic dyneins appear to be homodimers of heavy chains with presumably identical motor properties (Moss et al., 1992; Sakakibara et al., 1998). These proteins have a mass of ~530 kDa and consist of several distinct domains (Figure 1.3). The carboxy-terminal portions of these molecules comprise both the globular head and a stalk that terminates in a microtubule-binding domain. The amino-terminal heavy chain region forms an apparently flexible domain that mediates interactions with other heavy chains within the complex and is also involved in associations with other components that are required for assembly, cargo binding and regulation of the motor activity.

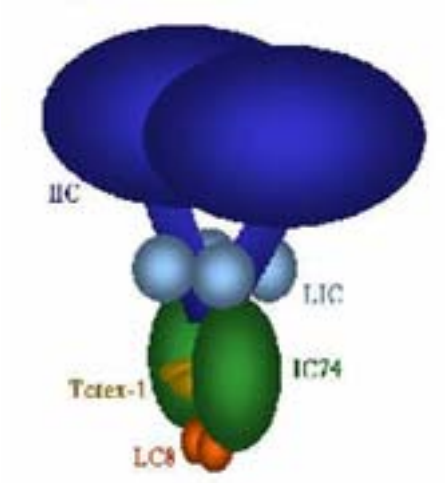

Figure 1.3. Cytoplasmic dynein structure. It contains two identical heavy chains of about 530 kDa, two 74 kDa intermediate chains and about four 53-59 kDa light intermediate chains. In addition, there are several light chains with unknown function (adopted **from www.ohiou.edu).**

Attaching individual motors to appropriate cellular cargoes and to generate the complex axonemal waveforms involve multiple accessory proteins, which are differentially expressed in different tissue types. The divergence in function has given rise to the notion that flagellar and cytoplasmic dyneins are quite distinct entities.

1.2 Dynein functional diversity

Defects in dyneins that power cilia and flagella lead to a wide variety of problems in the organisms. Genetic analysis of the unicellular green alga *Chlamydomonas* revealed that defects in dyneins and other flagellar structures such as the central pair microtubules and radial spokes lead to poor motility or paralysed flagella (Review Mitchell, 2000). Similarly, many instances have been reported in humans suffering from “Primary Ciliary Dyskinesia”

(PCD) or Kartagener Syndrome, in which often cilia exhibit ultrastructural defects (Afzelius et al., 1979). Mice having a mutation in the carboxy-terminal of an inner arm dynein heavy chain (*MDHC7*) are incapable of maintaining the normal fertility due to the reduced sperm motility (Neesen et al., 2001). Another mouse model with a mutation in the outer arm axonemal dynein heavy chain gene 5 (*Mdnah5*) exhibits most of the classical features of PCD, including recurrent respiratory infections, situs inversus and ciliary immotility. These mice also suffer from hydrocephalus and die perinatally (Ibanez-Tallon et al., 2003).

The multiple roles played by cytoplasmic dyneins, both alone and in combination with the adaptor complex dynactin, remain to be fully elucidated. However, to date there is a clear evidence for the involvement of this microtubule motor in vesicular trafficking and maintenance of the Golgi apparatus. Furthermore, during mitosis dyneins localized at the cell cortex act to pull the spindle poles apart during anaphase B, while dyneins located at the kinetochore move cell cycle checkpoint proteins (Wojcik et al., 2001). Recently, this complex has also been found to be necessary for dissolution of the nuclear envelope, where it appears to pull or tear the membrane and underlying lamina during prophase and prometaphase (Salina et al., 2002; Beaudouin et al., 2002).

Attempts to obtain mice deficient for cytoplasmic dynein heavy chains failed to produce any viable offspring suggesting that this motor is absolutely necessary at an early stage in mammalian development (Harada et al., 1998). The mouse mutant of cytoplasmic dynein intermediate chain revealed that *mD2LIC* is needed to maintain or establish ventral cell fates, for monocilium formation in the ventral node, and for correct signalling by the organiser and midline (Amer et al., 2004). *D2LIC* is present in the Golgi apparatus and in centrosomes (Grissom et al., 2002), and its loss may cause defects in protein maturation in the cytoskeleton or in cell polarity.

1.3 The p28 / *Dnali1* gene

Analyses of mutant strains of the green alga *Chlamydomonas reinharditii* contribute significant information to the function of different dynein genes (Silflow et al., 2001). Splice-site mutations in the gene encoding the 28 kDa dynein light chain (p28) are correlated in the IDA-4 mutant with a loss of a set of dynein inner arm classes, indicating an important role of p28 for the assembly of inner dynein arm isoforms (LeDizet, 1995).

The p28 light chain belongs to the I2/I3 group of inner dynein arm isoforms (Piperno et al., 1990; LeDizet and Piperno, 1995). I2/I3 series of inner arm dyneins consists of only one

heavy chain that unlike other dynein complexes interacts with actin together with either centrin or p28 light chains. The role of actin in the inner dynein arm isoform remains unknown (Kagami et al., 1992; Piperno et al., 1990), while loss of *p28* gene function in *Chlamydomonas* resulted in impaired flagellar motility.

Orthologous *p28* genes have been analyzed in the sea urchin and in the human (Gingras et al., 1996; Kastury et al., 1997). The sea urchin p33 protein shares 66% identical amino acids with p28. Moreover, incubation with p33 specific antibodies inhibits the motility of demembranated-reactivated sperm, supporting the role of this dynein light chain for the flagellar motility (Gingras et al., 1996). The human *hp28* (*DNALI1*) gene was localized on chromosome 1 region p35.1 (Kastury et al., 1997). The *hp28* gene consists of seven exons and it was suggested that this gene could be a candidate gene in the patients suffering from PCD. This suggestion was supported by expression analyses detecting *DNALI1* transcripts in several tissues having cilia or flagella (Kastury et al., 1997). In addition, *DNALI1* expression was also observed in tissues without ciliary structures, e.g. skeletal muscle (Kastury et al., 1997). Although the expression of *DNALI1* was studied at RNA level, to date the function of this gene is unknown in mammals.

The murine *p28* gene (*Dnali1*) was identified using an RT-PCR approach (Breckle, 2000). A cosmid clone was isolated containing the complete *Dnali1* gene. *Dnali1* gene consists of six exons and is located on mouse chromosome 4, region D. The *Dnali1* gene is expressed in almost every tissue at the RT-PCR level. However, it shows relatively high expression in the testis, where two *Dnali1* specific transcripts are detected by Northern blot experiment. The expression of both transcripts starts at the same time at day 15 during the development of testis (Breckle, 2000). By using Dnali1 polyclonal antibodies, the Dnali1 localization was demonstrated along the entire length of spermatozoa tails (Hupe, 2003). To elucidate the proteins that interact with Dnali1, a yeast-two-hybrid screen was performed using a murine testicular cDNA library (Hupe, 2003). By using this assay, no protein was found to be a member of axonemal inner arm dynein family. However, it was identified that Dnali1 interacts putatively with the carboxy-terminal part of the cytoplasmic dynein heavy chain (*Dnchc1).* This result indicates that Dnali1 not only functions as an inner dynein arm component but may also be a part of the cytoplasmic dynein complex.

1.4 The *Tcte3* gene

Another gene that might play a role in the axonemal as well as the cytoplasmic dynein complex is *Tcte3* (NM_011560). *Tcte3 (Tctex2)* gene was identified on mouse chromosome 17 in mice bearing the *t* haplotype (Lader et al., 1989; Huw et al., 1995; Artzt, 1995). It was originally described as a putative sperm membrane protein (Huw et al., 1995), but subsequent identification of the *Chlamydomonas* homolog LC2 revealed that this protein is actually a component of outer dynein arm (Patel-King et al., 1997). Complete deletion of the LC2/*oda12* gene in *Chlamydomonas* causes loss of all outer dynein arms and a slow jerky swimming phenotype (Pazour, 1999), indicating that LC2 is required for the outer arm assembly in *Chlamydomonas*, while another mutant lacking the 3'-end of the LC2 gene is partially functional and allows for the assembly of outer dynein arms.

The human orthologue *TCTE3* gene was mapped on chromosome 6q27 (Neesen et al., 2002). The gene consists of four exons. Both murine and human proteins share 87% homology in their coding sequence. Northern blot analysis using various human tissues resulted in a specific expression of *TCTE3* only in testis. At the RT-PCR level, it was found that the gene is expressed in several tissues including brain, lung and trachea (Neesen et al., 2002). Moreover, these analyses revealed that two transcript variants are expressed, which differ by the presence of exon 3. The two splice variants were also detected in the murine tissues. A cosmid clone was isolated harbouring the four exons of the *Tcte3* gene. Southern blot analyses using cosmid and genomic DNA indicated that *Tcte3* is a single copy gene in the murine genome (Drenckhahn, 2000).

However, the functions of the *Tcte3* gene as well as of the *Dnali1* gene have to be elucidated. Therefore, the generation of mice deficient for the *Tcte3* or the *Dnali1* gene product were the main aims of the present work.

1.5 Aims of the study

1) Expression analyses for *Dnali1* and *Tcte3* genes.
2) Generation of Tcte3 specific polyclonal antibodies.
3) Generation of *Tcte3* deficient mice by homologous recombination.
4) Characterization of *Tcte3* deficient mice.
5) *In-vitro* studies of Dnali1 by immunohistochemical analysis.
6) Verification of the putative interaction between Dnali1 and Dnchc1.
7) Generation of *Dnali1* deficient mice.
8) Characterization of *Dnali1*$^{-/-}$ embryos.
9) Evaluation of *DNALI1* as a candidate gene for asthenozoospermia in infertile males by DHPLC.

2. MATERIALS AND METHODS

2.1 Materials

2.1.1 Chemicals

Acrylamide/Bis-acrilamide 40% (w/v) (19:1)	Gibco/BRL, Karlsruhe
Acetic acid	Merck, Darmstadt
Agar	Fluka, Neu-Ulm
Agarose	Gibco/BRL, Karlsruhe
Ammonium acetate	Fluka, Neu Ulm
Ammonium persulfate	Sigma, Deisenhofen
Ampicillin	Sigma, Deisenhofen
Ampuwa	Fresenius, Bad Homburg
Bacto-tryptone	Difco, Detroit, USA
Bacto-Yeast-Extract	Difco, Detroit, USA
BCIP	Boehringer, Mannheim
Bisacrylamide	Serva, Heidelberg
Blocking reagent	Roshe, Penzberg
Bromophenol blue	Sigma, Deisenhofen
BSA (Factor V)	Biomol, Hamburg
Cell culture media (DMEM)	Gibco/BRL, Eggenstein
Coomasie G-250	Sigma, Deisenhofen
Choloroform	Baker, Deventer, Holland
DAPI	Vector, Burfingame
DMEM	GibcoBRL, Karlsruhe
Dimethyl pimelimidate dihydrochloride	Sigma Deisenhofen
Dextran sulfate	Pharmacia, Freiburg
Dimethyl sulfoxid (DMSO)	Sigma, Deisenhofen
Dithiothreitol	Sigma, Deisenhofen
dNTPs	GibcoBRL, Karlsruhe
Ethanol	Baker, Deventer, NL
Ethidium bromide	ROTH, Karlshure
FCS	Gibco/BRL, Karlsruhe

Formaldehyde	Gibco/BRL, Karlsruhe
Ficoll 400	Pharmacia, Freiburg
Formamide	Fluka, Neu Ulm
Glutaraldehyde	Sigma, Deisenhofen
Glycerol	Gibco/BRL, Karlsruhe
Glycine	Biomol, Hamburg
Goat serum	Sigma, Deisenhofen
HCl	Merck, Darmstadt
H_2O_2	Merck, Darmstadt
HEPES	Merck, Darmstadt
IPTG	Biomol, Hamburg
IVF medium	Medicult, Berlin
Isopropanol	Merck, Darmstadt
KCl	Merck, Darmstadt
M2-medium	Sigma, Deisenhofen
M16-medium	Sigma, Deisenhofen
Methanol	Merck, Darmstadt
$MgCl_2$	Merck, Darmstadt
MOPS	Merck, Darmstadt
Methyl benzoat	Fulka, Neu Ulm
β-Mercaptoethanol	Serva, Heidelberg
Mineral oil	Sigma, Deisenhofen
Na acetate	Merck, Darmstadt
Na citrate	Merck, Darmstadt
NaCl	Merck, Darmstadt
Na_2HPO_4	Merck, Darmstadt
NaH_2PO_4	Merck, Darmstadt
NaOH	Merck, Darmstadt
NBT	Boehringer, Mannheim
PBS	Gibco/BRL, Karlsruhe
Phosphoric acid	Merck, Darmstadt
Pepton	Gibco/BRL, Karlsruhe
Picric acid	Fulka, Neu Ulm
Phenol	Gibco/BRL, Eggenstein

Polyethylene glycol 6000	Serva, Heidelberg
Proteinase K	Pharmacia, Freiburg
[α^{32}P] dCTP	Amersham, Braunschweig
RNase A	Sigma, Diesenhofen
RNase Inhibitor	Roshe, Penzberg
RNAse away	Biomol, Hamburg
Salmon sperms DNA	Sigma, Deisenhofen
SDS	Serva, Heidelberg
Taq-DNA-Polymerase	Gibco/BRL, Eggenstein, FINNzymes, Finland, Amersham, Braunschweig
T4-DNA-Ligase	Gibco/BRL, Eggenstein
TEMED	Serva, Heidelberg
Triton X-100	Serva, Heidelberg
Tris	Sigma, Deisenhofen
Tween-20	Fluka, Deisenhofen
X-Gal	Biomol, Hamburg
Xylen cyanole	Bio-Rad, München

All those chemicals, which are not mentioned above were bought from Merck, Darmstadt, or ROTH, Karlsruhe.

2.1.2 Kits

DYEnamic ET-Terminator mix	(Amersham Pharmacia)
Endo Free Plasmid Maxi Kit	(Qiagen, Hilden)
GST-Bind kit	(Novagen, Darmstadt)
Maxi Plasmid Kit	(Qiagen, Hilden)
Mega Plasmid Kit	(Qiagen, Hilden)
Mini Plasmid Kit	(Qiagen, Hilden)
PCR Purification Kit	(Qiagen, Hilden)
pGEM-T Easy cloning system	(Promega, Mannheim)
QIAquick Gel Extraction Kit	(Qiagen, Hilden)
RNA Easy Kit	(Qiagen, Hilden)
RediprimeTM II Random Prime	

Labeling System	(Amersham Pharmacia)
ApopTag Plus Peroxidase *in situ* Apoptosis Detection Kit	(Chemicon International, Temecula,CA)

2.1.3 Solutions and buffers

Solutions were prepared according to Sambrook et al. (1989) with deionised dH_2O, unless, otherwise stated.

2.1.3.1 Agarose gel electrophoresis

5x TBE buffer	450 mM Tris 450 mM Boric acid 20 mM EDTA (pH 8)
Glycerol loading buffer -I	10 mM Tris/HCl (pH 7.5) 10 mM EDTA (pH 8) 0.025% Bromophenol blue 0.025% Xylenecyanol 30% Glycerol
Glycerol loading buffer -II	10 mM Tris/HCl (pH 7.5) 10 mM EDTA (pH 8) 0.025% Orange G 30% Glycerol

2.1.3.2 SDS-PAGE

40% Acrylamide stock solution	Acrylamide 29.2% (w/w) Bis-acrylamide 0.8% (w/w) 10% Ammonium persulfate solution in H_2O

Sample buffer (2x)	0.5 M Tris/HCl (pH 6.8) 20% Glycerol 4% SDS 10% β-Mercaptoethanol
Running buffer (5x)	25 mM Tris/HCl (pH 8.3) 192 mM Glycine 0.1% SDS
Stacking gel buffer (4x)	0.5 M Tris/HCl (pH 6.8) 0.4% SDS
Separating gel buffer (4x)	1.5 M Tris/HCl (pH 8.3) 0.4% SDS

2.1.3.3 Frequently used buffers and solutions

Bouin's solution	15 volumes of Picric acid (in H_2O) 5 volumes Formaldehyde 1 volume Acetic acid
Denaturation solution	1.5 M NaCl 0.5 M NaOH
Depurination solution	0.25 N HCl
DMPC-dH_2O	0.1 % (v/v) Dimethyl-dicarbonate (DMPC) was solved in dH_2O, incubated 24 h at RT and afterwards autoclaved.
E-buffer (10x)	300 mM $NaH_2 PO_4$ 50 mM EDTA

Elution buffer	1.5 M NaCl 20 mM Tris/HCl (pH 7.5) 1 mM EDTA
Hybridisation solution I	5x SSPE solution 5x Denhardt´s solution 0.1% SDS
Hybridisation solution II	5x SSC 5x Denhardt´s solution 10% Dextran sulfate 0.1% SDS
Ligation buffer (10x)	600 mM Tris/HCl (pH 7.5) 80 mM $MgCl_2$ 100 mM DTT
Lysis buffer I	100 mM Tris/HCl (pH 8.0) 100 mM NaCl 100 mM EDTA 0.5% SDS
Lysis-buffer II	100 mM Tris/HCl (pH 8.0) 5 mM EDTA 200 mM NaCl 0.2% SDS 100 µg/ml Proteinase K
10x MOPS Buffer	41.8 g MOPS 16.6 ml 3 M Sodium acetate 20 ml 0.5 M EDTA in 1 litre of DMPC H_2O, adjust pH to 6.75

Neutralisation solution	1.5 M NaCl 1 M Tris/HCl (pH 7.0)
10x PBS buffer	1.3 M NaCl 70 mM Na_2 HPO_4 30 mM NaH_2 HPO_4, (pH 7.4)
PBT buffer	0.1% Tween-20 in PBS (1x)
SSC (20x)	3 M NaCl 0.3 M $Na_3C_6H_5O_7$ (pH 7.0)
SSPE (20x)	0.02 M EDTA 0.2 M NaH_2 PO_4 3.6 M NaCl (pH 7.0)
Stop-Mix I	95% Formamide 20 mM EDTA 0.05% Bromphenol blue 0.05% Xylene cyanol
Stop-Mix II	15% Ficoll 400 200 mM EDTA 0.1% Orange G
TE-buffer	10 mM Tris/HCl (pH 8.0) 1 mM EDTA
5x TBE buffer	450 mM Tris-bases 450 mM Boric acid 20 mM EDTA (pH 8)
Washing solution I	2x SSC 0.1% SDS

Washing solution II	0.2x SSC

2.1.4 Laboratory Material

All laboratory materials, which are not listed here, were bought from Schütt or Krannich (Göttingen).

Whatman blotting paper (GB 002, GB 003 and GB 004)	Schleicher and Schüll, Dassel
Cell culture flask	Greiner, Nürtingen
Disposable filter Minisart NMI	Sartorius, Göttingen
Filter Paper 0858	Schleicher and Schüll, Dassel
Hybond C	Amersham, Braunschweig
Hybond N	Amersham, Braunschweig
Petri dishes	Greiner, Nürtingen
Pipette tips	Eppendorf, Hamburg
Micro centrifuge tubes	Eppendorf, Hamburg
Transfection flasks	Lab-Tek/Nalge, Nunc, IL, USA
X-ray films	Amersham, Braunschweig
Superfrost Slides	Menzel, Gläser

2.1.5 Sterilisation of solutions and equipments

All solutions that were not heat sensitive were sterilised at 121°C, 105 Pa for 60 min in an autoclave (Webeco, Bad Schwartau). Heat sensitive solutions were filtered through a disposable sterile filter (0.2 to 0.45 µm pore size). Plastic wares were autoclaved as above. Glass-wares were sterilised overnight in an oven at 220°C.

2.1.6 Media, antibiotics and agar-plates

2.1.6.1 Media for Bacteria

LB Medium (pH 7.5)	1% Bacto-trypton 0.5% Yeast extracts 1% NaCl
LB-Agar	1% Bacto-trypton 0.5% Yeast extracts 1% NaCl 1.5% Agar

The LB medium was prepared with distilled water, autoclaved and stored at 4°C.

2.1.6.2 Media for cell culture

ES-cell medium	DULBECCO´s MEM (DMEM) 0.1 mM non essential amino acids 1 mM Sodium pyruvate 10 µM ß-Mercaptoethanol 2 mM L-Glutamine 20% Fetal calf serum (FCS) 1000 U/ml Recombinant leukaemia inhibitory factor (LIF)
Fibroblast cell medium	DULBECCO´s MEM (DMEM) 2 mM L-Glutamine 1 % Sodium pyruvate 1 % Pen/Strp 10% FCS
Neuroblastoma cell medium	DULBECCO´s MEM (DMEM) 200 mM L-Glutamine 1 % Sodium pyruvate

	1 % Pen/Strep
	1% non-essential amino acids
	10% FCS

For long-term storage of cells in liquid nitrogen, the following freezing media were used,

ES cell – freezing medium	30% ES cell medium
	50% FCS
	20% DMSO

2.1.7 Antibiotics

Stock solutions were prepared for the antibiotics. The stock solutions were then filtered through sterile disposable filters and stored at –20°C. When antibiotics were needed, in each case, it was added after the autoclaved medium has cooled down to a temperature less than 55°C.

	Master solution	**Solvent final**	**Concentration**
Ampicillin	50 mg/ml	H_2O	50 µg/ml
Kanamycin	25 mg/ml	H_2O	50 µg/ml
G 418	40 mg/ml	PBS	400 µg/ml
Gancyclovir	100 mM	PBS	2 µM

2.1.8 IPTG / X-Gal plate

LB-agar with 50 µg/ml ampicillin, 100 µM IPTG and 0.4% X-Gal was poured into petri-dishes. The dishes were stored at 4°C.

2.1.9 Bacterial strains

E. coli DH5α	K-12 strain,F^- Φ80d *lac*ZΔM15 endA1 *rec*A1 hsdR17 (r_k^-, m_k^+) sup E44 *thi*-1 d^- *gyr*A96 Δ(lacZYA-arg)

E. coli BL21	B strain, F^- *omp*T *hsd*S_B(r_B^- m_B^-) *gal* *Dcm*
E. coli BL21 (DE3)	B strain, F^- *omp*T *hsd*S_B(r_B^- m_B^-) *gal* *dcm* (DE3)

2.1.10 Cell lines

- Swiss 3T3, mouse embryonic fibroblast cell line, American Type Culture Collection, Rockville, USA "NIH Swiss Mouse".
- NS20Y "Mouse Neuroblastoma cells" American Type Culture Collection (Rockville, MD).
- RI mouse embryonic stem cell line (Passage 11), Dr. A. Nagi, Toronto, Canada.

2.1.11 Plasmids

pBluescript SK (+/-)	(Stratagene, La Jolla, USA)
pBluescript KS (+/-)	(Stratagene, La Jolla, USA)
pGEM-T Easy	(Promega, Wisconsin, USA)
pTriEX-1.1 Neo	(Novagen, Darmstadt, Germany)
pPNT	Tybulewicz et al., 1991
pZERO-2	(Invitrogen, Karlsruhe, Germany)
pTKNeo	MPI for experimental medicine, Göttingen, Germany

2.1.12 Synthetic oligonucleotides

Synthetic oligonucleotide primers were obtained from Qiagen (Hilden, Germany), and dissolved in water to a final concentration of 100 pmol/µl.

Primer name	**Sequence**
mpcDNA-F:	**5' CCT GAA TTC ATG ATA CCA GCA GAC TCT 3'**
mpcDNA-R:	**5' AAC TTC TTC GGT GCG ATA ATG CC 3'**
mp28-probe-F:	**5' GGC GGA CAG ACA GTC AGA CA 3'**

mp28-probe-R:	**5’ GTG GTG CGT GCA TGT AAT TC 3’**
mp-ext1-f:	**5’- CCA GAG CAC CAA TGC TAA AGG AAA TAG GAAT- 3’**
mp-ext1-r:	**5’ – CTC ACA AAG GTC GGG ACT TAG GAT CAG – 3’**
mp-cla-F:	**5’ AGA ATT CCA GCT CAT GGT TCT ATG TAT 3’**
mp-cla-R:	**5’ TAA CTC GAA GAA GGA AAA CAA CAA ATA 3’**
mp28-5’-frag F:	**5’ TAC TCC CAG TGT TTT GGT GAG TAG 3’**
mp28-5’-frag R:	**5’ CCA GGA CTA GAT ATT GAG ACC TTT A 3’**
mp28-3’-frag F:	**5’ CCC ATA AGC CCA TTG TAA TAA AAG 3’**
mp28-3’-frag R:	**5’ TAT AGC TAT CTA GGG AGT GTG GAG T 3’**
mp-gen-F2:	**5’ GAG AGA GAG GTG TCA TTT ACT AGT GG 3’**
mp-gen-R:	**5’ ACC AAA ACA CTG GGA GTA GAG TT 3’**
mp-X-F:	**5’ TTA CTG CTT CTG TCT GAA CTT GTT G 3’**
mp-X-R:	**5’ CCT GTT CTT TCT GAA ACC AGA ATT T 3’**
mp-B-F:	**5’ CCA TCA AGA GTC CTC ATA GAG AGC 3’**
mp-B-R:	**5’ GAC ACA GAA CAC CAT AAA CCT CAT 3’**
Mp-for	**5’- GTT GTA GTC TTG TGG AGA ACA GAG A– 3’**
Mp-rev	**5’- TAC TCA CAC AAA ACA CTG GGA GTA G – 3’**
Neo-F1	**5’ – CGA TCC ATG AGC TAA GCT AGC TAT A – 3’**
hp-exon1-F:	**5’ CTA AGA AGT CAG GCA CAA GAG GTT T 3’**
hp-exon1-R:	**5’ CTC TGA CTT CCC AAT TCC CTT TAC T 3’**
hp-exon2-F:	**5’ GTG ACA TAA TTT CTG CTG AGA AGA CC 3’**
hp-exon2-R:	**5’ CCA TAT GTA AGT TCT AGG AGC TCT GTG 3’**
hp-exon3-F:	**5’ GTG CTA GGG ACC TTC AAG TCA AA 3’**
hp-exon3-R:	**5’ CTT GGA TCT GTG CTG AAG GTG A 3’**
hp-exon4-F:	**5’ AGG AAG GGT GTT TGC AGT AGA CAT AC 3’**
hp-exon4-R:	**5’ GTC AGA ATG TAG TGC TGG AAT GAT AAG 3’**
hp-exon5&6-F:	**5’ AGT ATA TAC CCT GGC AAT GTC ATG T 3’**
hp-exon5&6-R:	**5’ AAA CAT TTA AAA GCC ATG GAA AAG G 3’**
hp-exon7-F:	**5’ ATT TGA TCA CCT CTC AGC TAT TTG TAT 3’**
hp-exon7-R:	**5’ TAG GTG TCT GAT GAC ATT GGA GTA ATA 3’**
T7:	**5’ TAA TAC GAC TCA CTA TAG GG 3’**
T3:	**5’ ATT AAC CCTT CAC TAA AG 3’**
SP6:	**5’ AGG TGA CAC TAT AGA ATA C 3’**
Tc-sp-F:	**5’ ACT TGA AGA AGT GCT GTG CTC TG 3’**
Tc-sp-R:	**5’ AGA GTG AAG CTG ATC GAT AAC AAA G 3’**
Tc-xl-F:	**5’ AAG AAT TTA AAA TAG AAT CCC ACA CA 3’**
Tc-xl-R:	**5’ TTC TTT CAG TTG ATA TGA AAC CTT TA 3’**
Tc-2-F	**5’- GCC CTG TGC TTC GCG GCA TCT GAG C - 3’**
Tc-2-R	**5’- GCT GGT CCT GAG CTA TTC ACA ATA G – 3’**
Tc-IBA-F	**5’ - CAT CCG AAT TCG GAA TGG AGC GGC GAG GCC GA – 3’**
Tc-IBA-R	**5’ – GGA TCC TTC ACA ATA GAG AGC AAA – 3’**
Tc-2-5	**5’ – GCC CTG TGC TTC GCG GCA TCT GAG C – 3’**
Tc-2-3	**5’ – GCT GGT CCT GAG CTA TTC ACA ATA G – 3’**
Tc-fin-F	**5’- CAC AGA TCT TAA GAG AAA GAC TGA GAG AGT C – 3’**
Tc-fin-R	**5’- GGT AGA GAG GTT CAG AGT ATG CTA CCT T – 3’**
Tc-geno-F	**5’ – ATG TCT GTT CTA ATC ATG CCT TTT T – 3’**

Tc-Probe-R	**5' – GTA CTG TGC TCC AGA CCA TGA TAA G – 3'**
Neo-3F	**5' – CCT TCT ATC GGC TTC TTG ACG AG – 3'**
Pelo-F	**5' – TGA GCC CAG ACT GTA CGT GAC – 3'**
Pelo-R	**5' – TCT GCA CCT TAG CGT GAA GCC – 3'**
Neo-447-f	**5'- C TTG TCG ATC AGG ATG ATC TGG – 3'**
Neo-597-r	**5'- G GCC ATT TTC CAC CAT GAT ATT – 3'**

2.1.13 cDNA probes

EF-2 cDNA (Hanes et al., 1992)

β-actin cDNA Clontech, Heidelberg, Germany

2.1.14 Mouse strains

Strains C57BL/6J, 129/Sv, and NMRI were initially ordered from Charles River Laboratories, Wilmington, USA and further inbred in animal facility of Institute of Human Genetics, Göttingen.

2.1.15 Antibodies

Mouse monoclonal α-tubulin	Sigma-Aldrich Chemie GmbH Munich
Anti-rabbit IgG Alkaline phosphatase conjugate	Sigma-Aldrich Chemie GmbH, Munich
Anti-mouse IgG Alkaline phosphatase conjugate	Sigma-Aldrich Chemie GmbH, Munich
Anti-rabbit IgG (whole molecule) Cy3 conjugate	Sigma-Aldrich Chemie GmbH, Munich
Anti-mouse IgG (whole molecule) FITC conjugate	Sigma-Aldrich Chemie GmbH, Munich
Anti-mouse 6xHistidine Antibody	R&D systems

2.1.16 Enzymes

Restriction enzymes (with supplied buffers)	(NEB, Invitrogen)
Collangenase (Type II)	(Sigma, Deisenhofen)
DispaseII (grade II)	(Roche)
Klenow Fragment	(GibcoBRL, Karlsruhe)
Proteinase K	(Sigma, Deisenhofen)
Platinum Taq polymerase	(GibcoBRL, Karlsruhe)
RNase A	(Qiagen, Hilden)
RNase H	(GibcoBRL, Karlsruhe)
RNase inhibitor	(GibcoBRL, Karlsruhe)
Superscript-II	(GibcoBRL, Karlsruhe)
Taq polymerase	(GibcoBRL, Karlsruhe)
T4 polynucleotide kinase	(NEB)
T4 DNA ligase	(Promega)
Tyrpsin	(GibcoBRL, Karlsruhe)

2.1.17 Instruments

Microscope BX60	(Olympus)
GeneAmp PCR System 9600	(Elmer)
Microtiterplate-Photometer	(BioRad)
Phosphoimager Screen	(Kodak)
Spectrophotometer Ultraspec 3000	(Amersham Pharmacia)
SpeedVac concentrator	SVC 100H (Schütt)
TurboblotterTM	(Schleicher & Schüll)
UV StratalinkerTM 1800	(Leica)
X-Ray Automatic Processor Curix 60	(Agfa)

2.2 Methods

2.2.1 Isolation of nucleic acids

2.2.1.1 Isolation of plasmid DNA

(Birnboim and Doly, 1979)

2.2.1.1.1 Small-scale isolation of plasmid DNA

A single *E.coli* colony was inoculated in 5 ml of LB medium with the appropriate antibiotic and incubated in a shaker for 16 hrs at 37°C with a speed of 160 rpm. 500 µl of this saturated culture was used for making glycerol stock and rest of the culture was centrifuged at 5000xg for 15 min. The pellet was resuspended in 150 µl of solution P1. The bacterial cells were lysed with 300 µl of P2 solution and than neutralized with 200 µl of solution P3. The precipitated solution was incubated on ice for 15 min, and centrifuged at 13000xg at 4°C for 15 min. The supernatant was transferred into a new tube, and 1 ml of 100% ethanol was added to precipitate the DNA. It was then stored on ice for 15 min, centrifuged at full speed for 20 min, and finally the pellet was washed with 70% ethanol and after air drying dissolved in 30 µl of TE buffer.

P1:	50 mM Tris-HCl, pH 8.0 10 mM EDTA 100 µg/ ml RNase A
P2:	200 mM NaOH, 1% SDS
P3:	3.0 M Potassium acetate, pH 5.5

2.2.1.1.2 Large-scale preparation of plasmid DNA using the Qiagen Midi Kit

A single clone was inoculated in 2 ml LB medium with appropriate antibiotic as a pre-culture for 8 hrs in a 37°C shaker. In 100 ml LB medium with appropriate antibiotic, this pre-culture was added in a dilution of 1/100 fold and incubated overnight at 37°C with shaking. The saturated culture was centrifuged at 6000xg for 15 min. The pellet was resuspended in 5 ml of

solution P1 and cells were lysed with 7.5 ml P2 and neutralized with 7.5 ml P3 as described above. The precipitated solution was centrifuged at 10000xg for 30 min at 4°C. Meanwhile, the column (Qiagen-tip 100) was equilibrated with 10 ml of QBT solution. After centrifugation, the lysate was poured into the column to allow the DNA to bind to the resin present in the bed of the column. The column was then washed twice with 10 ml of solution QC. Finally, the DNA was eluted with 5 ml of QF solution. To precipitate the DNA, 3.5 ml of isopropanol was added and mixed thoroughly and centrifuged at 14000xg for 30 min at 4°C. The DNA pellet was washed with 70% ethanol and dissolved in 100 µl of TE.

QBT:	750 mM Sodium chloride
	50 mM MOPS pH 7.0
	15 % Ethanol
	0.5 % Triton X-100
QC:	1 mM Sodium chloride
	50 mM MOPS pH 7.0
	15 % Ethanol
QF:	1.25 M Sodium chloride
	50 mM Tris/ HCl pH 8.5

2.2.1.1.3 Endotoxin free preparation of plasmid DNA

Endotoxins, also known as lipopolysaccharides or LPS, are cell membrane components of Gram-negative bacteria (e.g., *E.coli*). During lysis of bacterial cells, endotoxin molecules are released from the outer membrane into the lysate and strongly influence the transfection efficiency of cultured cells like embryonic stem (ES) cells. Increased endotoxin levels lead to sharply reduce transfection efficiencies. Endofree plasmid preparation kit integrates endotoxin removal into standard plasmid preparation procedure. The neutralized bacterial lysate was filtered through a QIA filter cartridge (provided in kit) and incubated on ice with a specific Endotoxin Removal buffer (patented by Qiagen). The endotoxin removal buffer prevents LPS molecules from binding to the resin in the columns (QIAGEN-tips) thus allowing purification of DNA containing less than 0.1 endotoxin units per µg plasmid DNA.

2.2.1.2 Isolation of genomic DNA from tissue samples

(Laird et al., 1991)

A 1 to 2 cm piece of the tail from a mouse was incubated in 700 µl of lysis buffer-I containing 35 µl proteinase K (10µg/µl) at 55°C overnight in a shaker. To the tissue lysate, an equal volume of phenol was added, mixed by inverting several times, and centrifuged at 8000xg for 5 min at room temperature. After transferring the upper aqueous layer into a new tube, the same procedure was repeated, first with a 1:1 ratio of phenol and chloroform and then with chloroform. Finally, the DNA was precipitated with 0.7 volume of isopropanol, washed with 70% ethanol, and dissolved in 100-200 µl of TE buffer and incubated at 60°C for 15 min.

Lysis buffer I:	50 mM Tris/HCl (pH 8.0)
	100 mM EDTA
	0.5% SDS

2.2.1.3 Isolation of genomic DNA from ES cells

To isolate the DNA from ES cells, cells in a 24 well plate were washed with PBS and incubated overnight in 500 µl of lysis buffer II at 37°C. Equal volume of isopropanol was added and mixed for 15 min to precipitate the DNA. After washing with 70% ethanol, the DNA was transferred into a microcentrifuge cup containing 60 µl of TE buffer and incubated at 60°C for 15 min.

Lysis-buffer II	100 mM Tris-HCl (pH 8.5)
	5 mM EDTA
	200 mM NaCl
	100 µg/ml proteinase K
	0.2% SDS

2.2.1.4 Isolation of genomic DNA from blastocysts

Intact and cultured blastocysts were genotyped by PCR. To isolate the genomic DNA, cultured blastocysts were lysed in 15µl lysis buffer III (100mM KCl, 20mM TrisCl, pH 8.0, 4 mM $MgCl_2$, 0.9 % NP-40, 0.9% Triton-X-100) containing proteinase K (300 µg/ml),

incubated for 1 hr at 37 °C, 4 hrs at 55°C and 90°C for 30 min. The DNA was stored at -20°C until use.

The intact blastocysts were lysed in 10 µl of lysis buffer III, incubated at 95°C for 10 min followed by an incubation at -80°C for 15 min. The chilling treatment was repeated and the PCR cups were stored at -20°C.

2.2.1.5 Isolation of total RNA from tissue samples and cultured cells

Total RNA isolation reagent is an improved version of the single-step method for total RNA isolation. The composition of reagent includes phenol and guanidine thiocyanate in a mono-phase solution. 100-200 mg of the tissue sample was homogenized in 1-2 ml of TRI Reagent by using a glass-teflon homogenizer. The sample volume should not exceed 10% of the volume of reagent used for the homogenization. To isolate total RNA from cultured cells, 350 µl of reagent was added to the petri-dish (6 cm diameter). Cells were homogenized with a rubber stick and the lysate was transferred into a microcentrifuge tube. The homogenate was incubated at 4°C for 5 min to permit the complete dissociation of nucleoprotein complexes. Then, 0.2 ml of chloroform was added, mixed vigorously, and stored at 4°C for 10 min. After centrifugation at 12000xg for 15 min at 4°C, the upper aqueous phase was transferred into a new tube. The RNA was precipitated by adding 0.5 ml of isopropanol. Finally, the pellet was washed twice with 75% ethanol and dissolved in 80-100 µl of DMPC-H_2O.

2.2.2 Electrophoresis methods

2.2.2.1 Agarose gel electrophoresis of DNA

Agarose gels are used to separate nucleic acid molecules from as small as 50 bases to more than 50 kb, depending on the concentration of the agarose and the precise nature of the applied electrical field (constant or pulse). Usually, 1 g of agarose was added in 100 ml of 0.5x TBE buffer (1%) and boiled in the microwave to dissolve the agarose, then cooled down to about 60°C before adding 3 µl of ethidium bromide (10 mg/ml). The agarose gel was poured into a horizontal gel chamber.

2.2.2.2 Agarose gel electrophoresis of RNA

(Hodge, 1994)

Single-stranded RNA molecules often have complementary regions that can form secondary structures. Therefore, RNA was run on a denaturing agarose gel that contained formaldehyde, and before loading, the RNA was pre-treated with formaldehyde and formamide to denature the secondary structure of RNA. 1.25g of agarose was added in 100 ml of 1x MOPS buffer and dissolved by heating in a microwave. After cooling it to about 50°C, 25 ml of formaldehyde (37%) were added, stirred and poured into a horizontal gel chamber.

RNA samples were treated as follows:

10 – 20 µg RNA
2 µl 10x MOPS Buffer
3 µl Formaldehyde
8 µl Formamide (40%)
1.5 µl Ethidium bromide (10 mg/ml stock)

Samples were denatured at 65°C for 10 min and chilled on ice before loading into the gel. The gel was run at 40 V at 4°C for about 12 hrs.

2.2.3 QIAEXII Gel Extraction method

To the excised DNA fragment from agarose, 300 µl of QX1 buffer was added in each 100 mg of gel slice followed by the addition of 10 µl of QIAEX II and incubated at 50°C for 10 min. To keep the QIAEX II in suspension, mixture was vortexed for every 10 min. After the gel slice was dissolved completely, the mixture was centrifuged at 10000xg for 1 min. The supernatant was discarded and the pellet was washed with 1 ml of QX1 buffer followed by two washing steps each with 1 ml of buffer PE. After drying the pellet, dissolved the DNA by adding 20-40 µl H_2O, centrifuged briefly and transferred the DNA into a new cup.

2.2.4 Enzymatic modifications of DNA

2.2.4.1 Restriction of DNA

Restriction enzyme digestions were performed by incubating double-stranded DNA with an appropriate amount of restriction enzyme in its respective buffer as recommended by the supplier, and at the optimal temperature for the specific enzyme. Restrictions include 2-10 U enzyme per microgram of DNA. These reactions were usually incubated for 1-3 hrs to ensure complete digestion. For genomic DNA digestion, the reaction solution was incubated for 2-16 hrs at 37°C.

2.2.4.2 Ligation of DNA fragments

The ligation of a DNA fragment into a vector was carried out in the following reaction mix:

30 ng vector DNA (digested)
50-100 ng insert DNA (1:3, vector: insert ratio)
1 µl ligation buffer (10x)
1 µl T4 DNA ligase (5U / µl)
in a total volume of 10 µl

Blunt-end ligations were carried out at 16°C for overnight, whereas overhang-end ligations were carried out at room temperature for 2-4 hrs.

2.2.4.3 TA-Cloning

(Clark, 1988; Hu, 1993)

Taq polymerase and other DNA polymerases have a terminal transferase activity that results in the non-template addition of a single nucleotide to the 3' ends of PCR products. In the presence of all four dNTPs, dATP is preferentially added. This terminal transferase activity is the basis of the TA- cloning strategy. For cloning of PCR products, the pGEM-T or pGEM-T easy vector systems that has 5‘ T overhangs were used.

The reaction mix contains the following components:

25 ng of pGEM-T or pGEM-T Easy vector DNA
PCR product (1:3, vector to insert ratio)
1 µl of T4 DNA ligase 10x buffer
1 µl of T4 DNA ligase
Total volume was 10 µl

The reaction was incubated overnight at 4°C.

2.2.5 Preparation of competent *E.coli* cells

By this procedure, the competence of *E. coli* cells to accept free DNA is artificially increased. This is achieved by modifying the cell wall with $CaCl_2$ and RbCl. Thirty ml of LB Medium were inoculated with a single bacteria colony (DH5α or BL21) and shacked overnight at 37°C. At the next day, 1 ml of this pre-culture was added to 100 ml of LB medium and incubated until an OD_{600}=0.5 was reached. Then, cells were cooled down on ice for 10 min and centrifuged at 5000x g, 4°C for 10 min (Sorvall RC5B). The cell pellet was resuspended carefully in 30 ml of TFB I (on ice) and was incubated 10 min on ice. After centrifugation at 5000x g at 4°C for 10 min, the bacteria were resuspended in TFBII, shock frozen in 200 µl aliquots in liquid nitrogen and stored at –80°C until their use.

TFB I:	100 mM	RbCl
	50 mM	$MnCl_2$
	10 mM	$CaCl_2$
	30 mM	KAc, pH 5.8
	15 % (v/v)	Glycerin
TFBII:	10 mM	RbCl
	75 mM	$CaCl_2$
	10 mM	MOPS, pH 7.0
	15 % (v/v)	Glycerin

2.2.6 Transformation of competent bacteria

(Ausubel et al., 1994)

Transformation of the bacteria was done by gently mixing one aliquot of competent bacteria (50 µl) with 10 µl of ligation reaction. After incubation for 30 min on ice, bacteria were subjected to heat shock for 45 sec at 37°C and cooled down for 2 min on ice. After adding 300 µl of LB medium, bacteria were incubated at 37°C, 200 rpm for 1 hr to grow and to allow the recovery from heat shock and were plated out on LB-agar plates containing appropriate antibiotic (50µg/ml) and whenever required, 1 mM IPTG and X-Gal 40mg/ml (X-Gal for "Blue-White" selection).

2.2.7 Polymerase Chain Reaction (PCR)

2.2.7.1 PCR amplification of DNA fragments

The amplification cycles were performed in an automatic thermocycler. The PCR reaction contains in general, the following components:

10 ng DNA
1 µl forward primer (10pmol)
1 µl reverse primer (10pmol)
1 µl 10mM dNTPs
5 µl 10x PCR buffer
1.5 µl 50mM $MgCl_2$
1 µl *Taq* DNA polymerase (5U/µl)
Up to 50 µl H_2O

The reaction mixture was added in a 200 µl reaction tube, vortexed slightly and placed in the thermocycler.

Standard PCR program:

Initial denaturation	95°C 5 min
Elongation	95°C 30 sec (denaturation)
30-35 cycles	58°C 45 sec (annealing)
	72°C 1-2 min (extension)
Final extension	72°C 10 min

2.2.7.2 Long-Range PCR

In order to verify the homologous recombination, long-range PCR analysis was performed using the TaKaRa LA Taq PCR kit (TaKaRa Bio Inc.). The PCR reaction contains the following components:

10 ng DNA
1 µl forward primer (10pmol)
1 µl reverse primer (10pmol)
8 µl 2.5mM dNTPs
5 µl 10x LA PCR buffer II (Mg^{2+} free)
5 µl 25mM $MgCl_2$
0.5 µl TaKaRa *Taq* (5 U/µl)
Up to 50 µl H_2O

The reaction mixture was added in a 200 µl reaction tube, vortexed slightly and placed in the thermocycler.

The PCR program is shown here:

Initial denaturation	94°C 1 min
Elongation	94°C 30 sec (denaturation)
30 cycles	60°C 2 min (annealing)

	72°C 5 min (extension)
Final extension	72°C 10 min

2.2.7.3 Colony PCR

Colony PCR allows rapid detection of transformation success when primers are available to allow determination of correct ligation products by size or hybridization. 500 µl of appropriate selection media (LB medium with appropriate antibiotic) for the plasmid of interest was added into the1.5 ml tubes (pre-labelled). The colonies were selected randomly and were picked with a sterile toothpick. After dipping the tootpick into the PCR master mix, they were inserted into the culture tubes. PCR was performed with appropriate conditions for the primers and expected product. The resulting PCR products were electrophoresed on 1% agarose gel. Having found a positive colony, the cultured colony was kept for plasmid DNA isolation.

2.2.7.4 Real-time PCR

DNA was isolated from *Tcte3*-deficient mice tails by the method described above (2.2.1.3) and quantified by spectrophotometer (OD260). Serial dilutions of sample and standard DNA's were made with buffer AE (Qiagen, Hilden). Standard DNA was serially diluted at 20, 10, 5, 2.5 and 1.25 ng/µl for the generation of standard curve, while each sample DNA (*Tcte3* mice) was used at a concentration of 10 ng/µl. Primers and TaqMan probes were designed accordingly to generate the amplicons <150 bp, enhancing the efficiency of PCR amplification.

Real-time quantitative PCR was performed using double stranded DNA binding dye Syber Green PCR Master mix (Applied Biosystems) in an ABI GeneAmp 7000 Sequence Detection System. Each reaction was run in triplicate and the melting curves were constructed by using the Dissociation Curves Software (Applied Biosystems), to ensure that only a single product was amplified. *pelota* gene (GenBank, NM_134058) primers (pelo-f and pelo-r) were used for the normalization of each DNA sample measured for *neomycin* copies.

Quantitative real-time PCR reactions of DNA specimens and standards were conducted in a total volume of 10 µl with 5 µl of 1 x TaqMan Master Mix, 2.5 µl of each forward and reverse primer in a final concentration of 1 µM and 2.5 µl of DNA. Thermal cycler parameters were 2

min at 50°C, 10 min at 95°C and 40 cycles involving denaturation at 95°C for 15 sec and annealing/extension at 58°C for 1 min.

Each reaction was run in triplicate and the melting curves were constructed by using the Dissociation Curves Software (Applied Biosystems), to ensure that only a single product was amplified. When the temperature reached the *Tm* (Tm = 87^{o}C) of the probes, a rapid loss of fluorescence was observed between the two adjacently bound probes. The negative derivative of fluorescence was plotted versus the temperature to define the template-specific melting curves. Standard curves of the threshold cycle number versus the log number of copies of genes were generated for *neomycin* resistance gene and were used to extrapolate the number of copies of *neomycin.* Quantitative real-time PCR results were reported as the number of copies for *neomycin* in *Tcte3* mice/ *neomycin* copies in homozygous null mice and the mean was calculated. The threshold cycle (Ct) of each sample was recorded as a quantitative measure of the amount of PCR product in the sample. The base line X-axis is set, which identifies the cycle in which the log linear signal can be distinguished from the background.

2.2.7.5 Genotyping of the knockout mice by using PCR

The genotypes of all offspring of mice were analyzed by polymerase chain reaction (PCR). For amplification of the wild type and the mutant allele, the DNA was extracted from mouse-tails as described in 2.2.1.3 and pipetted to the following reaction mixture:

2.2.7.5.1 *Tcte3* mice genotyping,

1 µl DNA (300-500 ng)
1 µl Tcfin-F (10 pmol/µl)
1 µl Tcfin-R (10 pmol/µl)
1 µl Neo-3F (10 pmol/µl)
1 µl dNTPs (10 mM)
5 µl *Taq* Polymerase buffer (10x)
3 µl $MgCl_2$ (25 mM)
0.5 µl *Taq* Polymerase (5 U/µl, Gibco)
Up to 50 µl H_2O

2.2.7.5.2 *Dnali1* mice genotyping,

1 µl DNA (300-500 ng)
1 µl mp-B-F (10 pmol/µl)
1 µl mp-gen-R (10 pmol/µl)
1 µl Neo-3F (10 pmol/µl)
1 µl dNTPs (10 mM)
5 µl *Taq* Polymerase buffer (10x)
3 µl $MgCl_2$ (25 mM)
0.5 µl *Taq* Polymerase (5 U/µl, Amersham)
Up to 50 µl H_2O

The mixture was subjected to the following program in the thermocycler,

2.2.7.5.3 *Tcte3* / *Dnali1* analysis,

Denaturation	95°C for 5 min
Elongation (for 35 cycle)	95°C for 30 sec (Denaturation)
	62°C (*Tcte3*) / 60°C (*Dnali1*) for 1 min (Annealing)
	72°C for 1 min (Elongation)
Final extension	72°C for 10 min

2.2.7.6 Reverse transcription PCR (RT-PCR)

RT-PCR was used to determine the expression of genes in specific tissues or in different developmental stages. 1-5 µg of total RNA was mixed with 1 µl of oligo $(dT)_{18}$ primer (10pmol/µl) in a total volume of 12 µl. To avoid possible secondary structures of the RNA, which might interfere with the synthesis, the mixture was heated to 70°C for 10 min, and then quickly chilled on ice. After a brief centrifugation, the following components were added to the mixture:

4 µl 5x first strand buffer
2 µl 0.1 M DTT
1 µl 10mM dNTPs
1 µl Rnasin (10U/µl)

The content of the tube was mixed gently and incubated at 42°C for 2 min. Then, 1 µl of reverse transcriptase enzyme (Superscript II) was added and further incubated at 42°C for 50 min for the first strand cDNA synthesis. Next, the reaction was inactivated by heating at 70°C for 15 min. One µl of the first strand reaction was then used for the PCR reaction.

2.2.7.7 One-Step RT-PCR

To obtain specific RT-PCR products, the QIAGEN OneStep RT-PCR kit was employed which contains optimized components that allow both reverse transcription and PCR amplification to take place in what is commonly referred to as a ”one-step” reaction.

Master mix	**per reaction**
5 x Qiagen OneStep RT-PCR buffer	10 µl
dNTP mix (containing 10 mM of each dNTP)	2 µl
Forward primer (10 pmol)	1 µl
Reverse primer (10 pmol)	1 µl
Qiagen OneStep RT-PCR Enzyme Mix	2 µl
RNase inhibitor (20 units/ l µl)	1 µl
RNase-free water	31 µl

2 µl (2 µg) of total RNA isolated from mouse tissues was added to 48 µl of prepared Master mix in a PCR tube, the sample was placed in the thermal cycler and the RT-PCR program runs according to the user manual. After the amplification step, the sample was checked on an agarose gel.

Thermal cycler conditions:

Reverse transcription	30 min 50 °C
Initial PCR activation step	15 min 95 °C
35 cycles	
Denaturation	30 sec 94 °C
Annealing	40 sec 56- 60 °C (depending on primers)
Extension	1 min 72 °C

2.2.8 DNA Sequencing

The sequencing method was derived from Sanger et al. (1977) where 4 different fluorescently marked ddNTPs (didesoxynucleosid-5´-triphosphate) were used. The sequence reaction was:

1- 1.5 µg	plasmid DNA or
0.2-0.5 µg	purified PCR products by Milipore columns
10 pmol/µl	specific primer
4 µl	ET reaction mix (dNTPs, dideoxy dye terminators and *Taq* polymerase.
x µl	Ampuwa H_2O
20 µl	Total volume

Elongation and chain termination took place in a thermocycler (MWG). The following sequence PCR program was used:

Initial denaturation	95°C	5 min
25 cycles	95°C	20 sec
	55°C	30 sec
	60°C	2 min
Extension	75 °C	10 min

The reaction products were analyzed with *automatic sequencing equipment*.

2.2.9 Blotting techniques

2.2.9.1 Southern blotting of DNA to nitrocellulose filters

(Southern, 1975)

In Southern blotting, the transfer of denatured DNA from agarose gel to nitrocellulose membrane is achieved by capillary flow. 20x SSC buffer, in which nucleic acids are highly soluble, is drawn up through the gel into the nitrocellulose membrane, taking with it the single-stranded DNA that becomes immobilised in the membrane matrix.
After electrophoresis, the gel was treated with 0.25 M HCl for depurination. It was followed by denaturation solution for 30 min and 45 min in neutralization solution. The transfer of the DNA to the nitrocellulose membrane was done using a Turbo-Blot-apparatus (Schleicher & Schuell, Dassel). About 20 Whatman filter papers (GB 003) were layered on a stack tray followed by 4 Whatman filter papers (GB 002) and 1 Whatman filter paper GB 002 soaked with 2x SSC. The equilibrated nitrocellulose filter that was also soaked with 2x SSC was laid on the top. The agarose gel, which was treated as described above, was placed on the filter and was covered with 3 Whatman filter papers GB 002 soaked with 2x SSC. The buffer tray was placed and filled with 20x SSC. The top of the blot was covered with a wick, which was soaked with 20x SSC. The transfer was carried out for overnight. Finally, after disassembling of the blot, the filter was washed briefly in 2x SSC and the DNA was fixed onto the filter by either incubating it at 80°C for 2 hrs or by UV-crosslinking in UV Stratalinker 1800 (60,000mJ/cm^2).

2.2.9.2 Northern blotting of RNA onto nitrocellulose filter

For the transfer of RNA onto a nitrocellulose filter, the same procedure as described above (2.2.9.1) was performed. In this case, however, the gel does not need to be denatured.

2.2.9.3 Colony Transfer

The colony hybridisation is a rapid and effective technique that detects recombinant sequences isolated directly from cells grown on plates and transferred to membranes. 88 mm

ϕ nitrocellulose or nylon membranes (Optitran BA-S85, Schleicher & Schuell) were placed on the plates for 1-2 min to transfer the colonies to the filters, whereas reference position points were marked to identify later the positive colonies. The culture plate was incubated at 37°C, so the colonies grow again. The marked membranes were placed on surfaces with the following solutions:

5 min	10% (w/v) SDS
3 min	denaturation solution
10 min	neutralisation solution
10 min	2xSSC

DNA was fixed by UV cross-linking. Then the membrane was ready for hybridization with a ^{32}P-labeled probe (2.2.10). After hybridization, the positive colonies were localized.

2.2.10 "Random Prime" method for generation of ^{32}P labeled DNA

(Denhardt, 1966; Feinberg and Vogelstein, 1989)

Rediprime™ II Random Prime Labeling System (Amersham Pharmacia) was used for labelling of DNA probes. The method depends on the random priming principle developed by Feinberg and Vogelstein (1989). The reaction mix contained dATP, dGTP, dTTP, Klenow fragment (4-8 U) and random oligodeoxyribonucleotides. Firstly, 25-50 ng of DNA were denatured in a total volume of 46 µl at boiling water for 10 min and chilled on ice for 5 min. After pipetting the denatured probe into the Rediprime™ II Random Prime Labeling System cup, 4 µl of [α-^{32}P] dCTP (3000 Ci/mmol) was added to the reaction mixture. The labelling reaction was carried out at 37°C for 1 hr. The labeled probe was purified from unincorporated [α-^{32}P] dCTP by using microspin columns (Amersham Pharmacia).

2.2.11 Hybridisation of nucleic acids

(Denhardt, 1966)

The membrane to be hybridised was equilibrated in 2x SSC and transferred to a hybridisation bottle. After adding 10 ml of hybridisation solution and sheared salmon DNA, the membrane

was incubated for at least 2 hrs in the hybridization oven at 65°C. Then, the labelled probe was denatured at 95°C for 10 min, chilled, and added to the hybridisation solution. The hybridisation was carried out overnight in the oven. Next day, the filter was washed for 10 min with 2x SSC at room temperature. Finally, it was washed with 0.2x SSC containing 0.1 % SDS at the hybridisation temperature. After drying the filter, it was sealed in Saran wrap and exposed to autoradiography overnight at -80°C or to Phosphoimager screen for 1-4 hrs. The film was developed in X-Ray Automatic Processor Curix 60 or the screen was scanned in the Phosphoimager. For quantification of detected bands, the program Quantity One (Bio-Rad) was used.

2.2.12 Protein and biochemical methods

2.2.12.1 Isolation of total proteins

100 mg of tissue was homogenized in 500 µl of 0.25 M Tris/HCl, pH 7.8, with a teflon glass headed pestle. The cell membrane was destroyed by freezing in liquid nitrogen and thawing at 37°C, which was repeated three times. The samples were centrifuged at full speed for 10 min at 4°C and supernatant was distributed in several microcentrifuge tubes. The tubes were frozen in liquid nitrogen and stored at –80°C.

2.2.12.2 Isolation of cell culture proteins

Lysis buffer	50 mM Tris-HCl, pH 7.5
	150 mM NaCl
	1 % NP-40
	1 mM dithiothreitol (DTT)
	2.5 mM EDTA
	1 µM aprotinin
	1 µM leupeptin
	1 mM phenylmethylsulphonyl fluoride (PMSF)

5 x 10^6 cells/ml were harvested and washed with cold phosphate buffered saline and resuspended in 100 µl of lysis buffer. The cells were allowed to swell on ice for 10 min

followed by brief sonication for 20 sec. The cellular extract was either used immediately or stored at –80°C for later use.

2.2.12.3 Determination of protein concentration

(Bradford, 1976)

To determine the protein concentration, the Bio-Rad protein assay was employed which is a dye-binding assay based on the differential colour change of a dye in response to various concentrations of protein. The assay is based on the observation that the absorbance maximum for an acidic solution of Coomasie Blue G-250 shifts from 494 to 595 nm when the binding to protein occurs. The BSA stock solution of 1 mg/ml was diluted in order to obtain standard dilutions in range of 10 µg/ml to 100 µg/ml. The Bio-Rad's color reagent was diluted 1:5 with H_2O, and filtered through 0.45 µm filters. In a 96-well microtiter plate, 20 µl of each standard dilution and the samples to be measured were pipetted with 280 µl of the color reagent. The absorption of the colour reaction was measured at 595 nm in a microplate reader (Microplate Reader 450, Bio-Rad).

2.2.13 Western blotting

(Gershoni and Palade, 1982)

2.2.13.1 SDS-PAGE for the separation of proteins

(Laemmli, 1970)

SDS-PAGE consists of two gels; firstly, a 10-12 % separating gel was poured. In order to achieve a smooth boundary between separating and stacking gel, the separating gel was covered with a layer of water. After polymerization of the separating gel, a 4 % stacking gel was poured over it. The samples were boiled in sample buffer for 10 min at 95°C before loading into the gel. The gel was run at 15 mA for 1 hr and then at a constant current of 30 mA.

The components for making protein gels of different concentrations are indicated below:

Separation gel	**10%**	**12%**	**15%**
Acrylamide 29:1 (40%)	5 ml	6 ml	7 ml
Lower Tris	5 ml	5 ml	5 ml
dH_2O	10 ml	9 ml	8 ml
SDS 10%	100 µl	100 µl	100 µl
APS 10%	200 µl	200 µl	200 µl
TEMED	6 µl	6 µl	6 µl

Collecting gel	**3%**
Acrylamide 29:1 (40%)	1.3 ml
Upper Tris	1.3 ml
dH_2O	7.4 ml
SDS 10%	50 µl
APS 10%	50 µl
TEMED	6 µl

Electrophoresis buffer	1.44% (w/v)	Glycine
	0.3% (w/v)	Tris base
	0.1% (w/v)	SDS
Acrylamide 29:1 (40%)	38.6% (w/v)	Acrylamide
	1.4% (w/v)	Bis-acrylamide
Lower Tris	1.5 M	Tris/HCl, pH 8.8
	0.4% (w/v)	SDS
Upper Tris	0.5 M	Tris/HCl, pH 6.8
	0.4% (w/v)	SDS

2 x SDS Loading Buffer	4.8% (w/v)	SDS
	20% (v/v)	Glycerin
	10% (v/v)	β-Mercapto-ethanol
	0.1% (w/v)	Bromphenol blue
	100 mM	Tris/HCl, pH 7.8

2.2.13.2 Staining of PAA gels

The PAA gels were stained with Coomassie Brilliant Blue 250. After the electrophoresis, the gel was introduced into the staining solution from 1 hr to overnight. To detect clearly the protein bands, the gel was incubated in a de-staining solution overnight under rocking. Alternatively, the „Simply Blue^{TM} SafeStain“ (Invitrogen, Groningen) staining solution was used to dye the protein PAA gel. The PAA gel was rinsed 3x for 5 min with dH_2O. Then, it was covered with SimplyBlue^{TM} solution and stained for 1 hr at room temperature under gentle shaking. The staining solution was discarded and the gel was washed with dH_2O for 1 hr. A second water wash was required for a clear gel background.

Staining solution:	30 % (v/v)	Methanol
	10% (v/v)	Acetic acid
	0.2% (w/v)	Coomassie Brilliant Blue R250
Destaining solution:	30% (v/v)	Methanol
	10% (v/v)	Acetic acid

2.2.13.3 Semi dry blot

The proteins were separated by SDS PAGE and transferred to a membrane. For this, 9 pieces of GB004 Whatman filter paper were cut at the size of the gel. For the blot, the graphite plates from the transfer equipment were rubbed down with dH_2O. Three pieces of filter paper were soaked in anode I buffer, 3 were soaked in anode II buffer and the paper pieces were piled up on the transfer plate respectively. The membrane was moistened with methanol and laid on the filter paper pile. The protein gel was taken out from the glass plates, the collecting gel was separated and eliminated; meanwhile the separating gel was carefully laid on the membrane.

Finally, 3 pieces of filter paper were soaked in the cathode buffer and placed on the gel. The air bubbles were eliminated with a roller. After the cathode plate was put in place, the transfer was done for 1 hr at 3.5 mA/cm^2. The membrane was subjected to immune detection.

Anode I buffer	0.3 M	Tris/HCl, pH 10.4
	20% (v/v)	Methanol
Anode II buffer	25 mM	Tris/HCl, pH 10.4
	20% (v/v)	Methanol
Cathode buffer	40 mM	ε-Aminocaproic acid
	25 mM	Tris/HCl, pH9.4
	20% (v/v)	Methanol

2.2.13.4 Immune detection on protein filters

The unspecific binding sites present in a membrane were saturated by using blocking buffer for 30 min-1 hr. Then, the filter was incubated in a plastic bag with 1:500 dilution of primary antibodies for overnight at 4°C. Unbound antibodies were removed by using washing buffer 3x 20 min. The secondary antibody coupled with alkaline phosphatase was diluted 1:10000 in washing buffer and added to the filter for 1 hr under swinging shaking. Later, the unbound antibodies were removed with washing buffer 3 times for 5 min each followed by 1 time washing with buffer P3 for 5 min and later incubated for reaction in a plastic bag with the chromogenic solution, containing 45 µl of NBT solution and 35 µl of BCIP solution in 10 ml of buffer P3. Then, the filter was washed shortly in dH_2O and dried on filter paper.

10x Washing stock	1.4 M	NaCl
	100 mM	Tris/HCl, pH 7.5
	0.5% (v/v)	Tween 20
Blocking buffer	5% (w/v)	Skimmed powder milk in 1x washing stock
Washing buffer	2% (w/v)	Skimmed powder milk in 1x washing stock

Buffer P3	100 mM	NaCl
	50 mM	$MgCl_2$
	100 mM	Tris/HCl pH 9.5
NBT solution	75 mg/ml	NBT
	70%	Dimethylformamide (DMF)
BCIP solution	50mg/ml	BCIP in DMF

2.2.14 Generation of polyclonal antibody

2.2.14.1 Production of a GST-Tag Fusion Protein

Tcte3 fusion protein with 220 amino acids GST-tag (at the amino-terminal) and a His-Tag (at the carboxy-terminal) was produced using the pET system (Novagen, Darmstadt). The pET 41b (+) expression vector carries strong bacteriophage T7 transcription and translation signals; expression can be induced by providing source of T7 RNA polymerase in the host cell (BL21 DE3). T7 RNA polymerase is very selective and active for fully induction by adding IPTG at a specific concentration and time.

The *Tcte3* cDNA was amplified by Tc-2-5 and Tc-2-3 primers and cloned into pGEM-T easy vector was restricted with *Eco*RI enzyme and ligated into the same site of pET 41b vector. The orientation of *Tcte3* cDNA fragment was checked by *Bgl*II restriction enzyme. In correct orientation, the length of cutted fragment from the pET41-b vector was 647 bp. The resulting ligation reaction was transformed into BL21- DE3 competent cells. The positive colony was picked up by colony PCR (2.2.7.3) and pre-cultured in 5 ml of LB Medium with kanamycin overnight at 37°C under shaking (200 rpm). 2 ml of this pre-culture was then used to inoculate 1000 ml of LB Medium-kanamycin and allowed to grow the bacteria at 37°C under shaking (200 rpm), until an OD_{550}= 6.0 was reached. For induction of the fusion protein, 10 ml of 100 mM IPTG solution was added to the culture stock and incubation continued for another 3 hrs. After that, the cells were harvested by centrifugation at 4,500x g, 4°C for 10 min. The supernatant was discarded carefully and the pellet was resuspended in 40 ml of ice-cold 1X GST buffer. For the analysis of total protein content via SDS-PAGE, suspension was taken and sonicated under ice cooling until lysis was complete. To remove insoluble

components, the suspension was centrifuged at 14000xg, 4°C for 20 min. The clear supernatant was carefully transferred to a clean tube. This extract was ready for affinity purification of the recombinant protein (GST-Bind Kits Novagen, Darmsdadt). 10 µl aliquots were separated in an SDS-PAA gel to check the induction of fusion protein. The purified fusion protein extract was then used to immunize the rabbits (New Zealand) and for subsequent isolation of the antibody from the antiserum of the rabbits.

2.2.14.2 Immunisation

Two rabbits were immunised with approximately 100 µg of purified fusion protein mixed with complete or incomplete Freund´s adjuvant (Sigma-Alderich Chemie, Deisenhofen, Germany) in a 1:1 ratio and injected subcutaneously into two rabbits for 3 times at the distance of 4 weeks. The rabbits were then sacrified and isolated antiserum was aliquoted and stored at -80°C.

2.2.14.3 Purification of specific polyclonal antibodies

The antibodies against the protein of interest present in the polyclonal serum have to be purified so that good protein analysis can be performed. For purification of Tcte3-specific antibodies through the serum, *Strep*-tag-Tcte3 fusion protein was generated by inserting the *Tcte3* cDNA in pASK-IBA2 vector (IBA GmbH, Goettingen). The *Tcte3* cDNA was obtained by RT-PCR of mouse testicular RNA using primers Tc-IBA-F (containing *Eco*RI site) and Tc-IBA-R (containing *Bam*HI site). The resulting 698 bp fragment was cutted by *Eco*RI and *Bam*HI restriction enzymes and ligated into the *Eco*RI and *Bam*HI sites of pASK- IBA-2 vector. The resulting ligation reaction was transformed into *E.coli* BL21- DE3 competent cells. Anaerobically grown *E.coli* (300 ml of a culture at an OD_{600} of 1 and induced by 30µl of Anyhydrotetracyclin) were recovered by centrifugation (3000 x g for 15 min at 4°C) and were subjected to isolation of the *Strep* tag-Tcte3 fusion protein.
The recombinant protein were separated by SDS PAA gel and transferred to a membrane (2.2.13.1). After the transfer, a stripe from the edge of the filter was cut out and fusion protein was detected with anti-His antibody to localize the fusion protein. Part of the filter containing the fusion protein was cut out, blocked for 1 hr and incubated for 1 hr with 200 µl of the polyclonal antiserum. The membrane was washed 3 times for 10 min with washing buffer and 2 times for 5 min with PBS. The bound specific antibodies were eluted from the membrane

with 1-5 ml of elution buffer under heavy shaking for 15 min. After a washing step with PBS for 5 min, the membrane was blocked again for minimum 15 min and the elution procedure was repeated 3 times more. The eluted antibodies were transferred to a Centrisart tube (Sartorius AG, Göttingen) and concentrated by centrifugation at 2500x g. The supernatant contained in the inner tube was removed and the outer tube was refilled with PBS and centrifuged again. These steps were repeated until the KSCN was completely removed from the antibody solution (3-4 times). The monospecific antibody solution was stored at 4°C.

Elution buffer:	3 M	KSCN
	0.1% (w/v)	BSA in 1x PBS

2.2.15 Histological techniques

2.2.15.1 Pre-treatment of glass slides

Glass slides were coated so that the paraffin sections have a better adhesion on them. The slides were sterilized boiling with a solution of HCl 0.1N and the resulting sterile slides were incubated in 1x Denhardt´s solution overnight. Later, they were fixed with ethanol/acetic acid (3:1) for 20 min. Then, rehydration of the slides was performed in decreasing series of ethanol (96%, 70%, 50%, 30%), each for 5 min. The slides were then incubated overnight in a 1% organosilan solution at 70°C, and they were washed several times with dH_2O. Next, they were fixed at 100°C for several hrs. In this condition, the slides can be stored until 6 months at 4°C. Finally, the slides were activated in buffered glutaraldehyde for 30 min for a better adhesive power. After the glutaraldehyde was rinsed for 5 min in dH_2O, the activation was stabilized in a 0.1 M Sodium-m-periodate solution for 15 min. After this, the slides were rinsed 3x for 5 min in 1x PBS and dried at 42°C. The activated slides can be used in 8 weeks and should be stored at 4°C.

Organosilan	1% (v/v)	γ-aminopropyltrithoxysilane pH 3.45
Buffered Glutaraldehyde	10% (v/v)	Glutaraldehyde in 1x PBS, pH 7.0

2.2.15.2 Preparation of paraffin sections

Bouin's solution	15 ml Picric acid
	5 ml 37% Formaldehyde
	1 ml Acetic acid

The tissue was fixed in Bouin's fixative for 12-16 hrs at room temperature and was dehydrated for 1 hr each in an increasing series of ethanol (50%, 70%, 90%, and 96%). For the paraffin embedding, removal of alcohol from the tissue was performed by incubation in methyl benzoate for 30 min. Washing twice for 10 min with Roticlear (Roth, Karlsruhe, Germany), the methyl benzoate was also removed. The embedding was done with a paraffin mixture with the commercial name of Paraplast^{TM}, which contains DMSO for a better infiltration into the tissue. The jars used in the procedure were temperated at 60° C. The Paraplast^{TM} was melt at 60°C in an oven for 1 hr. The Roticlear was replaced with a 1:1 mix of Roticlear and Paraplast^{TM}, and the tissue was incubated at 60°C in this medium twice for 30 min. Then, the tissue was incubated 2x 30 min in Paraplast^{TM} alone. The tissue was transferred to the embedding mould, which was filled with liquid Paraplast^{TM} and placed at room temperature to solidify. The paraffin block was clamped onto the microtome (Leica Microsystems, AG Wetzlar) for section cutting of 2-10 µm thickness. The sections were laid on pre-treated slides with the help of a 70% ethanol drop at 42°C and laid at this temperature until the liquid evaporates. The paraffin sections were then stored at 4°C.
The tissue sections were incubated twice for 10 min in Roticlear to remove paraffin. Then, the sections were re-hydrated in a descending ethanol series (100%, 96%, 70%, 50%, and 30%) for 2 min each, finally washed in PBS or dH_2O.

2.2.15.3 Staining of histological sections (Hematoxylin-Eosin staining)

The slides containing the paraffin sections were stained by treating with H_2O for 1 min and then 15 min in Hematoxylin followed by placing under the running tap water (control) for 10 min, then 1 min in dH_2O. The slides were covered with Eosin 0.1% + 2 drops acetic acid for 5 min, then washed in dH_2O for 1 min. Incubations were carried out in 50%, 70%, 80%, 90%, 96% and 100% ethanol for 2 min in each. Slides were then incubated two times in histoclear (Xylol) for 3 min.

2.2.15.4 Immunostaining of mouse testis and trachea sections

Sections were incubated in PBT (2 x 10 min) and blocked for 1 hr in PBS containing 2% goat-normal-serum, 3% BSA and 1x roti-block-solution (Roth, Karlsruhe, Germany). Thereafter, they were covered with 20 µl purified anti-Tcte3/anti-Dnali1 antibody-solution and incubated over night in a humidified chamber at 4°C. For detection of bound antibodies, slides were incubated with a 1:100 dilution of alkaline phosphatase conjugated goat anti-rabbit IgG (Sigma-Alderich Chemie, Deisenhofen, Germany) and were visualized with 0.35 mg/ml NBT (nitroblue tetrazolium salt) and 0.18 mg/ml BCIP (5-bromo-4-chloro-indolylphosphate) substrate.

The trachea was isolated from adult mice and additional material was removed. Then single tracheal rings were cutted with a micro-sissor. A single tracheal ring was placed onto a slide and dissociated using two forceps. Thereafter, tissue was fixed in 4% paraformaldhyde and washed two times in PBS buffer. Then the slides were incubated in PBT (2 x 10 min). After a blocking step for 1 hr in PBS containing 5% goat-normal-serum, 3% BSA and 1x roti-block-solution (Roth, Karlsruhe, Germany), cells were covered with 20 µl purified anti-Dnali1 antibody solution and incubated over night in a humidified chamber at 4°C. Additionally, monoclonal anti-α-tubulin antibody was added in a final dilution of 1:50. After 4 washes with PBT, slides were incubated with secondary antibodies (goat-anti-rabbit-Cy3 and goat-anti-mouse-FITC) in a final concentration of 1:50 in PBS for 1 hr at room temperature. Finally, slides were washed again in PBT four times, covered with a drop of vector shield solution containing DAPI stain and examined using a BX60 microscope (Olympus, Hamburg, Germany) with fluorescence equipment and "Analysis" software program (Soft Imaging System, Muenster, Germany).

2.2.15.5 Immunofluorescence staining of mouse blastocysts and morula (Moreno 2002)

Mouse blastocysts and morula stage embryos were collected by flushing the oviducts of female mice at 3.5 dpc and 2.5 dpc respectively and were fixed in 2% formaldehyde, PBS for 10 min at room temperature, followed by a 1-2 hrs incubation at 4°C. The samples were then permeabilized with cold methanol for 15 sec, washed in PBS twice and non-specific reactions were blocked by further incubation in PBS containing 2 mg/ml BSA and 100 mM glycine. An appropriate primary antibody was solubilized in this blocking solution and incubated with the

slides for 1–2 hrs. After extensive washing in PBS containing 0.1% Triton X-100, the samples were sequentially labelled with indocarbocyanine (Cy3) or fluorescence isothiocyanate (FITC)-conjugated secondary antibodies. After samples were washed 4 times with PBS containing 0.1% Triton X-100, the nuclei were counterstained with DAPI. Immunostaining of the sections was examined using a fluorescence-equipped microscope (BX60; Olympus).

2.2.15.6 Immunofluorescence staining of mouse ES, 3T3 and NS20Y cells

The cells were grown over night on the cover slips, in DMEM medium (2.1.5.3.) and fixed in ice cold methanol : aceton (ratio 1:1) solution for 10 min at RT. Samples were rinsed in PBS and an initial blocking step was performed with the blocking solution (PBS containing 5% goat serum, 3% BSA and 1x roti block solution) for 1 hr. An appropriate primary antibody solution (in PBS) was applied for overnight in a humidified chamber at 4°C. After four washes with PBS/0.2% Tween-20, the cover slips were incubated with FITC- or Cy3-conjugated goat anti-rabbit or goat anti-mouse IgG for 1 hr at room temperature. One drop of mounting medium with DAPI was dispensed onto the slides after washing with PBS/0.2% Tween-20. Fluorescent cells were visualised with Olympus BX60 microscope.

2.2.16 Generation of a Green Fluorescent Fusion Protein (GFP)

The green fluorescent protein (GFP) is a very useful tool to perform sub-cellular localization of proteins and to observe their expression, due to the green fluorescent light that emits at 507 nm after being excited at 488 nm. A fusion protein with the enhanced green fluorescent protein (EGFP) was produced by cloning in frame the entire or truncated coding regions of the protein of interest in carboxy-terminal position with respect to the EGFP sequence. The pEGFP-C1 vector (Clontech, Heidelberg) carries a strong promoter (pCMV) and the SV40 polyadenylation site, which directs the proper processing of the 3´end of the EGFP mRNA. The sequence of interest was cloned in the multiple cloning site using the restriction sites of *Sal*I and *Apa*I. This ligation reaction (2.2.4.2) was transformed in DH5α competent cells (2.2.6) and a positive clone was selected for further analysis. After verifying the correct reading frame and sequence (2.2.8), the DNA was used for transfection.

2.2.17 Transfection

The transfection involves the introduction of foreign DNA into mammalian cells for its expression. There are different types of procedures to perform a transfection. The reagent used in this study was "Lipofectamine 2000 TM" (Invitrogen, Karlsruhe, Germany).
For transfection, approximately, 80,000-100,000 of 3T3 NIH Swiss albino mouse fibroblast cells were plated in flaskettes (Lab-Tek/Nalge Nunc, IL, USA) with DMEM (2.1.5.3.), and incubated overnight at 37°C with 5% CO_2. 10 µl of Lipofectamine 2000 TM reagent and 3 µg of the DNA of interest were diluted each in a total volume of 100 µl, respectively, with optiMEM I reduced serum medium (invitrogen, Karlsruhe, Germany), incubated at room temperature for 5 min and subsequently mixed together in a reaction tube, which was then incubated at room temperature for 20 min. The DMEM containing cells were washed with PBS and the medium was replaced with 1 ml of OptiMEM I medium without antibiotics/FKS. The reaction mixture was added in the flask drop-by-drop and incubated for 3-3.5 hrs at 37°C followed by the replacement of old medium with DMEM medium containing FKS/antibiotics. The cells were then incubated at 37°C for 24-48 h.

2.2.18 Co-immunoprecipitation

Immunoprecipitation is a technique that permits the purification of specific proteins for which an antibody has been raised. This primary antibody is either already bound to dynabeads or can be bound to the protein/dynabeads during the procedure in order to physically separate the antibody-antigen complex from the remaining sample. Total cell extract or nuclear extract is used to analyze putative protein-protein interactions in eukaryotic cells. Mouse neuroblastoma cells (NS20Y) were transfected with the appropriate expression vectors (protein A and protein B), using Lipofectamin 2000 transfection reagent (2.2.17). Cells were grown for 48 hrs at 37°C, then collected and homogenized in 200 µl buffer containing 50 mM Tris/HCl pH 7.5, 150 mM NaCl, 2.5 mM EDTA, 1% NP-40, 0.5 mM PMSF and 0.5% protease inhibitor cocktail. The homogenized mixture was then incubated on ice for 10 min. Cell extracts were spinned down at 14000xg for 10 min at 4°C, and the lysates were transferred into new cups. Cross-linking of IgG molecules to protein-A coupled immuno-magnetic beads was achieved by incubating in 1 ml solution containing 0.2 M triethanolamine (pH 8.0) and 5.4 mg of dimethyl pimelimidate dihydrochloride for 30 min with constant agitation at 20°C. The reaction was stopped by incubation with 1 ml 50 mM Tris/HCl (pH 7.5) at 20°C for 15 min.

Thereafter, beads were washed four times with 0.1% Na-phosphate buffer (pH 8.1) and collected using a magnet for 2 min. Magnetic beads coupled either with specific antibodies were incubated with 400 µl of the cell lysate overnight at 4°C. Then the beads were collected using the magnet and washed three times with phosphate buffer (pH 8.1). For SDS-PAGE analysis, collected beads were boiled in 50 µl of SDS sample buffer for 5 min and proteins were separated on a 12% acrylamide gel. Finally, precipitated proteins were detected by a Western blot analysis.

2.2.19 Techniques for Recovery and Culture of Preimplantation Embryos

2.2.19.1 Superovulation

Seven to eight week old female mice were superovulated by intraperitoneal injections of 5 IU of pregnant mare's serum gonadotropin (PMSG, Sigma St Louis, MO, USA) followed 44-48 hrs later by 5 IU of human chorionic gonadotrophin (HCG, Sigma). After the second injection, female mice were housed overnight with males and were checked for a vaginal plug the following morning. The E0.5 was considered to be 12:00 noon at the day of vaginal plug.

2.2.19.2 Recovery of 3.5 days old embryos

3.5 days old embryos (blastocyst stage) can be flushed out from the uterus. Plugged female mice (3.5 days pc) were killed by cervical dislocation. The skin and peritoneum were opened with the large transverse incision to expose the abdominal cavity. The upper part of the uterus was dissected and placed into a drop of M2 medium (2.1.1). Under the dissection microscope, the needle attached to a 1 ml syringe was inserted in the lower end of the uterine tissue. Embryos were flushed with 0.05 ml of M2 medium. Embryos were collected with a pipette and washed through several M2 drops. To remove the zona pellucida, embryos were treated in one drop of Tyrode's acid solution and transferred into the drop of M2-medium as soon as their zona pellucida was dissolved. The collected embryos were washed five times in a drop of PBS and each single embryo was transferred into a PCR cup (0.2 ml) containing 5 µl dH_2O. Those samples were used for genotyping.

2.2.19.3 Culture of blastocysts

The 2 cell stage embryos were cultured in the M16 medium (2.1.1) until they developed to the blastocyst stage. Clearly formed blastocysts were washed five times in drops of ES cell medium and placed individually in gelatinized 96-well plate containing 20 µl of ES cell medium. The plate was incubated at 37^0C, 5% CO_2 for 3-5 days. ES cell medium was changed every second day of the culture.

2.2.20 Determination of sperm parameters

2.2.20.1 Sperm count in epididymes, uterus and oviduct.

Epididymes of mice were dissected under aseptic condition and put in 0.5 ml of IVF medium (2.1.1). Spermatozoa were allowed to swim out of the epididymes for 1 hr at 37°C, 5 % CO_2. Sperm suspension was diluted 40 times with PBS before counting. 5 µl of this suspension was put into a Neubauer counting chamber and sperms were counted in 8 independent fields (each having an area of 0.0025 mm^2) under the microscope (Olympus BX60) with 20X magnification. Total sperms were calculated by following formula,

Total no. of Sperms = average of sperms x 10 x 40 x 500

For determination of sperm number in the uterus and the oviduct, female wild type mice were mated with *Tcte3*$^{-/-}$ males. Uteri and oviducts of those mice, which were positive for vaginal plug, were dissected in IVF medium and the sperm were flushed out.

2.2.20.2 Sperm motility analysis

10 µl of sperm suspension was put on a dual sided sperm analysis chamber. Sperm motility was quantified using the computer assisted semen analysis (CASA) system (CEROS version 10, Hamilton Thorne Research). Then, 6,000-10,000 spermatozoa from 4 mice of mutant line and wildtype were analysed using the following parameters: straightness (STR), path velocity (VAP), straight line velocity (VSL). For statistical analysis, frequencies of the six sperm motility parameters VAP, VSL, VCL, ALH, BCF and STR were examined by probability

plots categorised by mouse type (wildtype/mutant) and by time of observation (1.5, 3.5 and 5.5 hrs after preparation).

2.2.20.3 Morphological examination

Male mice of 2 months old were killed in accordance with the Animal Welfare Act and international guidelines. Testes were immediately excised and sliced in half. The halves were fixed either Bouins solution or 5% glutaraldehyde in collidine buffer (0.05 M, pH 7.4). Tissues fixed in Bouin solution were processed and embedded in paraffin. The morphology analysis of *Tcte3* mice testis was performed by staining the thin sections (~5 μm) with toluidine blue (1% in 01% borax) and examined under the microscope (Olympus BX60). For electron microscopy, sections of testis and epididymis fixed in glutaraldehyde were examined and photographed with a transmission electron microscope.

2.2.20.4 Apoptotic assay

The slides containing the thin sections of testis were processed for a TUNEL assay to assess the possible number of cells undergoing apoptosis by an ApopTag *in situ* detection kit (Chemicon International, Inc.,Temecula, CA). The slides were pretreated with H_2O_2 and incubated with the reaction mixture containing TdT and digoxigenin-conjugated dUTP for 1 hr at 37°C. Labeled DNA was visualized with peroxidase-conjugated anti-digoxigenin antibody with 3,3'-diaminobenzidene as the chromagen. The percentage of cell death was determined by counting the cells exhibiting brown nuclei (TUNEL-positive) and comparing with wildtype littermate.

2.2.21 Techniques for production of targeted mutant mice

(Joyner, 2000)

The discovery that cloned DNA introduced into cultured mouse embryonic stem cells can undergo homologous recombination at specific loci has revolutionized our ability to study gene function in vitro and in vivo. In theory, this technique will allow us to generate any type of mutation in any cloned gene. Over twenty years ago, pluripotent mouse embryonic stem cells (ES) derived from inner cell mass cells of mouse blastocysts were isolated and cultured (Martin, 1981; Evans and Kaufman, 1981). Using stringent culture conditions, these cells can maintain their pluripotent developmental potential even after many passages and following

genetic manipulations. Genetic alterations introduced into ES cells in this way can be transmitted into the germline by producing mouse chimeras. Therefore, applying gene targeting technology to ES cells in culture gives the opportunity to alter and modify endogenous genes and study their functions *in vivo*.

2.2.21.1 Production of targeted embryonic stem cell clones

2.2.21.1.1 Preparation of MEFs feeder layers

A frozen vial of MEFs (mouse embryo fibroblasts) was quickly thawed at 37°C and transferred to 10 ml EMFI medium. After centrifugation at 270xg for 5 min, the cell pellet was gently resuspended in 10 ml MEFs medium and plated on a 50mm culture flask. Cells were incubated at 37°C in 5% CO_2. When the cells formed a confluent monolayer (three days), they were trypsinized, transferred to five 150 mm dishes and grown until they formed confluent monolayer, or directly treated with mitomycin C. To treat the MEFs with mitomycin C, the medium was removed and 10 ml fresh medium containing 100 µl mitomycin C (1mg/ml) was added. After 2-3 hrs of incubation, the monolayer of cells was washed twice with 10 ml PBS. The cells were then resuspended with 10 ml medium and gentle pipetting dissolved any cell aggregates. The cells were centrifuged, resuspended in MEFs medium and plated onto dishes, which were treated with 0.1% gelatine for 30 min. The feeder cells were allowed to attach by incubation overnight at 37°C, 5% CO_2 or used after 2 hrs of incubation. Before adding ES cells on the feeder layer, the medium was changed to ES cell medium.

2.2.21.1.2 Growth of ES cells on feeder layer

One vial of frozen ES cells was quickly thawed at 37°C and cells were transferred to a 12 ml tube containing 6 ml ES cell medium. After centrifugation, the cell pellet was resuspended in 5 ml ES cell medium and plated on 60 mm dishes containing MEFs at 37°C, 5% CO_2. Next day the medium was changed. The second day, cells were washed with PBS, treated with 2 ml trypsin/EDTA at 37°C, 5% CO_2 for 5 min. The cells were gently pipetted up and down to dissolve cell clumps, resuspended with 5 ml ES medium and centrifuged. The cell pellet was resuspended in 10 ml ES cell medium and distributed either to 5 or 6 dishes (60 mm),

containing feeder layers or to 2 dishes (100 mm) containing feeder layers. The cells were passaged every second day as described above.

2.2.21.1.3 Electroporation of ES cells

ES cells, which have grown for two days on 100 mm dishes, were trypsinized. The cell pellet was resuspended in 20 ml PBS and centrifuged .The cell pellet was then resuspended in 1 ml PBS. 0.8 ml of cell suspension was mixed with 40 µg of linearized DNA-construct and transferred into an electroporation cuvette. The electroporation was performed at 240 V, 500 µF with the BIO RAD gene pulser™. After electroporation, the cuvette was placed on ice for 20 min. The cell suspension was transferred from cuvette into 20 ml of ES cell medium and plated onto two 100 mm dishes containing feeder layers. The medium was changed every next day. Two days after the electroporation, the drugs for the selection were added (active G418 at 400µg/ml and gancyclovir at 2 µM). The medium was changed every day. After about eight days of selection, drug resistant colonies have appeared and were ready for screening by Southern blot analysis.

2.2.21.1.4 Growing ES cells for Southern blot analysis

The drug resistant colonies that were formed after about eight days of selection were picked with a drawn-out Pasteur pipette under a dissecting microscope. Each colony was transferred into a 24 well plate containing feeders and ES cell medium. After 2 days, the ES cells were trypsinized with 100 µl trypsin for 5 min and resuspended in 500 µl ES cell medium. Half of the cell suspension in each well was transferred to a well on two different 24 well plates, one gelatinised plate, and the other containing feeder cells (master plate). The gelatinised plate was used for preparing DNA and the master plate was kept frozen.

2.2.21.2 Production of chimeras by injection of ES cells into blastocyst

The ability of mammalian embryos to incorporate foreign cells and develop as chimeras has been exploited for a variety of purposes including the perpetuation of mutations produced in embryonic stem (ES) cells by gene targeting, and the subsequent analysis of these mutations. The standard procedure is to inject 10-20 ES cells, which are recombinant for targeted locus, into the blastocoel cavity of recently cavitated blastocysts that have been recovered by

flushing the uteri of day 4 pregnant mice (C57BL/6J). After injection, embryos are cultured for a short period (2-3 hrs) to allow re-expansion of the blastocoel cavity and then transferred to the uterine horns of day 3 CD1 pseudopregnant mice. Pseudopregnant females are obtained by mating 6-8 weeks old oestrous females with vasectomized males.

2.2.21.3 Detection of chimerism and mice breeding

The most convenient and readily apparent genetic marker of chimerism is coat colour. Chimeric males (and sometimes females) are bred to wild-type mice to ascertain contribution of the ES cells to germline. Once a germline chimera has been identified, the first priority will be to obtain and maintain the targeted allele in living animals. The chimeras were bred with C57BL/6J and with 129/Sv mice to compare the phenotype in two different genetic backgrounds.

2.2.22 Mutation analysis by DHPLC (WAVE)

A total of 25 infertile patients due to asthenozoospermia were investigated by DHPLC. The seven exons of *DNALI1* gene were amplified by using the following primers,

hp-exon1-F:	**5’ CTA AGA AGT CAG GCA CAA GAG GTT T 3’**
hp-exon1-R:	**5’ CTC TGA CTT CCC AAT TCC CTT TAC T 3’**
hp-exon2-F:	**5’ GTG ACA TAA TTT CTG CTG AGA AGA CC 3’**
hp-exon2-R:	**5’ CCA TAT GTA AGT TCT AGG AGC TCT GTG 3’**
hp-exon3-F:	**5’ GTG CTA GGG ACC TTC AAG TCA AA 3’**
hp-exon3-R:	**5’ CTT GGA TCT GTG CTG AAG GTG A 3’**
hp-exon4-F:	**5’ AGG AAG GGT GTT TGC AGT AGA CAT AC 3’**
hp-exon4-R:	**5’ GTC AGA ATG TAG TGC TGG AAT GAT AAG 3’**
hp-exon5&6-F:	**5’ AGT ATA TAC CCT GGC AAT GTC ATG T 3’**
hp-exon5&6-R:	**5’ AAA CAT TTA AAA GCC ATG GAA AAG G 3’**
hp-exon7-F:	**5’ ATT TGA TCA CCT CTC AGC TAT TTG TAT 3’**
hp-exon7-R:	**5’ TAG GTG TCT GAT GAC ATT GGA GTA ATA 3’**

PCR schedule was following:

Steps	Hold		30 Cycles		Hold	
	Time	Temperature	Time	Temperature	Time	Temperature
	5 min	95°C				
Denaturation			30 sec	95°C		
Annealing			30 sec	63°C		
Elongation			1 min	72°C	10 min	72°C

Heteroduplex formation is necessary for detection of heterozygous mutations, while there is no requirement in case of homozygous mutations. The conditions for making heteroduplexes were:

95°C for 5 min
95°C for 22 sec 1 cycle
94°C for 22 sec 1 cycle
T-1°C for 22 sec up to 69 cycles
(T is the temperature of previous cycle)

The samples can be stored at -20°C at this step.

WAVE program for *DNALI1* amplicons:

Exon	Length (bp)	Elution temperature	Time shift
1	140	65°C	0
2	143	64°C 63°C	0 -0.3
3	170	63.8°C 64.3°C	-0.3 -0.3
4	176	65.4°C	0
5	43	62.9°C	-0.3
6	122	62.6°C 64°C	-0.3 -0.3
7	127	58.8°C	-0.3

2.2.23 Computer analysis

For the analysis of the nucleotide sequences, BLAST, BLAST2, MEGABLAST and other programs from National Center for Biotechnology Information (NCBI) were used (www.ncbi.nlm.nih.gov). Information about mouse alleles, phenotypes and strains were used from Jackson Laboratory (www.informatics.jax.org). For proteins studies ExPASy tools (www.expasy.ch) were used. Mouse genome sequence and other analysis of mouse genes, transcript and putative proteins were downloaded from Celera discovery system (www.celera.com).

3. RESULTS

3.1 Isolation and characterization of the *Dnali1* cDNA

In order to identify genes that are involved in the generation of flagellar and ciliary motility, an RT-PCR experiment was performed to generate a probe of the human *DNALI1* (*hp28*) cDNA. The resulting cDNA fragment was used to identify several clones from a murine testicular cDNA library. Sequence analysis of two of these clones (A and B) revealed similarity to the human *DNALI1* cDNA, however, differ in their size. The smaller cDNA clone B contains an insert of 891 bp with a putative start codon at position 55 and a termination codon at position 829 bp. The 3' UTR has a length of 74 bp and a putative polyadenylation signal was identified 23 bp upstream of the poly-A tail. The respective cDNA encodes a putative protein of 258 amino acids with a calculated molecular weight of 29680 daltons and a predicted pI of 8.21 (Figure 3.1).

Sequence analysis of the larger cDNA clone A showed complete similarity to the clone B, but has a 1174 bp additional sequence in the 3' untranslated end, containing a ploydenylation signal at position 2061 bp. Comparison with different databases identified several cDNA and genomic clones with high similarity (accession numbers: **NM077109**, **AK077109** and **AL626775**).

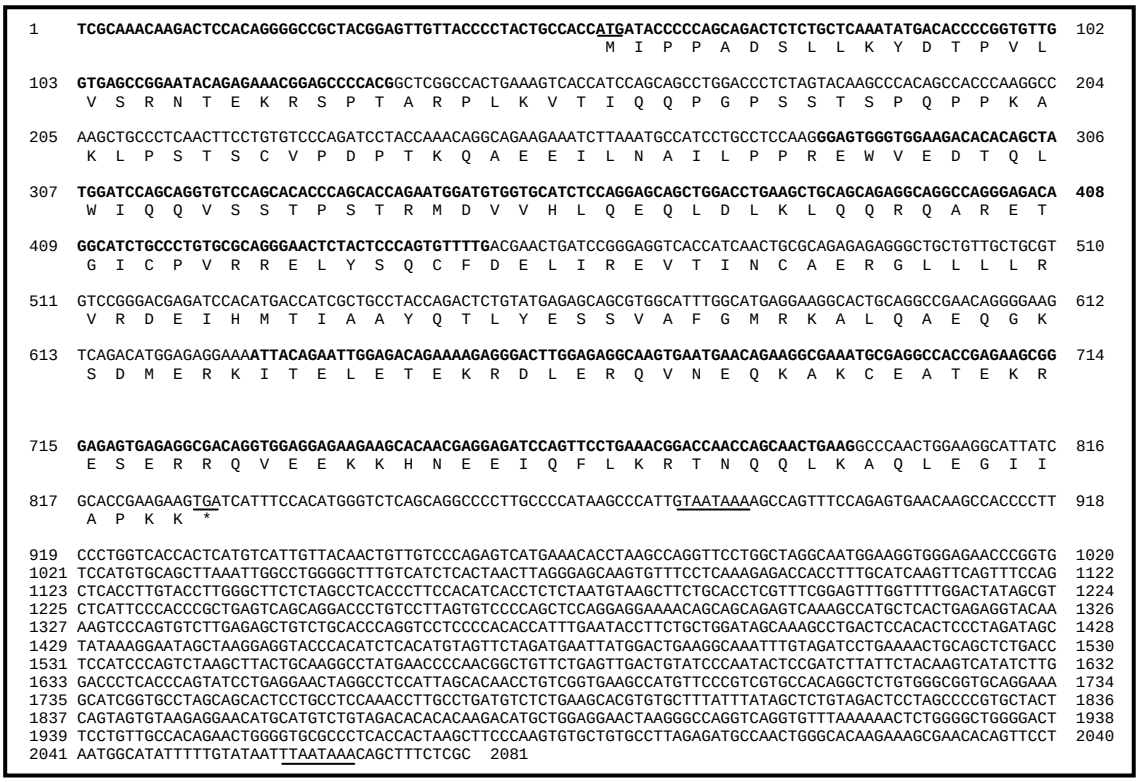

Figure 3.1. Nucleotide sequence and deduced amino acid sequence of the *Dnali1* cDNA. Numbering of nucleotides is assigned to both sides of the sequence; translation stop codon is indicated by an asterisk. Polyadenylation signals are underlined.

3.1.1 Genomic organization of *Dnali1* gene

Dnali1 gene comprises 6 exons of varying sizes (123 bp – 1299 bp), separated by introns of different length. The cDNA contains an open reading frame of 258 amino acids (Figure 3.1). In the *Dnali1* 3'-UTR, two polyadenylation signals were identified, resulting in two transcripts of approximately 0.9 kb and 2.3 kb (Figure 3.1).

Genomic structure of the human orthologue gene *DNALI1* is almost identical to that of the mouse; the first four exons of both *Dnali1* and *DNALI1* are of identical sizes, while the exon 5 and exon 6 of *DNALI1* are joined in the mouse genome (Figure 3.2B).

A

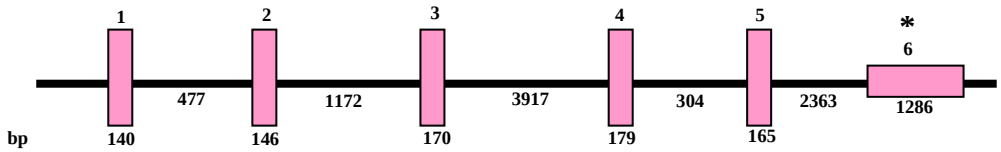

B

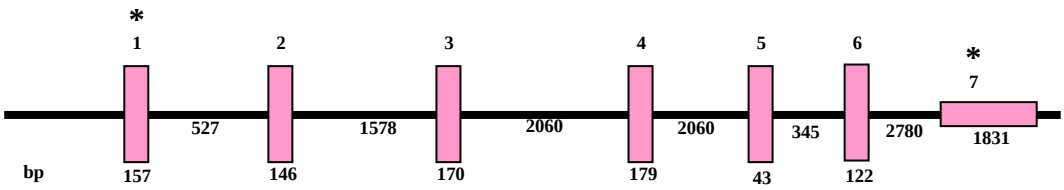

Figure 3.2. Schematic representation of the exon-intron structure of the murine *Dnali1* gene (A) and the human orthologue *DNALI1* (B). Positions of the translational start and stop sites are marked by asterisks. Numbers on the top of the pictures indicate exons, numbers on the bottom indicate length of the exons and introns.

The *Dnali1* gene is localized to the region D of the chromosome 4, which is syntenic to chromosome 1 p35.1 where the human *DNALI1* (GenBank accession no. AF006386, Kastury et al., 1997) gene was mapped.

3.1.2 Expression analysis of *Dnali1* gene

To analyse the expression pattern of the *Dnali1* gene at the RNA level, total RNA was isolated from multiple adult mouse tissues (2.2.1.5), including oviduct, epididymis, liver, heart, brain, placenta, colon, kidney, trachea, lung, spleen, pancreas, testis and ovary. By RT-PCR analysis, a *Dnali1* fragment could be amplified from samples of testis, ovary, brain, lung, trachea, kidney, colon, placenta, liver, epididymis and oviduct RNA (Figure 3.3), while *Dnali1* is not found to be expressed in heart, spleen and pancreas. Integrity of the RNA used for RT-PCR was proven by amplification of a fragment of the *Gapdh* cDNA. The specificity of the PCR products were verified by hybridisation using the murine *Dnali1* cDNA as a probe (Figure 3.3).

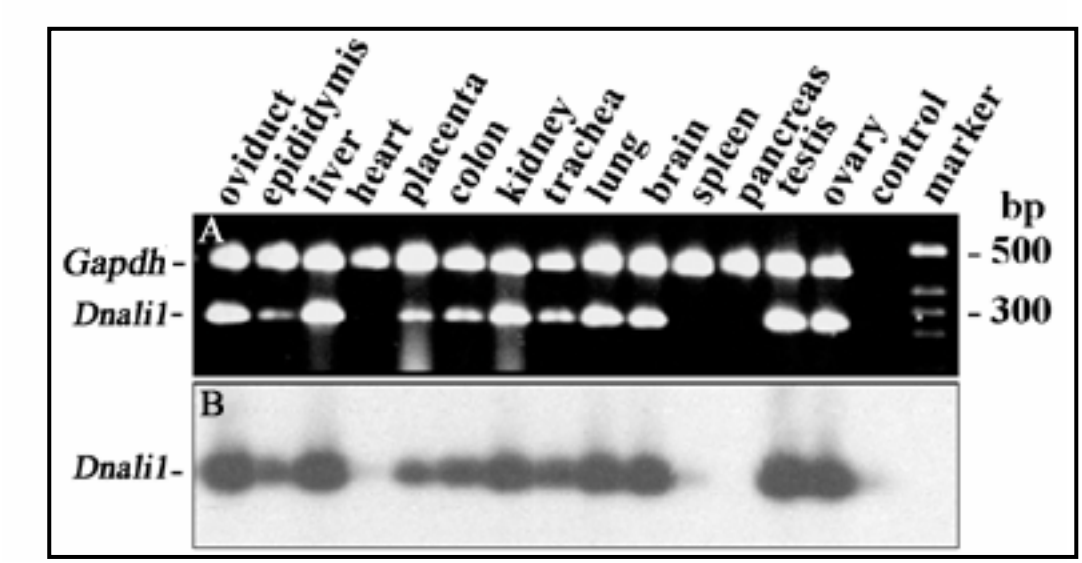

Figure 3.3. Expression analysis of *Dnali1* in different adult mouse tissues using an RT-PCR approach (A) *Dnali1* transcripts were observed in oviduct, epididymis, liver, placenta, colon, kidney, trachea, lung, brain, testis and ovary. The quality of the RNA probes was proven by amplification of a 458 bp fragment of the murine glyceraldehyde-3-phosphate dehydrogenase transcript (*Gapdh*). (B) Amplification of specific *Dnali1* transcripts was proven by hybridisation with *Dnali1* cDNA probe.

To determine the expression of *Dnali1* at the Northern blot level, total RNA from brain, testis, liver, intestine, ovary, lung, heart, colon and kidney was size fractioned in an 1% agarose gel containing formaldehyde and transferred to nitrocellulose membrane. Equivalent loading and integrity of RNA was checked by hybridization with *β-actin* probe. The Northern blot was hybridised with a ^{32}P-labelled *Dnali1* cDNA probe, which detected two transcript variants of approximately 0.9 kb and 2.3 kb in RNA from adult testis. No signal was visible in other adult tissues tested (Figure 3.4).

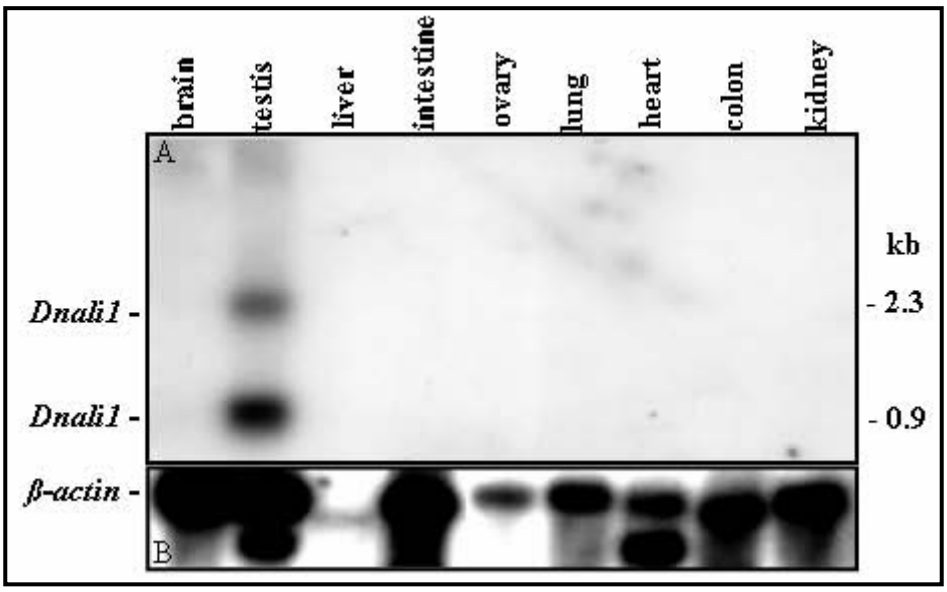

Figure 3.4. Northern blot analysis of *Dnali1* gene expression in different adult mouse tissues. Total RNA (20 µg) was extracted from various tissues including brain, heart, liver, intestine, ovary, lung, heart, colon and kidney of the adult mouse and subjected to Northern blot hybridization using the *Dnali1* cDNA as a probe (A). The integrity of the RNA was checked by hybridization with *β-actin* probe (B).

Northern blot analyses of *Dnali1* using testicular RNA of different developmental stages revealed that the expression of *Dnali1* started at day 15 during the development of testis and both smaller and larger transcripts exhibited initiation of expression at the same time (Breckle, 2000). The expression of *Dnali1* in mouse mutant lines for different spermatogenesis defects at different stages was checked by Northern blot analyses and demonstrated that the expression of *Dnali1* is restricted to germ cells (Breckle, 2000). Moreover, RT-PCR experiment was performed by using the total RNA isolated from ES cells, blastocysts and different embryonic stages (8.5 – 16.5 dpc), which resulted in the amplification of *Dnali1* transcript at all stages, indicating that *Dnali1* expression is initiated very early during the embryogenesis (Breckle, 2000**).**

3.1.3 Localization and expression analyses of the Dnali1 at protein level

In order to analyse the *Dnali1* gene product and to study the intracellular localization of Dnali1 protein, Dnali1-specific antibodies were generated (Hupe, 2003). These antibodies detected an approximately 30 kDa protein in testicular extracts, corresponding to the predicted

size for the Dnali1 protein. By using these antibodies, the Dnali1 localization was demonstrated along the entire axoneme of spermatozoa (Hupe, 2003).

3.1.3.1 Tracheal epithelial cilia staining

In order to find out whether Dnali1 could be detected in cilia of tracheal epithelial lining, the trachea of an adult mouse was isolated and cutted with a micro-scissor (Figure 3.5G-I). Tracheal rings were then stained with Dnali1 specific antibodies to localize the protein. Dnali1 signals were detected in the cytoplasm of epithelial cells, which exhibit cilia. Moreover, immunostaining together with tubulin staining indicates that Dnali1 is localized along the whole length of tracheal cilia (Figure 3.5A-F).

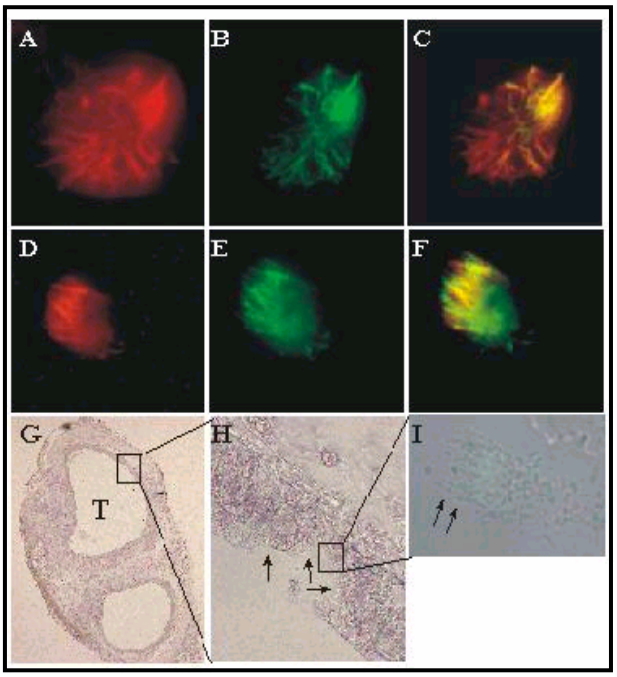

Figure 3.5. Immunohistochemical localization of Dnali1 in mouse trachea. (A-F) Cilia of the inner lining of mouse tracheal epithelium were probed with anti-Dnali1 (red) and with anti-α-tubulin (green) antibodies. The apparent staining of Dnali1 was observed along the axoneme of cilia (C and F). Figures G and I show light micrographs of mouse tracheal cells in 10X and 60X magnifications, respectively.

3.1.3.2 Brain lateral ventricles cilia staining

To gain insight into the different functions attributed to Dnali1 and in view of its relative abundance in mouse brain, its distribution was examined in the newborn (P0.5) mouse brain by immunohistochemical staining. Dnali1 was observed in the ependymal layer lining the lateral ventricles (Figure 3.6 A, B).

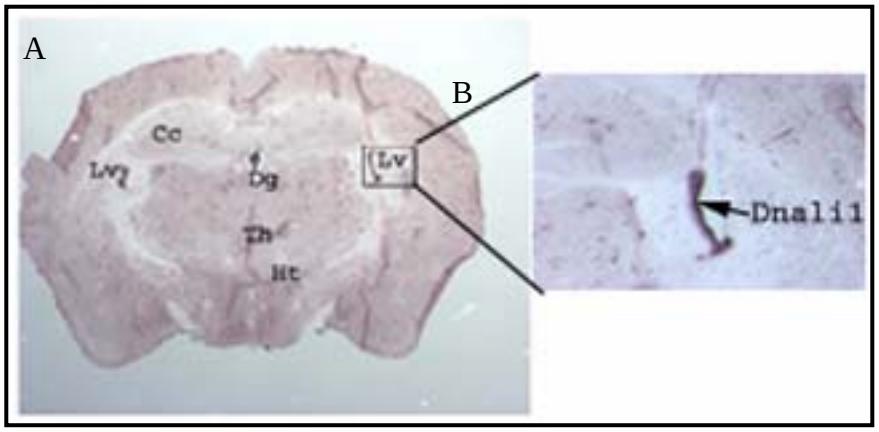

Figure 3.6. Expression of Dnali1 in brain ciliated ependymal cells lining the lateral ventricle by immunohistochemistry; transverse section of newborn mouse brain was treated with Dnali1 specific antibodies and counterstained with Alkaline Phospatase conjugated secondary antibodies (A), arrow indicates the specific staining of Dnali1 in the cilia of lateral ventricle (B). LV, Lateral ventricles; dg, Dentate gyrus; Ht, Hypothalamus; Th, Thalamus; Cc, Cerebral cortex.

3.1.4 Targeted Disruption of the *Dnali1* gene

3.1.4.1 Construction of targeting vector for *Dnali1* disruption

In order to generate the targeting vector, a 3.5 kb region of the *Dnali1* gene containing exons 1, 2 and part of exon-3 was deleted and replaced by *neomycin* phosphotransferase gene cassette (*Neo*) under the control of phosphoglycerate kinase promoter. Induction of the negative selection marker, the Herpes simplex virus thymidine kinase (*TK*) gene enabled us to use both positive and negative selection (Mansour et al., 1988).

3.1.4.2 Subcloning of 5’ flanking region of the *Dnali1* gene into the pTKNeo vector

A 3.2 kb *Xba*I fragment containing the 5’-flanking region of the *Dnali1* gene (upstream region of exon-1 (Figure 3.6) was isolated from the cosmid clone (MPMGc121L23271Q2) and purified from the agarose gel. This fragment was subcloned into pBlueScript vector using the *Xba*I site. A fragment of 2.3 kb was cutted through by using the *Xho*I and *Cla*I restriction enzymes and ligated with *Sal*I and *Cla*I digested pTKNeo vector.

3.1.4.3 Subcloning of 3’ flanking region of the gene into pTKNeo vector

A fragment of 7.8 kb containing exons 4, 5 and 6 was isolated from the cosmid using *Bam*HI and *Xba*I restriction enzymes (Figure 3.6) and was subcloned into pBlueScript vector. The fragment was again extracted from pBlueScript vector by *Bam*HI and *Not*I enzymes and cloned into the pTKNeo vector using the same sites. The replacement vector (*DnaliI-Neo-Tk*; pTKNeo vector containing 5’- 2.3 kb arm and 3’- 8 kb arm) was subjected to multiple restriction analyses for verification (Figure 3.7) and was linearized at the unique *Not*I site present in the polylinker site before transfection.

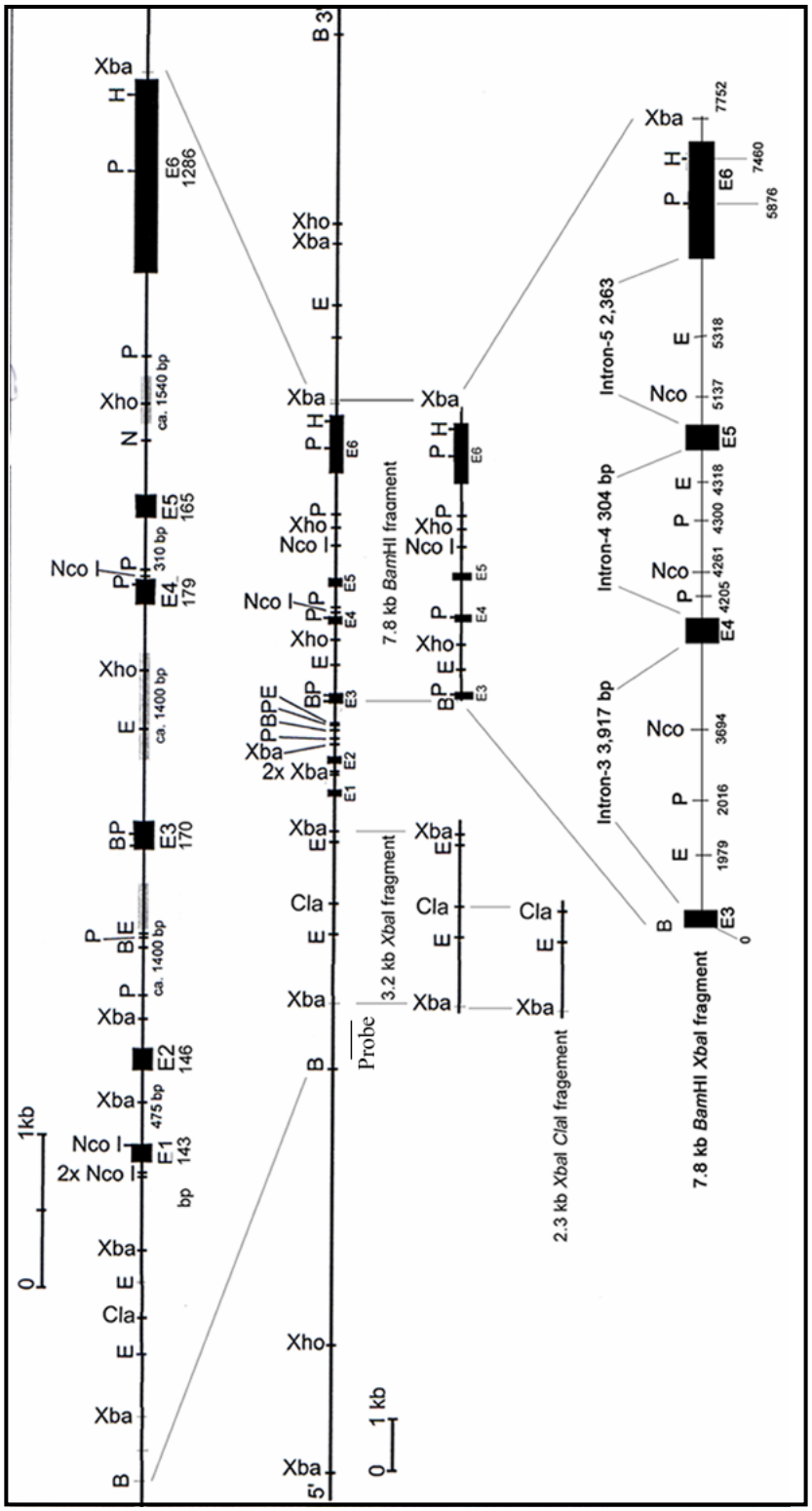

Figure 3.6. Genomic structure of the *Dnali1* gene and generation of the targeting vector. The 2.3 kb fragment was cloned as 5'-arm and 7.8 kb fragment served as 3'-arm for the targeting construct. The probe used for recombinant ES cells screening is indicated. The restriction site abbreviations are: E; *Eco*RI, P; *Pst*I, H; *Hind*III, B, *Bam*HI; N, *Not*I; E, exons; bp, base pairs; kb, kilo base pairs.

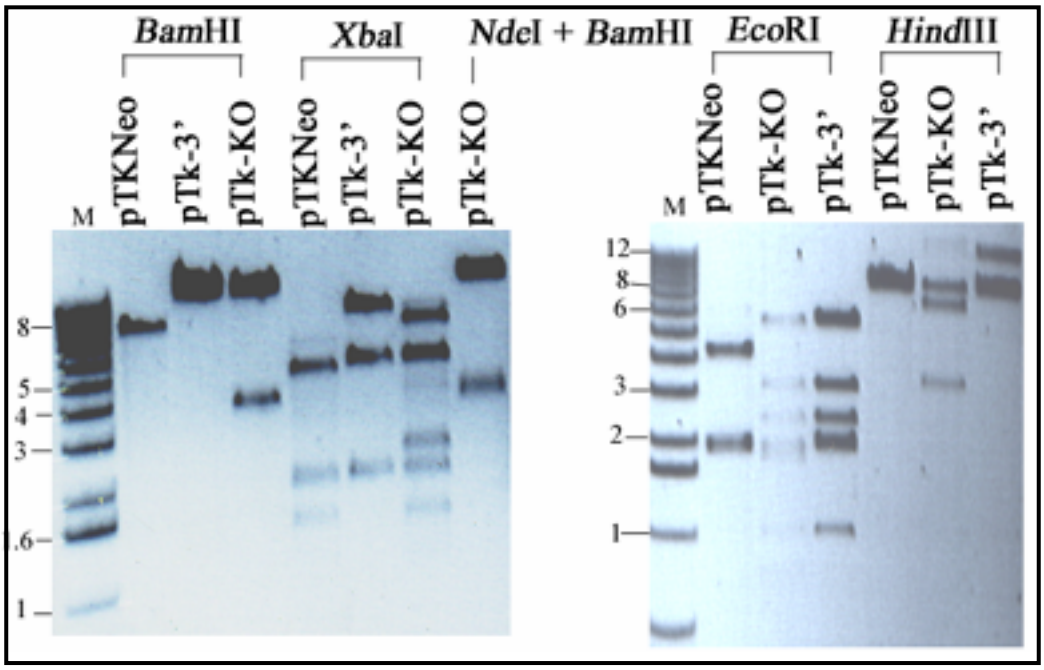

Figure 3.7. Restriction analysis of pTKNeo vector, pTKNeo + 3'-arm and knockout construct DNA's with different restriction enzymes. *Bam*HI, (1; pTKNeo vector, 2; pTKNeo + 3'-arm, 3; knockout construct), *Xba*I, (4; pTKNeo vector, 5; pTKNeo + 3'-arm, 6; knockout construct), *Nde*I + *Bam*HI, (7; knockout construct), *Eco*RI, (8; pTKNeo vector, 9; knockout construct, 10; pTKNeo + 3'-arm) and *Hind*III, (11; pTKNeo vector, 12; knockout construct, 13; pTKNeo + 3'-arm).

3.1.4.4 Subcloning of the 5'-external probe

A 0.5 kb fragment of 5'-region of the *Dnali1* gene was amplified by PCR using the mp-ext1-f; 5'- CCA GAG CAC CAA TGC TAA AGG AAA TAG GAAT - 3' and mp-ext1-r; 5'- CTC ACA AAG GTC GGG ACT TAG GAT CAG - 3' primers. The PCR product was subcloned into the pGEM-T Easy vector and subsequently sequenced. Following the DNA digestion by *Eco*RI enzyme, the 0.5 kb fragment was isolated from agarose gel and was used as probe for screening of recombinant ES-clones.

3.1.4.5 Electroporation of R1 ES-cells

ES cell lines were cultured in the culture medium (2.1.6.2). Confluent plates were washed in PBS buffer, trypsinized and the cells were suspended in the same buffer at 2 x 10^7 cells/ml. Aliquots of this cell suspension were mixed with 50 µg of linearized targeted vector *Dnali1-Neo-Tk* and electroporated at 240V and 500 µF using a Bio-Rad Gene Pulser apparatus. The

cells were plated onto nonselective medium in the presence of G418- resistant embryonic mouse fibroblasts. After 36 hrs, selection was applied using medium containing G418 at 400 µg/ml and gancyclovir at 2 µM. After 10 days of selection, 200 individual drug-resistant clones were picked into 24-well trays for freezing and isolation of DNA.

To screen the recombinant ES-clones for homologous recombination events, genomic DNA was extracted from the recombinant ES-clones (2.2.1.3), restricted with *Bam*HI, electrophoresed and blotted onto nitrocellulose filters. The blots were hybridized with the ^{32}P-labeled 0.5 kb 5'- probe. In case of a homologous recombination event two fragments were detected, the wildtype allele resulted in a hybridization signal of 6.7 kb and the targeted allele was 5.3 kb fragment (Figure 3.8). Of the 150 colonies tested, 3 clones were found showing the expected hybridization pattern.

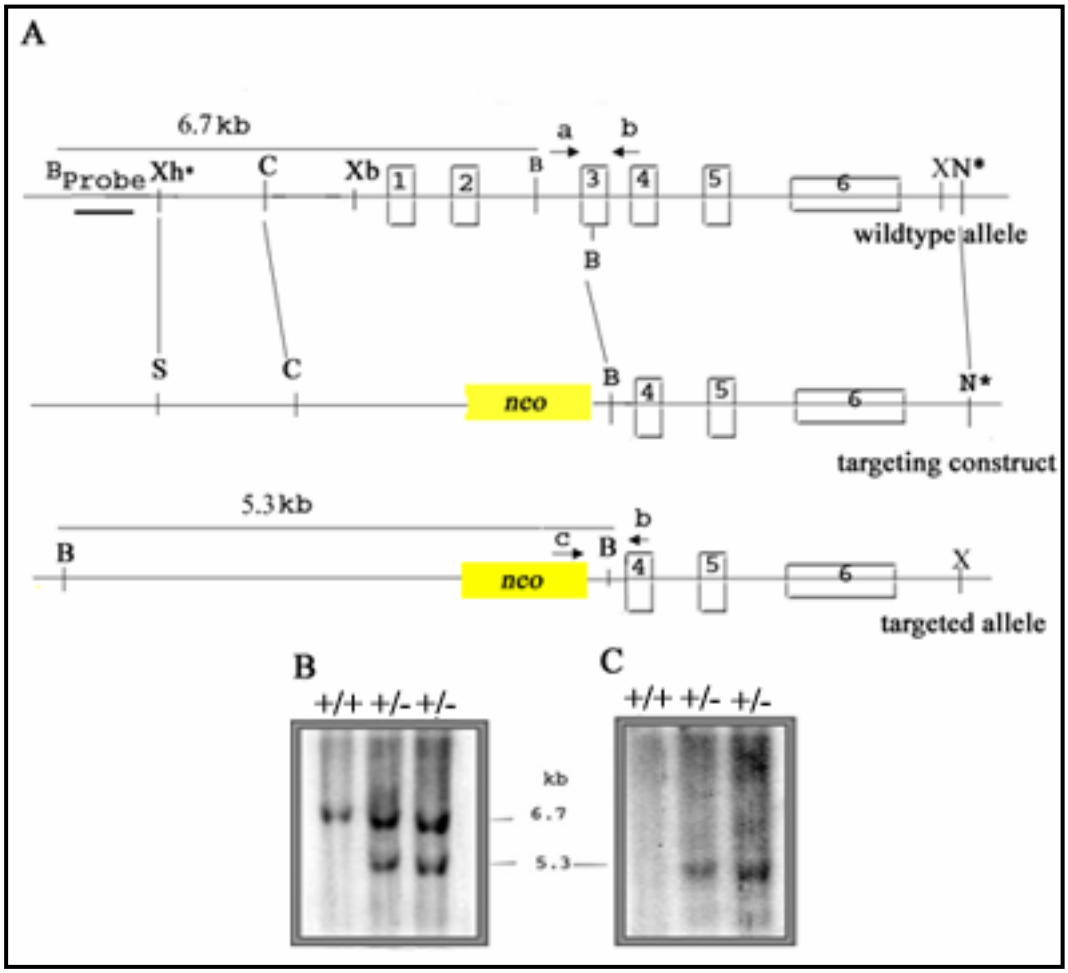

Figure 3.8. Targeted disruption of *Dnali1* gene by homologous recombination. (A) Schematic representation of Southern blot strategy to screen for recombinant ES clones. Wildtype *Dnali1* gene (at the top), targeting construct (middle) and recombinant allele (at the bottom) are shown.

ES cell DNAs were digested with *Bam*HI and hybridized with the 0.5 kb *Dnali1* specific external probe (B). The probe detected a ~6.7-kb fragment (wildtype allele) and a ~5.3-kb fragment (targeted allele). (C) The same blot was rehybridized with neomycin resistance gene specific probe, which showed hybridization signal of 5.3 kb corresponding to the recombinant allele. Site of external probe is indicated (probe). Arrows indicate the position of primers used for genotype analyses: a; mp-B-f, b; mp-gen-r and c; Neo3F. The restriction site abbreviations are: Xh; *Xho*I, S; *Sal*I, X, *Xba*I; C, *Cla*I; B, *Bam*HI; N, *Not*I; *neo*, neomycin resistance gene; asterisks represent the restriction sites deriving from cloning vectors.

3.1.4.6 Generation of chimeric mice

The recombinant ES cells were injected into 3.5 dpc blastocysts derived from C57BL/6J mice. The blastocysts were implanted into the pseudopregnant CD1 mice to generate the chimeric mice. This work was performed in the Max Planck Institute for experimental Medicine Göttingen.

Five chimeras were obtained by two independent injections of recombinant ES clones. The chimeras were scored according to the coat colour (in percentage), two males with 90%, one male with 30%, and two females with 80% chimerism were obtained. Two male chimeras with 90 % chimerism were bred with C57BL/6J and 129X1/SvJ mice, respectively to obtain F1 animals in respective background (C57BL/6J x 129/Sv) and in (129X1/SvJ). Germ line transmission was detectable only on C57BL/6J x Sv/129 background after one and half month breeding, while on inbred 129/Sv background, no offspring was obtained during a long-term breeding of about four months. The germ line transmission of the mutant allele was verified by genomic PCR using mp-B-f, mp-gen-r and Neo3F primers (Figure 3.9) with genomic PCR on DNA isolated from tail biopsies of the offspring.

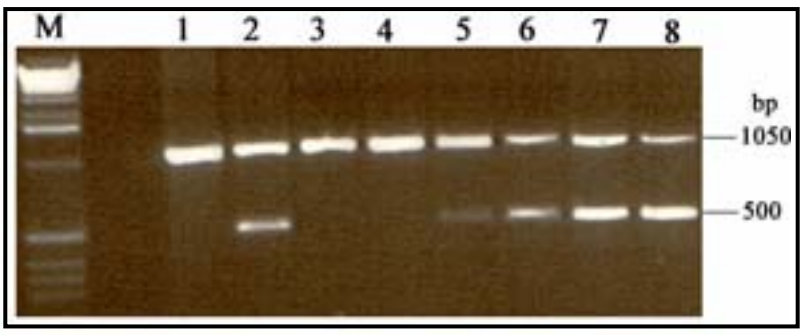

Figure 3.9. Genotyping of *Dnali1* mutant mice. The wildtype allele for *Dnali1* is amplified by mp-B-f and mp-gen-r primers (figure 3.8) resulting in a PCR product of about 1 kb. The mutated *Dnali1* allele generated a fragment of 500 bp by using the Neo-3F and mp-gen-r

primers (figure 3.8). The PCR products were separated on an 1% agarose gel and stained with ethidium bromide.

3.1.4.7 Generation of *Dnali1* deficient mice

Mice with homologous recombination in the *Dnali1* gene at C57BL6/J x 129 SvJ background, were appeared to have no overt phenotype and were fertile. Heterozygous animals were crossed to generate the *Dnali1* deficient mice. The resulting offspring were genotyped by PCR analysis. The statistical analysis is summarized in Table 3-1. The sex ratio for 67 offspring of the heterozygous matings was not affected, with approximately equal numbers of 35 males and 32 females (Table 3-1). On heterozygous matings, no viable *Dnali1*$^{-/-}$ mice were identified among 104 mice checked for the *Dnali1* gene mutation, suggesting that homozygosity for the *Dnali1* deficiency results in embryonic lethality (Table 3-1).
Out of the 104 offspring, 67 were heterozygous and 37 were wildtype for *Dnali1* mutation (Table 3-1). The observed ratio of homozygous wildtype (WT) offspring to heterozygous offspring to homozygous knockout offspring was approximately 1:2:0, which was deviating from the Mendelian expected genotypic ratio (1:2:1). In 15 throws, derived from seven successive heterozygous breeding pairs, an average litter size was calculated to be 6.9, which was reduced significantly as compared to the normal one (9.5)

	+/+		+/-		-/-	
Total offspring	**M**	**F**	**M**	**F**	**M**	**F**
104	17	20	35	32	0	0
Observed no.	37 (34.5 %)		67 (62.6%)		0	
Expected no.	26 (25%)		52 (50%)		26 (25%)	

Table 3-1. Analysis of genotype distribution of F2 generation at C57BL/6J x 129X1/SvJ background. Total of 104 animals from heterozygous breeding were genotyped. M, male; F, female.

3.1.5 Embryonic lethality of *Dnali1* deficient embryos

Genotyping of 104 newborn offspring by PCR analysis (Figure 3.9) revealed the absence of mice homozygous for the *Dnali1* mutation (Table 3-1). In order to determine when the *Dnali1* mutation results in a lethal phenotype, embryos at developmental stages E8.5 and E7.5 were investigated. No homozygous mutants were observed by genotyping PCR (Table 3-2). However, a great number of empty deciduae (17 out of 62) was detected at E8.5 stage. Resorbed embryos were also notified at E9.5 and genotyping of these embryos failed. In contrast, both wildtype and heterozygous embryos could be identified at 9.5 dpc and seemed to show a normal development, except a few absorptions (2-3)(Figure 3.10). To investigate whether the *Dnali1* deficient embryos die during preimplantation stages, embryos at E3.5 were isolated and genotyped by PCR (Figure 3.11). Blastocysts flushed from the uteri of *Dnali1* heterozygous females bred with heterozygous males. *Dnali1* null embryos were detected by genotyping at the expected ratio as defined by the Mendelian distribution. The results collectively suggest that *Dnali1* deficient embryos die between E3.5 and E7.5.

Figure 3.10. Dissected uterus of *Dnali1*$^{+/-}$ female mouse. F1 animals heterozygous for the *Dnali1* mutation were intercrossed and vaginal plug positive female mice were sacrified on day 8. Arrows indicate the absorbed embryos.

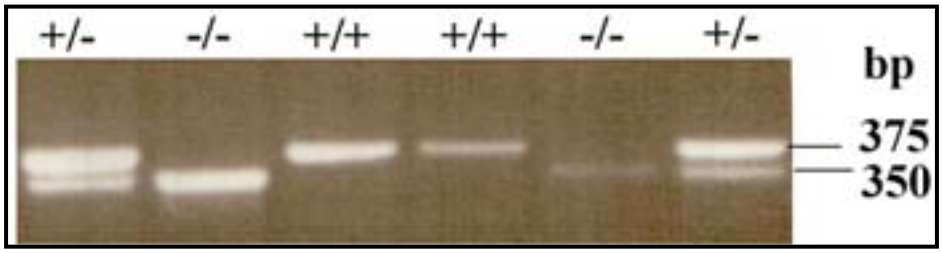

Figure 3.11. Genotyping of blastocysts. Blastocysts were flushed from the uteri and were genotyped using mp-for, mp-rev and Neo-F1 primers. Wildtype (+/+), heterozygous (+/-) and homozygous (-/-) embryos for the targeted allele were found.

Stage	Genotype			
	+/+	+/-	-/-	ND
E 3.5	9	19	6	4
E 7.5	10	17	0	3
E 8.5	12	32	0	6

Table 3-2. Genotyping of offspring derived from *Dnali1* heterozygous matings. Staged embryos were genotyped by PCR. At E3.5, in 4 blastocysts, PCR analysis gave no result. Three and six embryos were being resorbed at E7.5 and E8.5 respectively, and therefore unable to be genotyped. ND, not determined.

3.1.5.1 Expression of *Dnali1* during mouse embryonic development

3.1.5.1.1 Expression of *Dnali1* mRNA during mouse embryogenesis

Dnali1 expression in the early stages of embryogenesis was determined by RT-PCR approach using the primers mpex-f and mpcDNA-r, which amplified a PCR product of 815 bp. Total RNAs isolated from the mouse ES cells, blastocysts (3.5 dpc) and the mouse embryos from E7.5 to E15.5 (dpc) were subjected to RT-PCR analysis. *Dnali1* transcripts could be detected in all stages starting from ES cells to 15.5 dpc indicating the vital role of *Dnali1* during mouse embryogenesis (Figure 3.12). The RNA integrity was controlled based on the *Gapdh* expression. The identity of PCR products obtained was verified by sequence analysis.

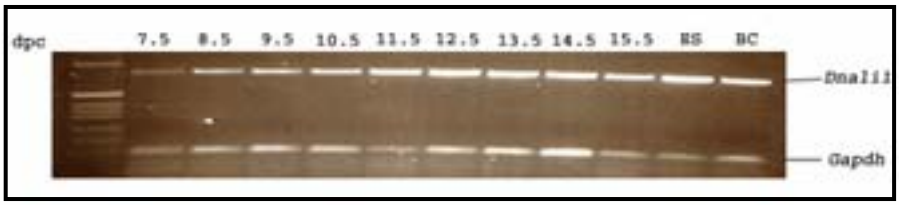

Figure 3.12. RT-PCR analysis on total RNA isolated from embryonic stem cells (ES), blastocysts (BC) and mouse embryos from 7.5 to 15.5 dpc using *Dnali1*-specific primers. Transcripts of *Dnali1* are detected at all analysed stages. RT-PCR for *Gapdh* transcript was performed as positive control.

3.1.5.1.2 Immunofluorescence microscopy

3.1.5.1.2.1 Expression of Dnali1 at E2.5 and E3.5

The spatial expression profiles of *Dnali1* in mouse embryogenesis at E2.5, E3.5 and E7.5 were studied by using Dnali1 specific antibodies. At the morula stage (E2.5), Dnali1 localization was found prominently in the cytoplasm (Figure 3.13 A-C). Comparable results were observed in blastocysts. Dnali1 was detected only in the inner cell mass (ICM) uniquely in the cytoplasm, while no staining was observed in the trophectoderm cells, indicating that Dnali1 expression is restricted to inner cell mass (Figure 3.13 D-F). These data suggest that Dnali1 accumulates in the cytoplasm of growing embryos and persists throughout the preimplantation stages.

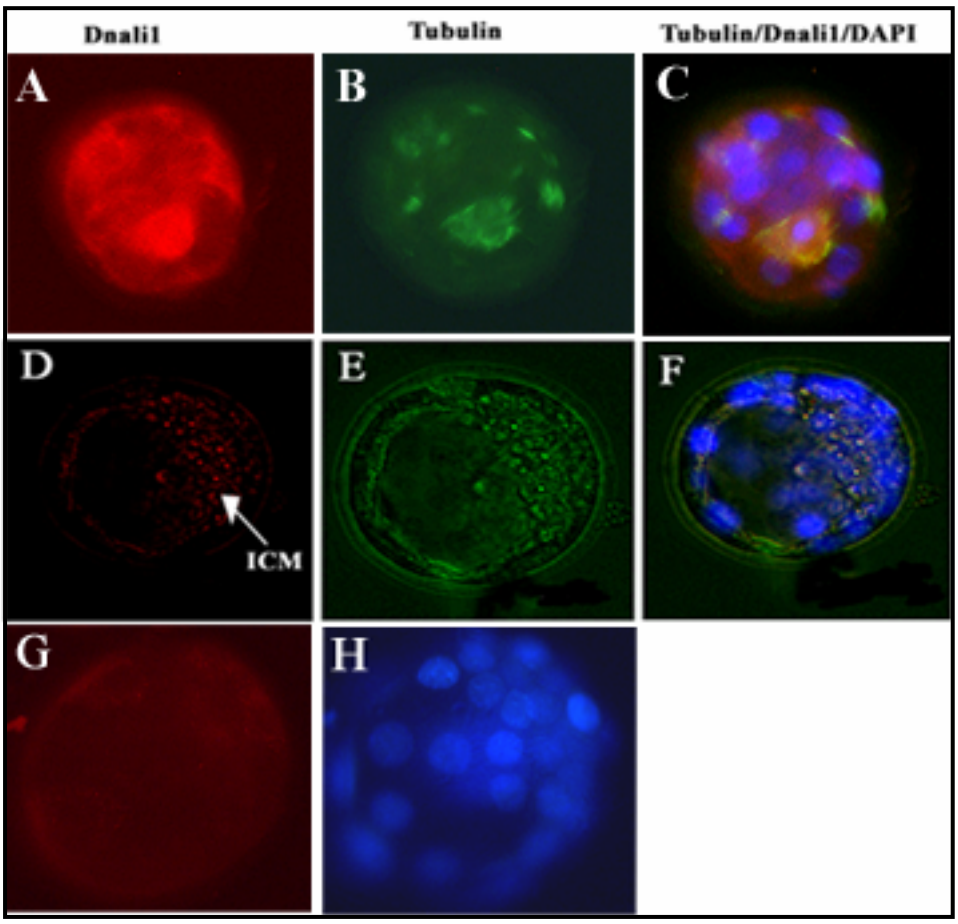

Figure 3.13. Expression of Dnali1 in wildtype morula (E2.5) and blastocysts (E3.5) stages. Mouse morulae (A-C) and blastocyt (D-F) were stained with Dnali1 specific antibodies (red) and α-tubulin (green). Dnali1 protein is expressed typically in the cytoplasm of morula and ICM of blastocysts (arrow). Additionally, DAPI was used to stain the nucleus (blue colour). No staining of Dnali1 was detected in the trophectoderm cells (D). Merge of Dnali1,α-tubulin staining and DAPI (C, F). Figure G shows control with no staining or weak background staining of DAPI stained blastocyst (H).

3.1.6 *Dnali1*-deficient blastocysts cultured *in vitro* show impaired ICM outgrowth

Due to the lethal phenotype of *Dnali1* null mutants, an *in vitro* blastocyst culture system was employed. Embryos at E3.5 were flushed out from the uteri of *Dnali1*$^{+/-}$ female mice mated with heterozygous *Dnali1* males and cultured in ES cell medium containing leukaemia inhibitory factor (LIF). Under these conditions, inner cells should expand, outgrow and frequently differentiate into extra-embryonic endoderm, while the trophectoderm layer should become adherent and differentiate into giant cells. At the beginning of the culture, putative *Dnali1* null blastocysts were morphologically normal and indistinguishable from wildtype or

heterozygous embryos. Embryos hatched from their zona pellucida and attached to the gelatine-coated dishes. During a 6-day culture, the wildtype or heterozygous blastocysts showed continuous growth and the inner cells mass (ICM) formed the typical structure of dense cell masses (Figure 3.14 A). In contrast, none of the putative *Dnali1* null mutants showed a distinguishable ICM-like structure, although the trophectoderm layer differentiated into giant cells (Figure 3.14 B). Among the 38 blastocysts tested, 2 embryos revealed delayed attachment, although they exhibited similar outgrowth to other embryos of the same genotype over a prolonged culture period. As summarized in the Table 3-3, the null mutants were lacking the robust outgrowth of the inner cells.

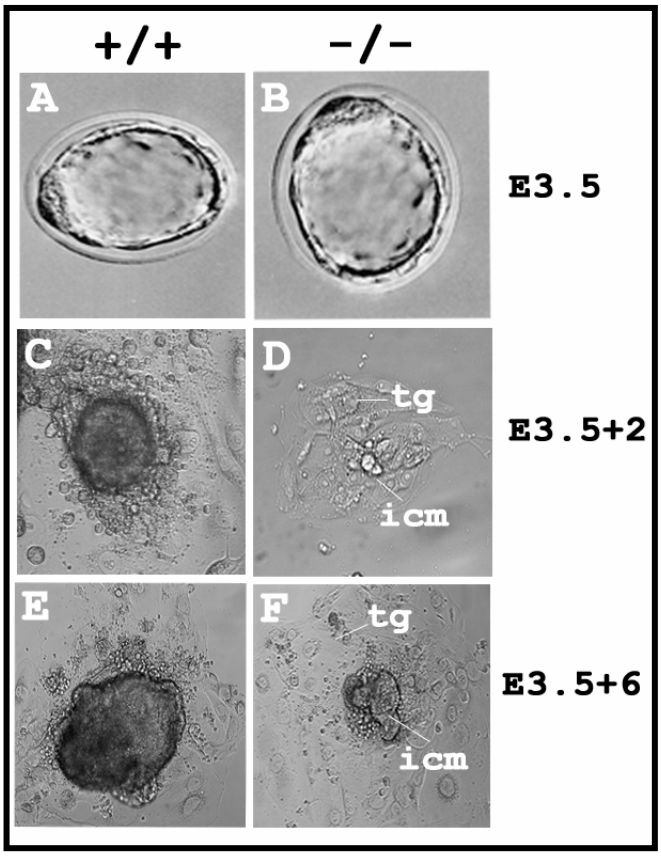

Figure 3.14. *In vitro* outgrowth of cultured blastocysts. Isolated blastocysts were grown *in vitro*. A representative heterozygous (A) and a homozygous (B) blastocyst are shown. At the beginning of the culture (0 d), blastocysts of both genotypes are phenotypically similar. The blastocysts hatched and attached to the gelatine-coated dishes at around day 1 of culture. The inner cells of the heterozygous embryo continued to proliferate and formed a dense core structure (A, C and E) surrounded by primitive endoderm cells. However, distinct ICM differentiation remained undone in the homozygous embryo culture (B, D and F). Outgrowth of polyploid trophectoderm cells was observed in all cultures (marked by tg).

Development	Genotype		
	+/+	+/-	-/-
Trophoblast and ICM	11	19	0
Trophoblast only	0	0	**6**
Delayed attachment	0	2	0

Table 3-3. Summary of the blastocyst outgrowth. Genomic DNA was isolated from the cultured blastocysts and genotyped by PCR (Figure 3.15).

3.1.7 Dnali1 interaction studies

Our results demonstrate that *Dnali1* is localized in sperm flagella and tracheal cilia. These observations suggest that Dnali1 is a component of axonemal dynein complexes. Analyses in the green algae *Chlamydomonas reinharditii* have demonstrated that the p28 protein is a component of the inner dynein arm isoforms. To elucidate whether Dnali1 is also an integral part of the inner dynein arm, we tried to identify those axonemal proteins, which interact with Dnali1. Therefore, a yeast-two-hybrid screen was performed using a murine testicular cDNA library (Hupe, 2003). Several proteins could be isolated. However, we did not detect a fragment encoding a known component of axonemal inner dynein arm complexes. Surprisingly, three of the identified two-hybrid clones encode fragments of the cytoplasmic dynein heavy chain 1 gene (*Dnchc1*). Sequence analysis of these fragments revealed that all three clones contain a part of the 3' UTR as well as approximately 318 bp encoding the last 106 amino acids of the cytoplasmic dynein heavy chain. To prove this putative interaction, immuno-precipitation and co-localization experiments in mammalian cells were performed using different approaches. Firstly, different cell lines were analysed for endogenous expression of *Dnali1* by RT-PCR. *Dnali1* expression was found in GC4, MA10, NS20Y and murine embryonic stem cells (Figure 3.14). For further experiments the neuroblastoma cell line NS20Y was selected.

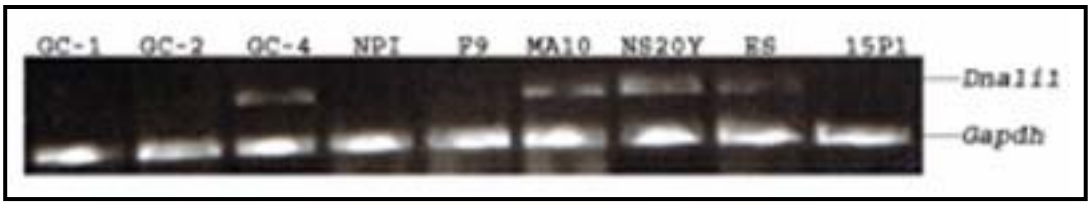

Figure 3.14. Expression of *Dnali1* in cell lines. Total RNA was extracted from GC1: mouse spermatogonia, GC2: spermatocyte immortalized, GC4: secondary spermatocyte, NPI: mouse epithelial cells from distal tubules, F9: mouse embryonic carcinoma, MA10: mouse Leydig cell tumor, NS20Y: mouse neuroblastoma, ES: embryonic stem cells and 15P1: mouse Sertoli cells and performed RT PCR analysis using mp-ex-F and mp-cDNA-R primers. *Dnali1* transcripts could be verified in GC4, MA10, NS20Y and ES cells. Integrity of the RNA used was proven by amplification of a *Gapdh* cDNA fragment.

3.1.7.1 Cellular localization of Dnali1 protein in NS20Y cells

Because actin microfilaments and MTs are the major determinants of neuronal shape (Tanaka and Sabry, 1995), the subcellular distribution of Dnali1 in mouse neuroblastoma cells (NS20Y) was analysed by immunofluorescence microscopy. Double immunostaining of NS20Y cells with Dnali1 specific antibodies and α-tubulin revealed localization of Dnali1 protein to the axonal part and vesicular like compartments around the nucleus (Figure 3.15). Extending axons arise form the growth cone a specialized structure at the tip of the axon-like processes in neurons, typically endowed with numerous fine processes, called filopodia that rapidly form and disappear.

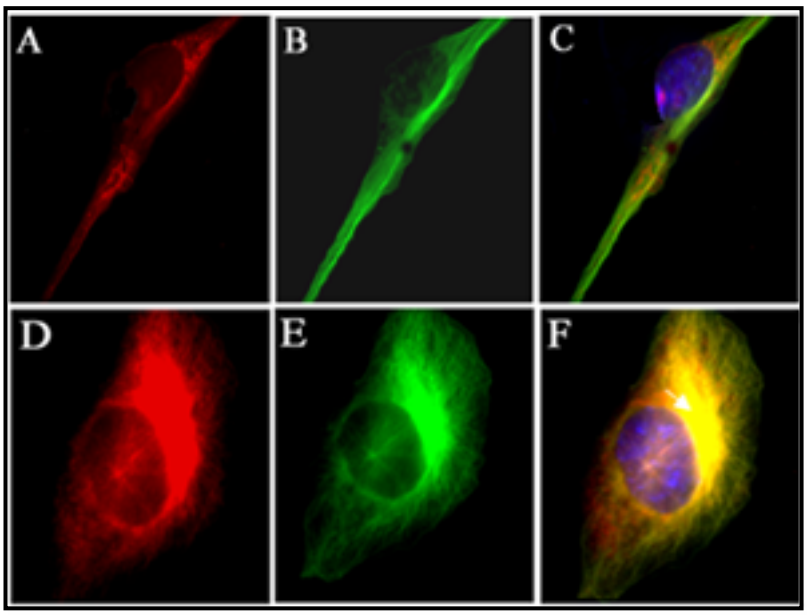

Figure 3.15. Endogenous Dnali1 expression in murine neuroblastoma cells (NS20Y) cultured for two weeks in vitro, fixed and immunostained with antibodies against Dnali1 and α-tubulin (A-F); Dnali1 localization could be detected in the cytoplasm of axon (red). (F) A high proportion-staining pattern of Dnali1 is visualized at the perinuclear region (arrow). Nuclei were counterstained with DAPI (blue colour).

3.1.7.2 Cloning of *Dnali1* cDNA in expression vector

For studying the biochemical interaction of *Dnali1* and *DnchcI*, the full-length *Dnali1* coding sequence was amplified by polymerase chain reaction by using the mpcDNA-f and mpcDNA-r primers from mouse testicular RNA. The resulting 815 bp *Dnali1* cDNA fragment was cloned into the pGem-T Easy vector and sequenced (Figure 3.16A). The DNA was restricted by *Eco*RI and *Not*I enzymes and a 838 bp fragment was inserted into the *Eco*RI and *Not*I sites of the pcDNA3.1(-)/*myc*-His-A vector. The resulting plasmid encoding *Dnali1* with a *myc*-His-tag at the C-terminus (Figure 3.16B) was then tested by transfection in NS20Y cells followed by immunostaining using α-*myc* antibodies. The over-expressed Dnali1 protein showed localization around the nucleus and in the axonal part of the neuronal cells (Figure 3.15). The pcDNA3.1-*Dnali1-myc* clone was used for further analysis, including the co-localization and co-immunoprecipitation studies.

3.1.7.3 Cloning of the cytoplasmic dynein (*Dnchc1*) fragment in an expression vector

The 3'-end fragment of the cytoplasmic dynein heavy chain (*Dnchc1*) cDNA was amplified by PCR, cloned into the pGem-T Easy vector and was subsequently sequenced. After restriction of the plasmid DNA with *Bam*HI and *Bgl*II, the 400 bp fragment (Figure 3.17) was cloned into the *Bam*HI and *Bgl*II digested pQM-Ntag/B vector (Abcam, Cambridge, UK). The resulting pQM-cytoplasmic-dynein-fragment-E2 plasmid was transiently transfected into the NS20Y cells and the fixed cells were then subjected to incubation with α-E2-tag specific antibodies to visualize the expression pattern of cytoplasmic dynein. Dnchc1 protein could be uniquely detected in the cytoplasm and Golgi apparatus of NS20Y cells (Figure 3.18 A-D).

```
  1 - ctggaagtcaatgtcaccgcctcacagagtgccacccttgatgcctgcagctttggagtc -  60
      L  E  V  N  V  T  A  S  Q  S  A  T  L  D  A  C  S  F  G  V
 61 - acaggtctgaagctccaaggggccacgtgcagcaacaacaagctatcactctccaatgcc - 120
      T  G  L  K  L  Q  G  A  T  C  S  N  N  K  L  S  L  S  N  A
121 - atctccacagtcctccccctcacacagctgcgctgggtgaaacaaacaagcgccgagaag - 180
      I  S  T  V  L  P  L  T  Q  L  R  W  V  K  Q  T  S  A  E  K
181 - aaggccagcgtggtgaccttacctgtctacctgaacttcacccgggcagacctcatcttc - 240
      K  A  S  V  V  T  L  P  V  Y  L  N  F  T  R  A  D  L  I  F
241 - accgtggactttgaaattgctacaaaggaagatcctcgcagcttctatgagcgtggagtt - 300
      T  V  D  F  E  I  A  T  K  E  D  P  R  S  F  Y  E  R  G  V
301 - gccgttctgtgcactgagtaaagctagacttttctccagtcctctttctggaataggaaa - 360
      A  V  L  C  T  E
```

Figure 3.17. Nucleotide and deduced amino acid sequence of *DnchcI* carboxy-terminal coding region (NM_030238), cloned in the reading frame of pQM-NTag vector.

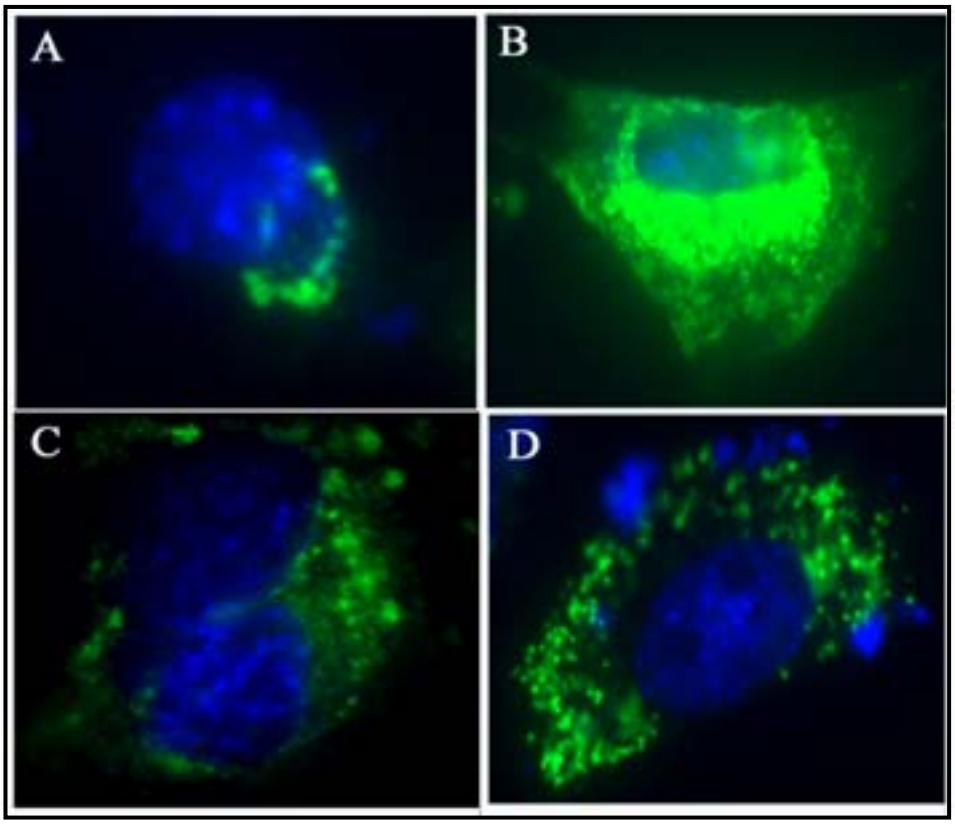

Figure 3.18. DnchcI (cytoplasmic dynein) localization in NS20Y cells. The pQM-cytoplasmic-dynein-fragment-E2 plasmid was transiently transfected into the NS20Y cells. On fixation with 4% PFA, NS20Y cells were incubated with α-E2-tag specific antibodies to visualize the expression pattern of cytoplasmic dynein (A-D) The α-E2-antibody was detected using a FITC-coupled secondary antibody. Blue colour indicates the DAPI stained nuclei. (A) DnchcI localises with the Golgi apparatus. Figure B demonstrates a stronger staining of overexpessed DnchcI protein at the perinuclear structures. (C and D) Dnchc1 protein could be uniquely detected in the cytoplasm of NS20Y cells. A dotty, vesicular cytoplasmic dynein staining pattern, rather than a clear Golgi complex localization, was detected.

3.1.7.4 The interaction studies of Dnalil1 and cytoplasmic dynein chain

3.1.7.4.1 Colocalization studies of Dnali1 and Dnchc1

After transfection of cells with both E2-*Dnchc1* and Myc-*Dnali1* constructs, the localization of fusion-polypeptides within the cells was determined (Figure 3.24). The α-myc-antibody was detected using a Cy3-coupled secondary antibody. Signals were observed in the cytoplasm surrounding the nucleus and punctuated spots were visible in cell peripheries (Figure 3.19 a and d). Using the *Dnali1* specific antibody, a similar staining pattern was

obtained, indicating that the myc-epitope did not alter the Dnali1 localization within cells (Figure 3.15). The E2-Dnchc1 fragment was localized around the nucleus and in cellular boundaries (Figure 3.19 b and e). Although the pattern of both polypeptides did not overlap completely, a coincided localization was observed in some parts of cells. Especially, in the distal region of filopodia both polypeptides were detected (Figure 3.19 c and f).

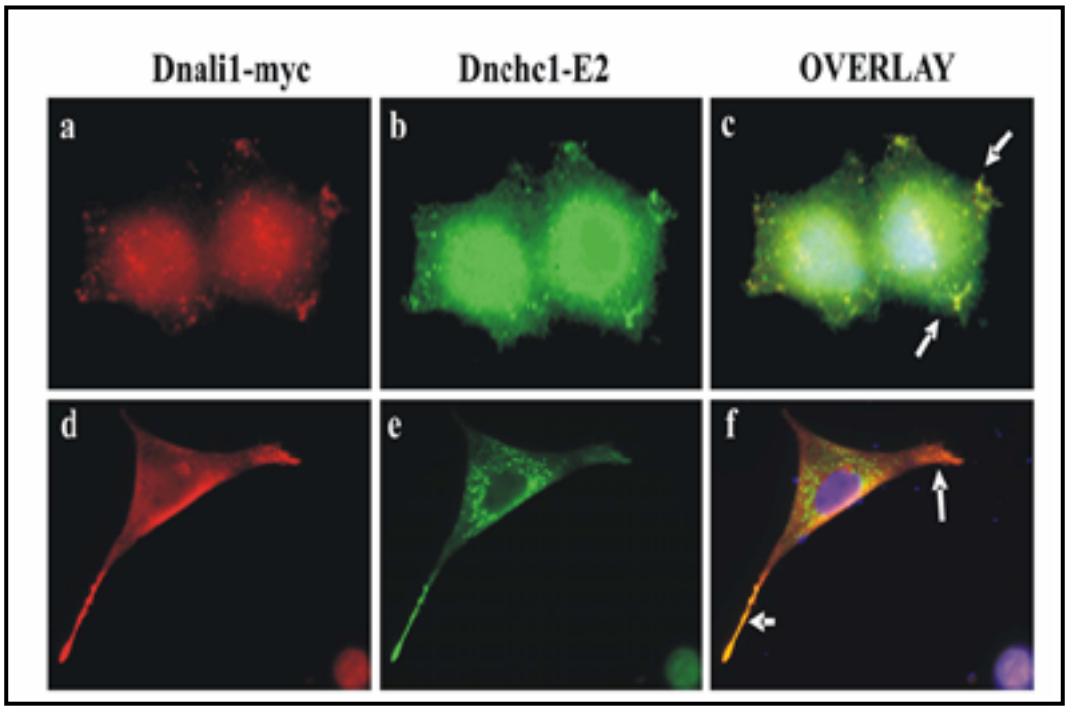

Figure 3.19. NS20Y cells were transfected with *Dnali1*-myc and *Dnchc1*-E2 constructs. For detection myc- and E2-epitope specific antibodies were used and visualized by Cy3-conjugated anti-rabbit secondary antibodies (red colour) and FITC conjugated anti-mouse IgG (green colour). Nuclei were counterstained with DAPI (blue colour). (a-c) A prominent signal of the Dnali1-myc fusion-protein is detectable around the nucleus. Moreover, some punctuate dots are located in the outgrowing regions of the cell. The cytoplasmic dynein is distributed over the whole cell, but punctuate signals are seen in the cell boundary. Yellow colour results from overlapping signals and indicates that in these cell compartments both dynein polypeptides co-localize. Figures d-f show one cell with filopodia. Especially in the distal region of filopodia both dyneins could be detected.

3.1.7.5 Dnali1 interaction with the cytoplasmic dynein heavy chain

3.1.7.5.1 Co-immunoprecipitation

Next it was analysed whether the putative interaction between both dynein chains could be verified by immunoprecipitation assay. An approximately 32 kDa polypeptide was observed by Western blot analysis, if the E2 monoclonal antibody was used for precipitation and the c-myc specific antibody for detection (Figure 3.20).

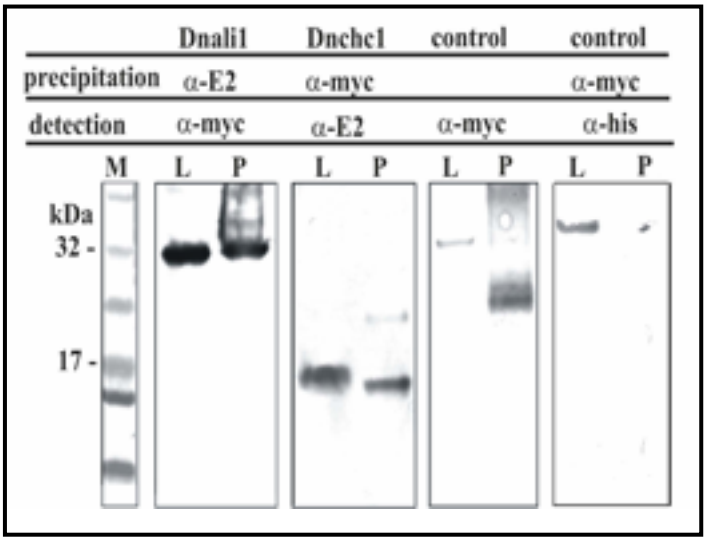

Figure 3.20. Co-immunoprecipitation of Dnali1-myc with Dnchc1-E2. NS20Y cells were transfected with *Dnali1*-myc and *Dnchc1*-E2 constructs. Either α-E2 or α-myc epitope antibodies were used for precipitation. In the left panel the result of the α-E2 precipitation and α-myc detection is shown. An approximately 32 kDa polypeptide was detected by Western blot analysis in the whole cell lysate (L) and in the precipitation pellet (P). Using α-myc antibodies for precipitation and α-E2 antibodies for Western blot detection, an approximately 15 kDa protein is detected in the middle panel. Third panel shows a control experiment with co-transfection of Dnali1-myc and Dnchc1-E2 constructs. The whole cell lysate was incubated with dynabeads without cross-linking with antibodies, demonstrating that Dnali1-myc and Dnchc1-E2 do not bind unspecific to the dynabeads. In the second negative control experiment (fourth panel), *Tcte3*-His and *Dnali1*-myc constructs were used for transfection and a 38 kDa Tcte3-His fusion-protein was detected in the whole cell lysate. The same procedure was applied for precipitation of Dnali1-myc polypeptide as described above. No precipitation or unspecific binding was determined by Western blot analysis using α-His antibodies.

The size of the co-precipitated polypeptide corresponds to the calculated molecular weight of the Myc-Dnali1 fusion-protein. Using c-myc antibodies for the precipitation and E2 antibodies for the detection, a 15 kDa polypeptide was confirmed, that complies the calculated size of the E2-Dnchc1-fragment (Figure 3.20). As negative control, a precipitation with an outer arm dynein light chain (*Tcte3*) and Dnali1 was performed; however, the Dnali1 polypeptide was not detected by Western blot analyses. Our results indicate that the axonemal dynein light intermediate chain Dnali1 interacts directly with the carboxy-terminal part of the cytoplasmic dynein heavy chain 1 within male germ cells.

3.1.8 Localization of Dnali1 in the Golgi apparatus

The association of Dnali1 and cytoplasmic dynein heavy chain was further explored in the mouse embryonic stem cells (ES) by immunocytochemistry. Dnali1 colocalized with vesicular compartments adjacent to the nucleus, as was observed in the neuroblastoma cells (Figure 3.15). In neuroblastoma cells, a dotty, vesicular cytoplasmic staining pattern, rather than a clear Golgi complex localization, was detected. It could be emphasized that Dnali1-Golgi localization is also present during the initial break down of the Golgi apparatus in the early stages of mitosis. To test the Golgi localization of Dnali1 in other cell lines, ES cells were co-stained with Dnali1 and GM130 (a marker for the Golgi compartments) antibodies. We observed nearly identical staining patterns (Figure 3.21 A-F). In control staining of ES cells by incubation with only secondary antibodies resulted in a barley background staining (Figure 3.21 G-I).

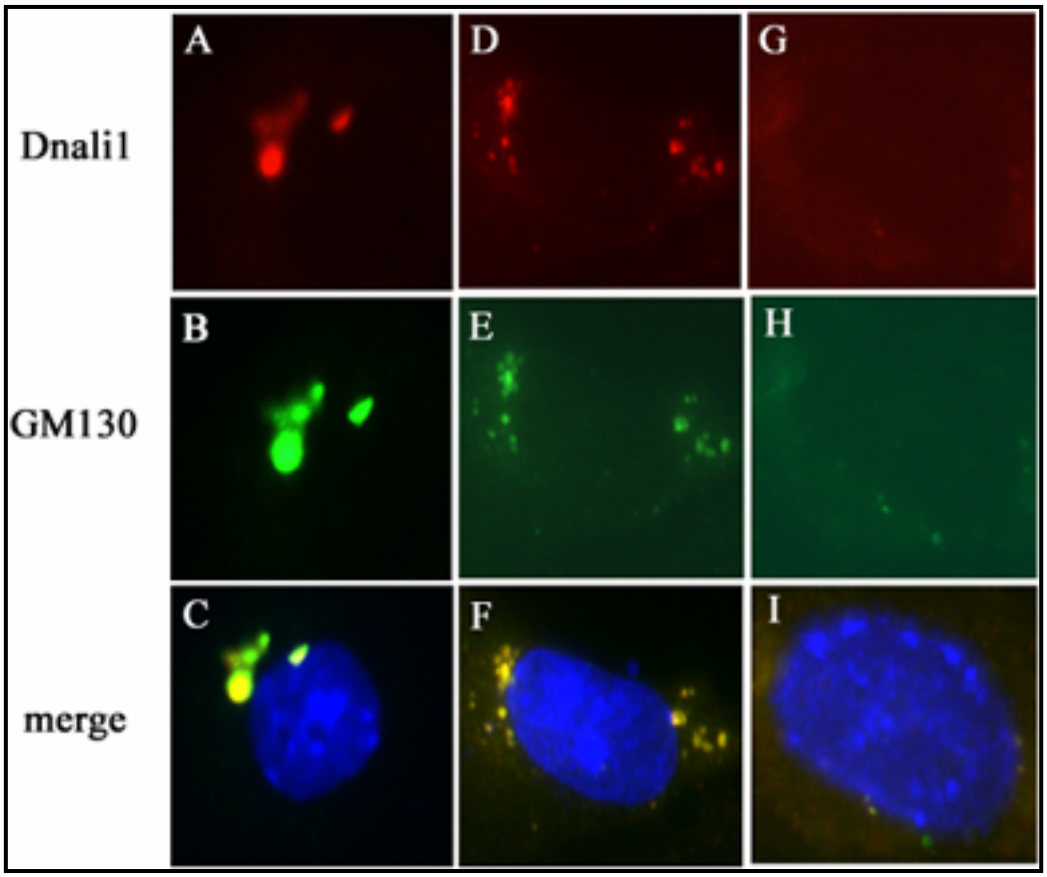

Figure 3.21. Localization of Dnali1 to the Golgi apparatus in ES cells (A-F). Methanol fixed murine ES cells were double labelled with Dnali1 (in red; A and D) and GM130 (in green; B and E) antibodies. The merged images are shown in C and F. The DNA is visualized with DAPI (blue). Figure G-I show the control staining for Dnali1 and GM130 specific antibodies.

3.1.8.1 Dnali1 association with Golgi structures in the absence of microtubules

Pharmacological agents depolymerise the microtubular network resulting in the dispersal of centrally located Golgi apparatus to numerous scattered, but functional Golgi stack-lets (for review Thyberg and Moskalewski, 1985). In order to determine if Dnali1 is localized to peripheral Golgi stack-lets, ES cells were treated with 10 μM nocodazole for 5-6 hrs at 37^{o}C to depolymerise the MTs, and were then stained with anti Dnali1 and γ-tubulin antibodies (a centrosomal marker). It was observed that Dnali1 colocalizes extensively on the clusters Golgi vesicles distributed in the cytoplasm (Figure 3.22 A-F). This pattern is consistent with the Golgi staining of nocodazole treated cells.

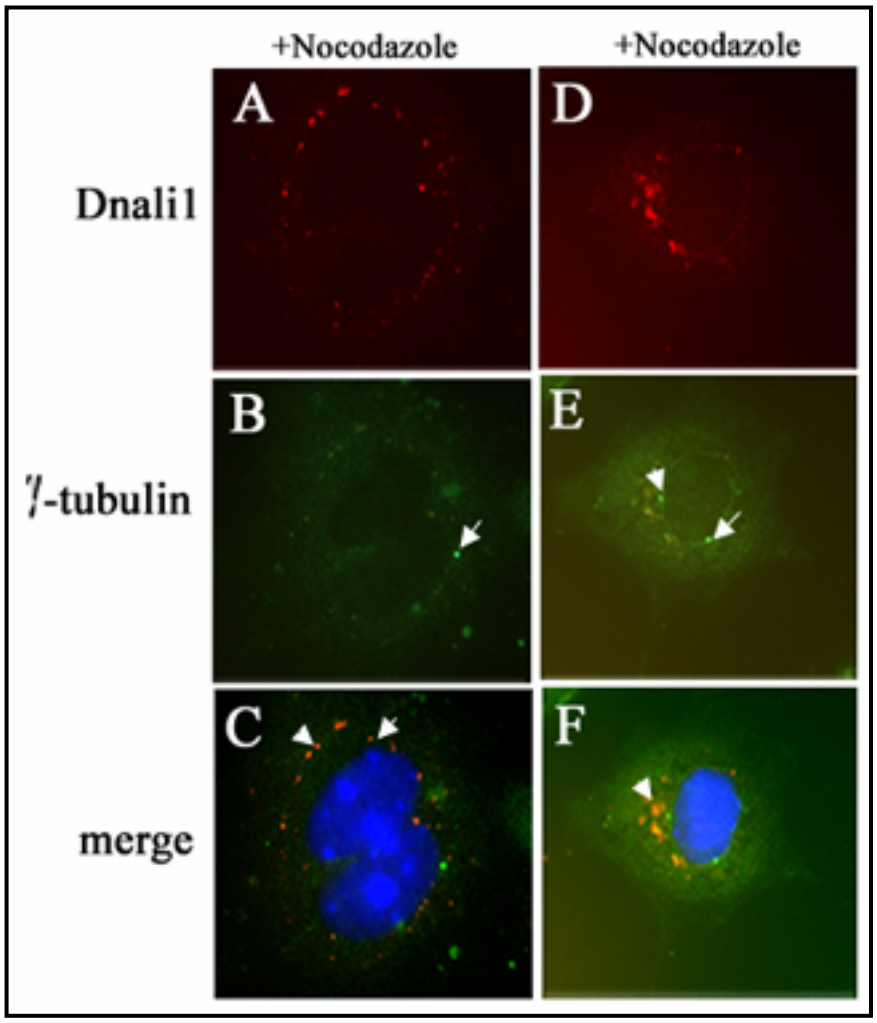

Figure 3.22. Dnali1 co-localization with the Golgi apparatus. Nocodazole-treated ES cells were methanol fixed and double labeled with anti-Dnali1 (red; A and D) and anti γ-tubulin (green; B and E) antibodies. After 6 hrs of nocodazole treatment, microtubule depolymerization was complete and only few nocodazole-resistant microtubules remained in some cells. Dnali1 co-localizes with Golgi elements scattered in the cytoplasm indicated by arrows (C and F). Centrosomal marker γ-tubulin staining could be visualized (B and E).

To understand the role of Dnali1 and its distribution with Golgi and centrosomes, ES cells were treated with higher concentration of microtubule-destabilizing agent; nocodazole (20 μM) for 3-4 hrs leading to complete depolymerization of microtubules and counter-stained with gamma-tubulin. The idea for doing this experiment was that as depolymerization of microtubules led to the dispersion of centrosomal proteins and cytoplasmic protein aggregates that contain the centrosomal components like pericentrin, ninein as well as dynein, whether this dispersal could affect the assembly of centrosomal proteins or the localization of Dnali1. We observed the localization of Dnali1 with large protein aggregates in the cytoplasm near

the nucleus (Figure 3.23). Consistent with this idea is the observation that by disruption of the microtubular organization, the centrosomal localization was disturbed, however, the localization of Dnali1 with the protein aggregates was not changed.

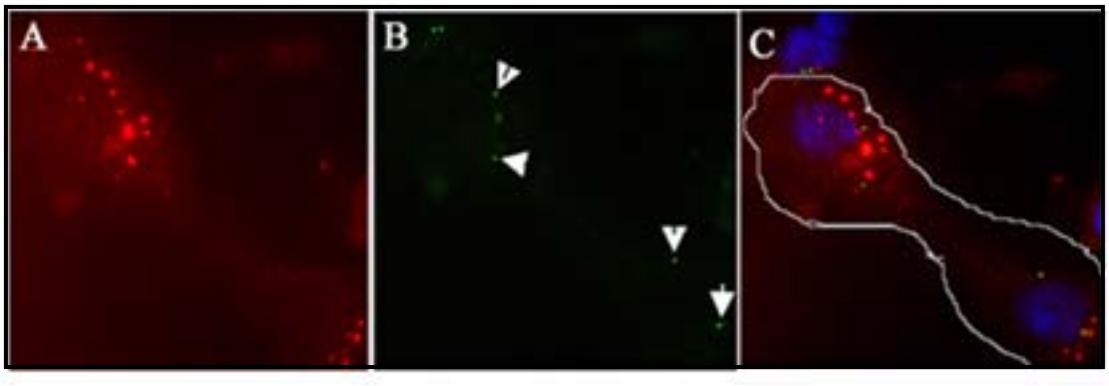

Figure 3.23. Dnali1 localization study with the centrosomes and distributional changes of Dnali1 with intense depolymerization of microtubules. Higher concentration of nocodazole (20 μM) treated ES-cells were methanol fixed and stained with affinity-purified antibodies against Dnali1 (red) or with γ-tubulin (green). DNA stained in blue. (A-C) Dnali1 localizes to the cytoplasmic granules that show distribution in the cytoplasm near the centrosome. Depolymerization of microtubules did not affect the localization of Dnali1. Arrowheads indicate the centrosomes stained with γ-tubulin.

3.1.9 Mutational analysis of human asthenozoospermia patients by DHPLC

Keeping in view the localization of *Dnali1* along the entire axoneme of sperm flagella, we investigated 25 infertile patients with asthenozoospermia by DHPLC. Exons 1 to 7 of the *DNALI1* gene were amplified by PCR using the following flanking intronic primers: hp-exon1-F and hp-exon1-R for exon 1, hp-exon2-F and hp-exon2-R for exon 2, hp-exon3-F and hp-exon3-R for exon 3, hp-exon4-F and hp-exon4-R for exon 4, hp-exon5&6-F and hp-exon5&6-R for exons 5 and 6, hp-exon7-F and hp-exon7-R for exon 7, with genomic DNA from patients and control DNA samples as templates. The resulting PCR products were then analysed by the "WAVE" mutational analysis system. The PCR program for the generation of heteroduplexes and WAVE program for *DNALI1* amplicons are indicated in 2.2.22. Specific melting temperatures for each fragment were selected with software to allow for partial denaturation of the DNA molecules measured as a 50% decrease in the DNA helicity, and this in turn resulted in adequate separation of homozygous from heterozygous double-stranded

DNA products. Single base-paired mismatches (SNPs) present within the DNA fragments produced different mobilities that were shown by altered retention times or chromatograms.

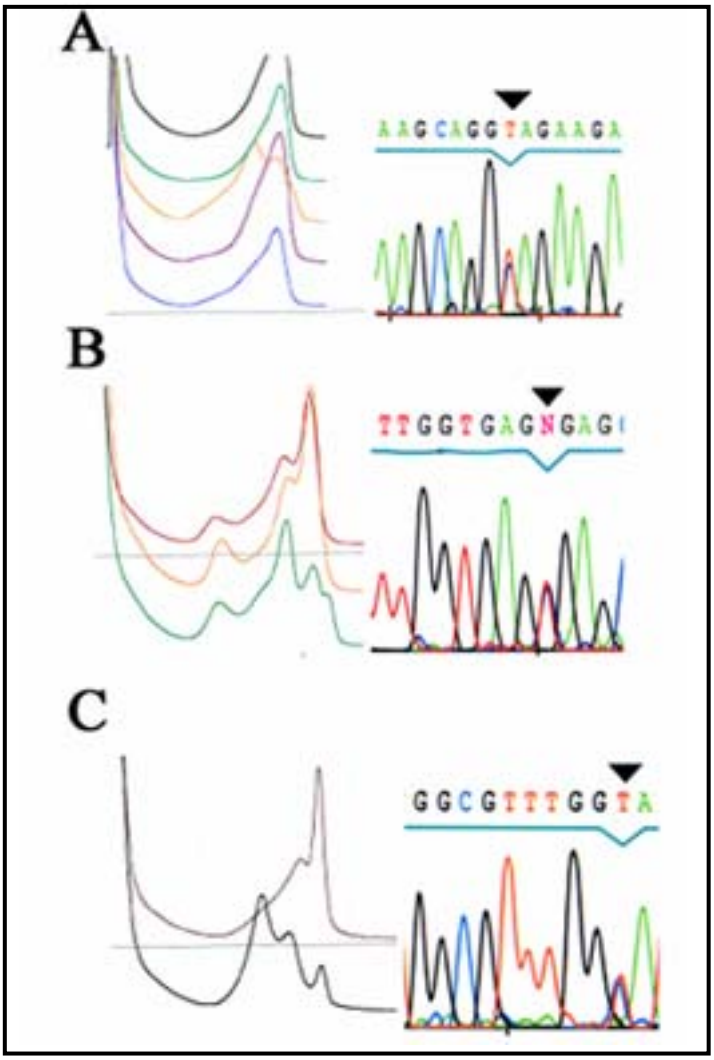

Figure 3.24. Chromatographic WAVE pattern and detection of mutations by DHPLC for the individual *DNALI1* PCR products. The sequences confirm the nucleotide changes of *DNALI1* gene with respect to change in WAVE pattern indicated by arrows. (A) exon 2; 194C>T, (B) IVS3 c.424+2T>C, (C) exon 4; 510C>T.

Referring to *DNALI1* sequence, a total of five nucleotide variations were identified in the 25 infertile patients (Figure 3.24 A-C). The results of DHPLC are summarized in the Table 3-4. The nucleotide substitutions 194C>T, IVS1 c.84–50T>C, 510C>T and IVS4 c.425-10G>A were likely to be polymorphisms as they were exonic silent substitutions, intronic variations located outside the splice sites, or were also present in control DNA samples. However, the

substitution IVS3 c.424+2T>C was notified as a putative splice site mutation and was not detected in the control samples.

Patient No.	Situs inversus	Other symptoms	Polymorphism
1	no	azs	no
2	yes	azs	IVS4 c.425-10G>A
3	no	azs	no
4	no	azs	no
5	no	azs	no
6	no	azs	no
7	no	azs	no
8	no	azs	no
9	no	azs	no
10	no	azs, br	no
11	no	azs	no
12	no	azs, br, li	510C>T, No exchange
13	no	azs	194C>T, A65V IVS3 c.424+2T>C IVS1 c.84–50T>C
14	no	azs	no
15	no	azs	no
16	no	azs, head ache	no
17	no	azs	no
18	no	azs	no
19	no	azs	no
20	no	azs	C-144A T808C
21	no	azs	no
22	no	azs, co, br	T808C
23	no	azs	194C>T, A65V
24	yes	azs	C-144A
			194C>T, A65V
25	no	azs	C-144T 194C>T, A65V

Table 3-4. Result of the "WAVE" analysis of patients suffering from reduced sperm motility. azs: asthenozoospermia, br: bronchitis, co: cough, li: lung infection. Base 1 corresponds to the first base of the initiation codon in the cDNA sequence.

3.2 Genomic organization and isolation of *Tcte3* cDNA

The murine *Tcte3* gene comprises of four exons spanning about 14 kb and is located on chromosome 17, which is syntenic to the human chromsome 6, where *TCTE3* is located.

Tcte3 cDNA was isolated by RT-PCR experiment from a mouse testis library by using the primer pair Tc2-5 and Tc2-3. The resulting PCR product was cloned into pGEM-T Easy vector and was subsequently sequenced. Sequence comparison of the cloned cDNA and genomic DNA revealed that *Tcte3* contains at least three alternative spliced variants in the mouse, named as I, II and III, whose exon structures are schematised in Figure 3.25A. *Tcte3*-I, II and III variants have a size of 768 bp, 510 bp and 738 bp, respectively. The deduced amino acid sequences are shown in Figure 3.26. Both *Tcte3*-I and *Tcte3*-III consist of an ORF of 191 AA, encoding protein with a molecular weight of approximately 22 kDa, while *Tcte3*-II encodes a protein of 136 amino acids. Sequence information of the *Tcte3* cDNA is indicated in the database (GenBank accession numbers: NM_011560, NM_198104). In the Ensemble Genome Browser, the accession numbers are ENSMUST00000040746, 73074 and 74495 respectively. Human orthologue *TCTE3* (NM_174910) cDNA is almost identical to that of the mouse, contains the coding region of about 747 bp (Figure 3.25B) and encode a protein of 198 amino acids residues (Neesen et al., 2002).

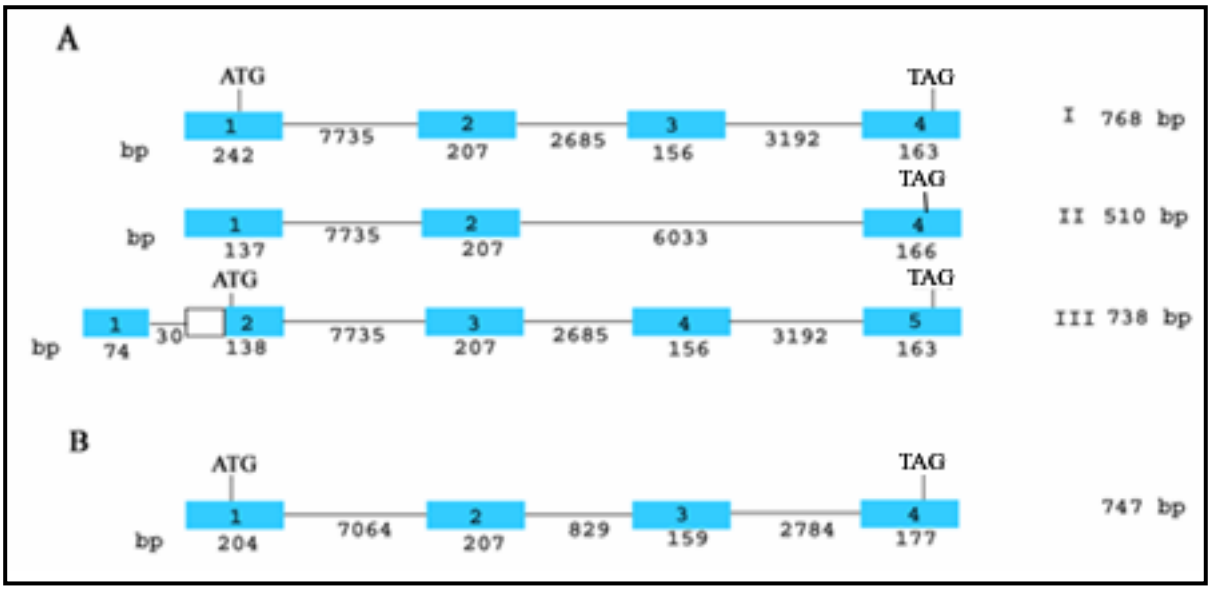

Figure 3.25. Schematic representation of the exon-intron structure of *Tcte3* gene (A) and human orthologue *TCTE3* (B). *Tcte3* splice variants are indicated by I, II and III with the specified

lengths, respectively. Blue boxes represent the exons of *Tcte3* variants. Translational start and stop sites are indicated. Numbers at the bottom indicate the length of exons and introns.

```
           ********************************************************************************
Tcte3-I    MERRGRMAKTPTGQTHQSPVSKRERKPSMFEKESYAQILRERLRESFHDVQYVEPPFDDSIADVGKEWKSALAKLKFANS 80
Tcte3-II   MERRGRMAKTPTGQTHQSPVSKRERKPSMFEKESYAQILRERLRESFHDVQYVEPPFDDSIADVGKEWKSALAKLKFANS 80
Tcte3-III  MERRGRMAKTPTGQTHQSPVSKRERKPSMFEKESYAQILRERLRESFHDVQYVEPPFDDSIADVGKEWKSALAKLKFANS 80

           **********************                                              *****
Tcte3-I    YRMEPLKKFQAHLVETKIQQILKDSLKDVKYDDKAPHLSLELADRILAAVKEFAYHRYKFIIQVLFIQKTGQAINIASRW 160
Tcte3-II   YRMEPLKKFQAHLVETKIQQILK----------------------------------------------------IASRW 105
Tcte3-III  YRMEPLKKFQAHLVETKIQQILKDSLKDVKYDDKAPHLSLELADRILAAVKEFAYHRYKFIIQVLFIQKTGQAINIASRW 160

           ******************************
Tcte3-I    IWDVAWDNWVEAKHETESYVVLALVFALYCE 191
Tcte3-II   IWDVAWDNWVEAKHETESYVVLALVFALYCE 136
Tcte3-III  IWDVAWDNWVEAKHETESYVVLALVFALYCE 191
```

Figure 3.26. Scheme shows amino acid sequence alignments of Tcte3 isoforms I, II and III. Amino acid residues derived from alternative exons are indicated by red and black colours. Asterisks label the identical amino acids in all three Tcte3 variants.

3.2.1 Targeted disruption of *Tcte3*

3.2.1.1 Construction of targeting vector for *Tcte3* disruption

In forerun work, the expression of *Tcte3* in the testis and other tissues was analysed. Moreover, a cosmid clone containing the complete *Tcte3* gene was isolated and characterised by restriction analyses and sequencing reactions (Drenckhahn, 2000; Tiede, 2001).

To generate mutant mice lacking *Tcte3* function, a replacement targeting vector was generated using the pPNT vector (Tybulewicz et al., 1991), which contains a bacterial phosphoribosyltransferase II gene conferring *neomycin* resistance (*Neo*) and a Herpes simplex virus thymidine kinase (*TK*) gene, each under the control of mouse phosphoglycerate kinase promoter. A total of 7.7 kb region was deleted containing the exon 2 of *Tcte3* gene. By deleting the region of *Tcte3* gene containing the exon 2 the activity of all three isoforms should be abolished.

A 5 kb *Spe*I/*Kpn*I fragment consisting of 156 bp of *Tcte3* coding sequence (exon 2) and about 4.8 kb of intronic region was isolated from the cosmid clone and inserted into pBlueScript vector using the same restriction sites. The plasmid DNA was digested with *Xba*I and *Eco*RI restriction enzymes. The resulting fragment of 3.5 kb length was then ligated into *Xba*I/*Eco*RI sites of the pPNT vector (Figure 3.29A).

A 3.8-kb *Xba*I fragment was isolated from the cosmid clone and was cloned into the *Xba*I site of the pBlueScript vector. Restriction analyses and DNA sequencing confirmed insertion and correct orientation of the fragment. The DNA was then restricted by *Not*I and *Xho*I enzymes

and was ligated into the *Not*I/*Xho*I sites of pPNT vector (Figure 3.29A). The resulting targeting construct was analysed by restriction analysis using different restriction enzymes (Figure 3.28).

A 1.4 kb fragment was isolated from the 5 kb *Spe*I/*Kpn*I fragment by cutting with *Eco*RI restriction enzyme, agarose gel extracted and was used as 3'-external probe for screening the DNA of recombinant R1 ES-clones (Figure 3.27, 3.29A).

To design the external probe at 5'-arm of the targeting construct, a 436 bp fragment of *Tcte3* gene was amplified by PCR, using the Tc-F, 5'- GAT CTG AAG TTC TGT GTT CAT CCA T – 3' and Tc-R, 5'- AAG CTG CCT TCT AGA GGA ACT AAA C – 3' primers and was subcloned into the pGEM-T Easy vector. The 436 bp fragment was cutted out from the pGEM-T Easy vector by *Eco*RI restriction enzyme, separated on 1% agarose gel and isolated from the agarose gel (2.2.3).

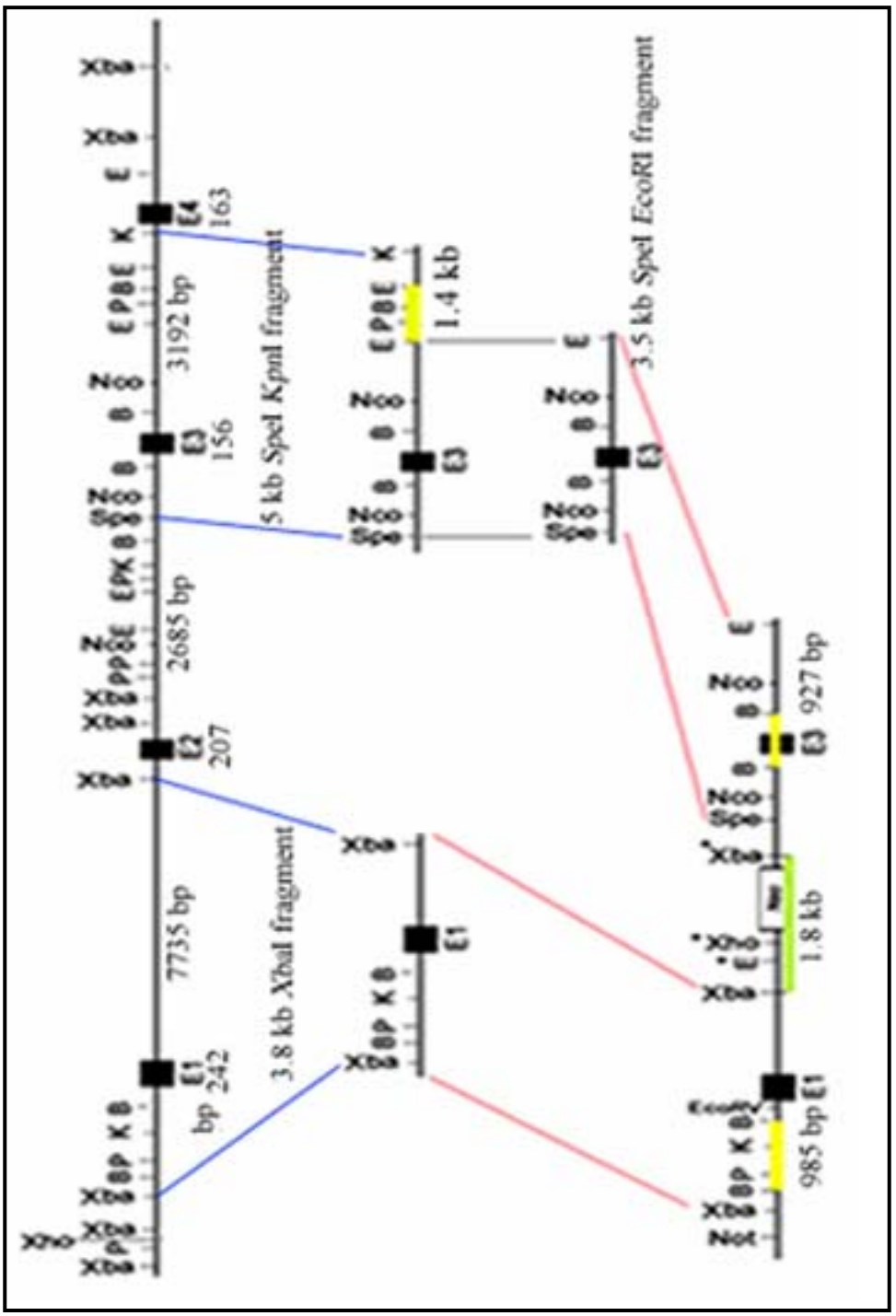

Figure 3.27. Genomic structure of the *Tcte3* gene and generation of targeting vector. The 3.8 kb fragment was cloned as 5'-flanking region and 3.5 kb fragment was inserted as a 3'-flanking region for the targeting construct. E, *Eco*RI; P, *Pst*I; B, *Bam*HI; K, *Kpn*I.

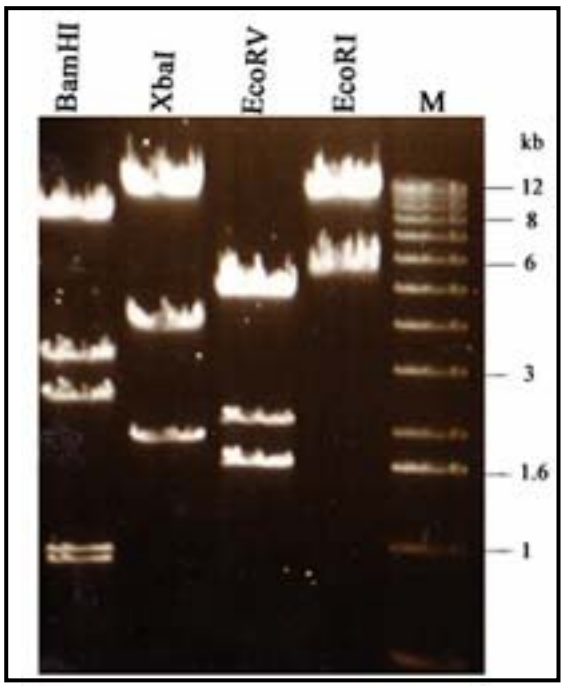

Figure 3.28. Restriction analysis of knockout construct with different restriction enzymes. M, marker; kb, kilo base pair.

3.2.1.2 Analysis of R1 ES-cells

RI embryonic stem (ES) cells were grown in Dulbecco's modified Eagle's medium (2.1.6.2). The plasmid DNA containing the targeting construct (pPNT-*Tcte3*) was purified using QIAGEN MaxiPrep kit (2.2.1.1.3) and was linearized by *Not*I restriction enzyme before introducing into early passage R1 ES cells by electroporation (500 μF, 0.24 kV) using a Bio-Rad Gene Pulser II (Bio-Rad Laboratories). After selection in medium containing G418 (200μg/ml) and ganciclovir (2 μM), individual drug resistance colonies were isolated, expanded and screened for the appropriate targeting event. The isolated DNA was subjected to restriction digest with *Kpn*I restriction enzyme, electrophoresed and transferred onto nitrocellulose filters. The 1.4 kb 3'-probe corresponding to the region indicated by yellow colour in Figure 3.27, was labelled with [^{32}P]-dCTP by random priming and hybridized overnight. Detection of a 5 kb DNA fragment indicated the presence of the wildtype allele, whereas a targeted allele was evident as a 9 kb DNA fragment (Figure 3.29B). The same membrane was probed with sequences specific for *neomycin* resistance gene and again the 9 kb band was detected (Figure 3.29B), confirming the targeted insertion of the *neomycin* gene in few ES cells. Three of 45 ES clones were identified to be positive for the homologous recombination.

3.2.1.3 Long-range PCR to confirm homologous recombination

In order to confirm the successful targeting at the *Tcte3* locus, long-range (LR) PCR was carried out by using the DNA from putative heterozygous ES cells detected by Southern blot analysis, encompassing the entire 3'-arm of the targeting vector. The LR-PCR covered the 5.1 kb of the genomic sequence with the primer set Neo3F and Tc-probe-r. The primer Tc-probe-r was located outside the recombination region, while Neo3F primer was neomycin resistance gene specific (Figure 3.29E). LR-PCR by using the primer pair Tc-geno-F (located in the deleted region) and Tc-probe-r amplified only the wildtype *Tcte3* locus of 4.8 kb size (Figure 3.29E). The 5.1 kb LR-PCR product confirms the successful homologous recombination event.

3.2.1.4 Southern blot analysis using 5'-external probe

The recombination event for *Tcte3* locus was further proven by Southern blot analysis using the 5'-end external probe (436 bp). Genomic DNA isolated from R1 ES clones was digested with *Bgl*II restriction enzyme, transferred onto membrane and hybridized with a 5'-external probe (436 bp). Using this probe, heterozygous clones showed two bands: a 4 kb band of the size expected for the endogenous *Tcte3* allele and a 6 kb band characteristic for the recombinant allele (Figure 3.29C). The results of Southern blot analysis using 5'-external probe, 3'-external probe and long-range PCR collectively confirm the successful targeting of *Tcte3* gene.

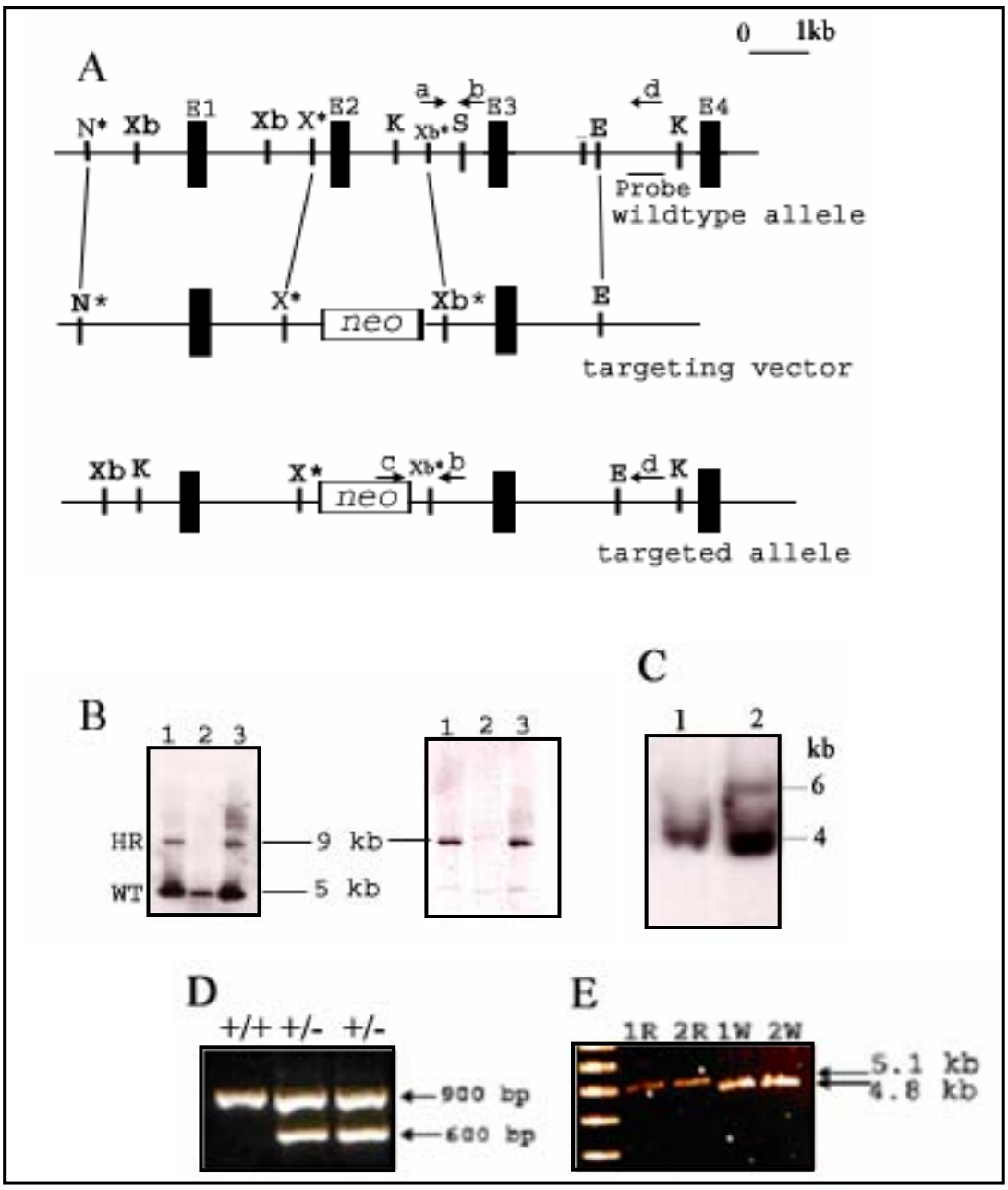

Figure 3.29. Targeted disruption of the *Tcte3* gene by homologous recombination. (A) Schematic representation of the wildtype allele, targeting vector for the disruption of *Tcte3* gene and the recombinant allele. Location of the probe (1.4 kb) used for genotyping the ES cell colonies is shown at 3'-end. Primers used for genotyping PCR are indicated by a;(Tc-fin-f), b;(Tc-fin-r) and c;(Neo3F) (B) Southern blot analysis for screening the ES cells. Genomic DNA from F1 offspring was digested with *Kpn*I restriction enzyme. Using the 3'-external probe, the wildtype allele yields a band of 5 kb, whereas the targeted allele give rise to a hybridisation signal of 9 kb. 1, +/-; 2, +/+; 3, +/-; HR, heterozygous, WT, wildtype. (C) Southern blot analysis using the 5'-external probe. Genomic DNA from F1 offspring was digested with *Bgl*II. The 436 bp external probe gave rise to a 4 kb (wildtype) and 6 kb (mutant allele) hybridisation signal, confirming the homologous recombination. (D) PCR genotyping of F1 offspring. The wildtype allele yields a

PCR product of 900 bp using the Tc-fin-f and Tc-fin-r primers, while the targeted allele is expected to generate a 600 bp fragment using the primers Tc-fin-r and Neo3F. (E) Long-range PCR analysis. Genomic DNA isolated Es cells was amplified by PCR by using the primers: a, Tc-geno-f; c, Neo3F and d, Tc-probe-r. The resulting wildtype PCR product was 4.8 kb (1W, 2W), while in case of recombinant allele, a product of 5.1 kb (1R, 2R) size was obtained. Arrows indicate the position of primers used for genotyping PCR and long-range PCR, restriction endonuclease sites abbreviations are: Xb, *Xba*I; K, *Kpn*I; S, *Spe*I; E, *Eco*RI; N, *Not*I and Xh, *Xho*I. *neo*, *neomycin* resistance gene; asterisks represent the restriction sites deriving from cloning vectors.

3.2.1.5 Production of chimeric mice

The *Tcte3* targeted 129/SvJ ES clones (no.15 and no.32) were cultivated and injected into the 3.5 dpc blastocysts derived from C57BL/6J mice, which were then implanted into pseudopregnant CD1 mice to generate chimeric mice. Nine chimeras were obtained by two independent injections of targeted ES clones. The chimeric offspring were identified by coat colour. Mice with high percentage of chimerism (80% - 100%) were selected for germline transmission and were subsequently bred with C57BL/6 and 129/SvJ female mice, respectively to generate F1 animals in respective background (C57BL/6J x 129/Sv and in 129/Sv). The germline transmission of the mutant allele was verified be genotyping PCR using Tc-fin-F, Tc-fin-R and Neo3F primers (Figure 3.29 D), with the isolated genomic DNA from tail biopsies.

3.2.1.6 Generation of *Tcte3* deficient mice

F1 heterozygotes were intercrossed to produce the homozygous offspring. No change in the sex ratio of *Tcte3* mice for the offspring of the heterozygous matings was noted in both backgrounds (C57BL/6J x 129/Sv and Table 3-5). Surprisingly, no homozygous null mice (*Tcte3*$^{-/-}$) were notified out of 112 C57BL/6J x 129/Sv offspring and 27 129/Sv offspring, derived from the heterozygous intercrosses. In addition, there seemed to be no reduction in litter size (8.6) in comparison to matings of wildtype animals. The ratio of wildtype to heterozygotes was approximately 1: 4 (Table 3-5) and among the 112 live-born offspring, 91 were heterozygous and 21 were wildtype mice (Table 3-5) in the C57BL/6J x 129/Sv genetic background, while in case of 129/Sv inbred background, 18 were heterozygous and 9 were wildtype for *Tcte3* mutation out of 27 animals genotyped (Table 3-5).

Background	+/+		+/-		-/-	
	M	F	M	F	M	F
C57BL/6J x 129/Sv	11	10	42	49	0	0
	21 (18.7%)		91 (81%)		0	
129/Sv	3	6	11	7	0	0
	9 (33.3%)		18 (66.6%)		0	

Table 3-5. Result of the genotype analysis of the F2 generation. In C57BL/6J x 129X1/SvJ hybrid background, the observed ratio was found to be approximately (1:4). A total of 112 animals were genotyped. In 129/Sv inbred genetic background, the ratio was 1:2:0. Total number of animals genotyped in this background is 27. M, male; F, female.

3.2.2 Murine *Tcte3* is present in more than one copy

Huw et al., (1995) suggested that *Tcte3* exists in multiple copies, which are clustered in tandem array in the mouse genome. However, in the database, the sequence of only one gene is indicated (accession number: NT_039641). In order to evaluate the *Tcte3* copy number, genomic DNA isolated from the C57BL/6J mice was digested with multiple restriction enzymes including *Bgl*II, *Nde*I, *Afl*II, *Sma*I, *Eco*RI, *Hind*III, *Hinc*II and *Bam*HI and was probed with the *Tcte3* 5'- probe (436 bp). The expected hybridization signals were: *Bgl*II, 4.3 kb; *Afl*II, 1.7 kb; *Nde*I, 3.8 kb; *Hind*III, 7.4 kb; *Hinc*II, 10.5 kb; *Eco*RI, 13.5 kb; *Bam*HI, 2.8 kb and *Sma*I, 19 kb. Southern blot analysis revealed a complex hybridization pattern (Figure 3.30). Yet presence of more than one signal indicates that *Tcte3* gene is present in more than one copy. One hybridization signal was obtained by *Bgl*II, *Hinc*II, *Kpn*I and *Hind*III restriction enzymes. Extra hybridization signals were detected in DNA restricted with *Afl*II, *Nde*I, *Hind*III, *Eco*RI, *Bam*HI, and *Sma*I. Although the DNA restriction was no complete in some samples (line 6 and 9 in figure 3.30), the resulting hybridisation pattern indicates the existence of more than one *Tcte3* gene in the genome of C57BL/6J mice.

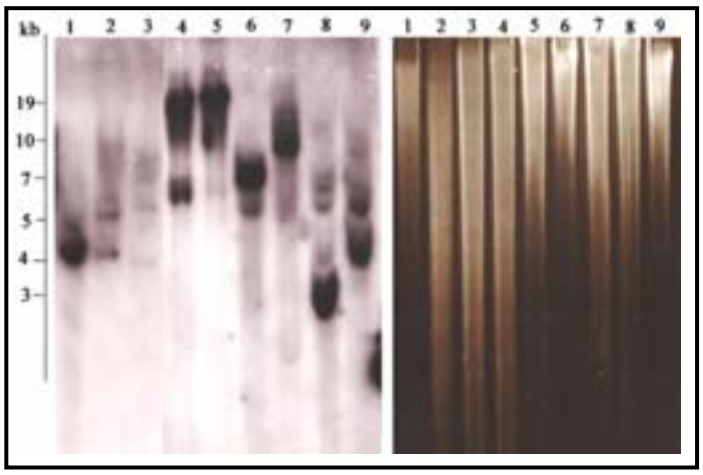

Figure 3.30. Southern blot analysis to determine the *Tcte3* copy number. Genomic DNA from C57BL/6J mice was digested with multiple restriction enzymes: 1, *Bgl*II; 2 & 9, *Nde*I; 3, *Afl*II; 4, *Sma*I; 5, *Eco*RI; 6, *Hind*III; 7, *Hinc*II and 8, *Bam*HI and were probed with the *Tcte3* specific 5'-probe (436 bp). Molecular size markers are indicated at left side. At the right side, agarose gel is shown to visualize the quality of the restriction of genomic DNA's.

3.2.2.1 More than one copy of murine *Tcte3* is transcribed

To investigate whether multiple copies of *Tcte3* genes were active in the mouse, an RT-PCR experiment was performed using adult mouse testicular RNA. Resulting PCR products were cloned into pGEM-T Easy vector and were subsequently sequenced. Three different *Tcte3* cDNA sequences were identified. (1) The original *Tcte3* cDNA sequence represented by A in this study, (2) the splice variant with missing exon-3 and (3) a cDNA sequence similar to *Tcte3* cDNA indicated by 'B' in this study, with the difference of three synonymous polymorphisms, which did not change the open reading frame. One polymorphism resulting in substitution of C into T was located at 5'-UTR, while the other two were present in the putative coding region; 143C>T in exon-2 and 455 C>G in exon-3, respectively.

3.2.3 Genotyping by quantitative real-time PCR

Quantitative real-time PCR is a powerful tool to ascertain putative copy number differences. Due to the putative presence of identical copies of *Tcte3* genes in the mouse genome, genotyping of the mice homozygous for *Tcte3* mutant allele was impossible by conventional genotyping approaches. Therefore, genotyping of *Tcte3* mice was based on doing simultaneous quantitative PCR amplification of the *neomycin* gene (*neo*) using specific

primers (Neo-447f and Neo-597r) for *Tcte3* mice and control homozygous null mice having two copies of the *neomycin* resistance gene (Table 3-6). Amplification of the *pelota* gene on another chromosome (GenBank, NM_134058) was carried out by using the same DNA of *Tcte3* mice for the normalization of each sample DNA concentration. *Pelota* specific primers (pelo-f and pelo-r) of 21-mer were used for the amplification (Sallam, 2001).

Mice no.	Ct. value for neo copies in *Tcte3* mice	Quantity-neo1	Ct. value for neo copies in -/- mice	Quantity-neo2	neo1/neo2	mean	st.dev
1	24,257	7,550	23,330	7,037	1,07	**0,958**	0,16
	24,514	6,377	23,219	7,571	0,84		
2	23,596	11,657	22,644	11,076	1,05	**1,052**	0.11
	23,709	10,818	22,828	9,90	1,09		
3	25,235	3,969	24,289	3,729	1,06	**1,024**	0,06
	25,465	3,413	24,397	3,471	0,98		
4	24,078	8,494	23,242	7,459	1,14	**1,145**	0,01
	24,244	7,612	23,425	6,607	1,15		
5	23,848	9,880	22,786	10,085	0,98	**0,998**	0,03
	23,828	10,008	22,823	9,842	1,02		
6	22,871	18,776	21,834	17,725	1,06	**1,008**	0,07
	23,027	16,943	22,786	16.265	0,96		
7	25,185	4,101	23,366	6,870	0,60	**0,554**	0,06
	25,245	3,943	23,188	7,729	0,51		
8	25,731	2,866	23,598	5,891	0,49	**0,459**	0,04
	25,979	2,434	23,665	5,635	0,43		
9	25,344	3,695	23,331	7,029	0,53	**0,536**	0,01
	25,234	3,971	23,279	7,278	0,55		
10	25,642	3,038	23,805	5,139	0,59	**0,563**	0,04
	25,876	2,605	23,887	4,866	0,54		
11	24,207	7,802	22,276	14,135	0,55	**0,488**	0,09
	24,390	6,916	22,060	16,309	0,42		
12	25,019	4,577	22,830	9,795	0,47	**0,500**	0,05
	24,913	4,904	22,925	9,195	0,53		

Table 3-6. Real-time PCR genotyping results of *Tcte3* heterozygous and homozygous mice. Ct. indicated the threshold cycle; the value used in the calculation of template quality during quantitative real-time PCR.

The amplification curve for two copies of the *neomycin* cassette was achieved in the exponential phase at the 23rd cycle (Figure 3.31A), while for one copy of neomycin cassette, a shift of approximately 2 more cycles was occurred and the amplification plot was obtained at the 25th cycle (Figure 3.31A). *Insl5*$^{-/-}$ (Shrinshaan, 2005) and *alt*$^{-/-}$ mice (Altmann, 2000) having two copies of the *neomycin* resistance gene were used as a measure of accurate amplification (Figure 3.32, mice no. 5 and 6). A total of 47 F2 animals were tested by real-time PCR, out of which, 10 were wildtype, 26 were heterozygous, while 11 mice were found to be homozygous for the *Tcte3-A* mutation (Table 3-7).

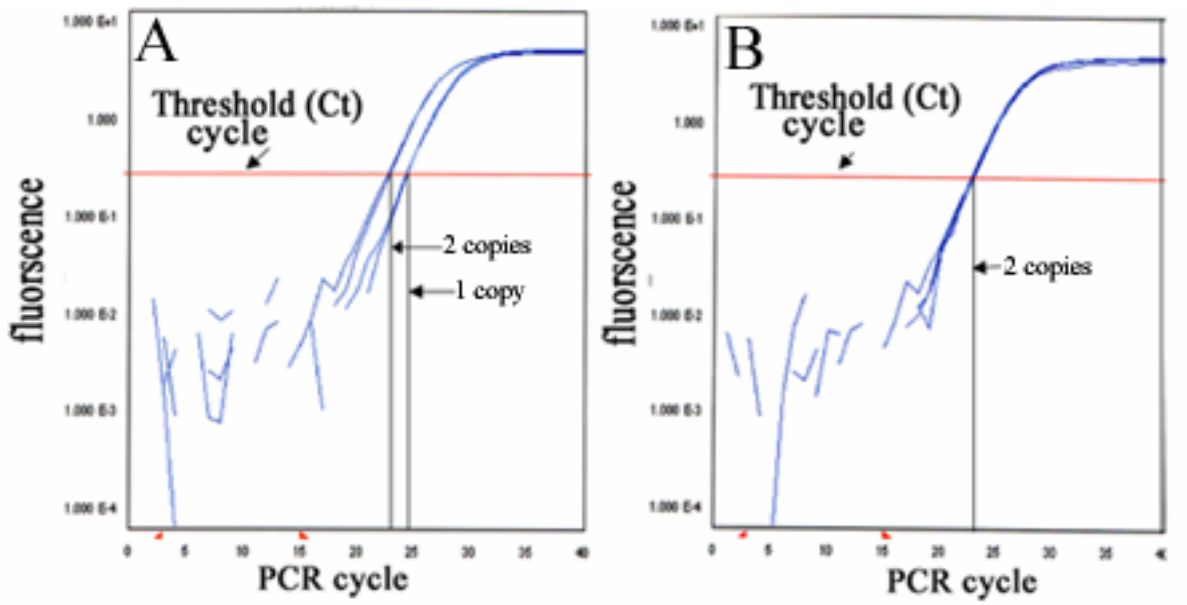

Figure 3.31. Amplification profile for *neomycin* copy number. Number of the *neomycin* resistance gene was calculated by software by plotting the log of copy number versus cycle number. (A) The amplification plot for mice containing two copies of the *neomycin* resistance gene needed less cycles to shift from the initial linear phase to the exponential phase, while amplification plot for one *neomycin* copy was needed 25 cycles. (B) The amplification plot for one and two copies of *neomycin* gene is shown.

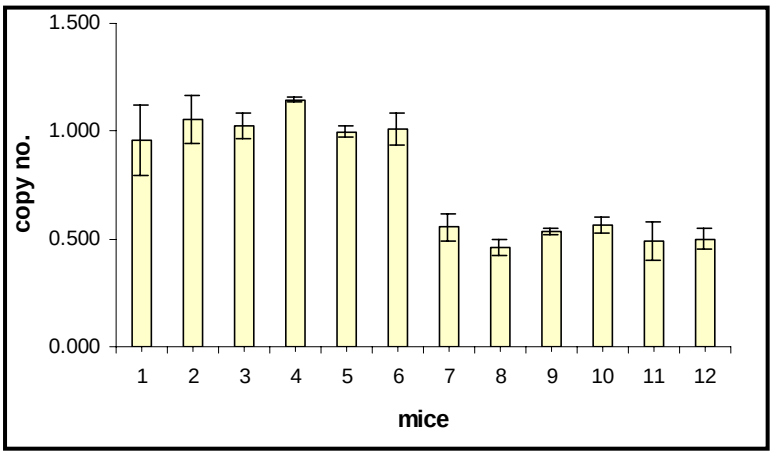

Figure 3.32. Quantitative real-time PCR analysis of *Tcte3* mice. The average mean calculated for the quantity of neomycin for each sample is plotted versus number of mice. Putative homozygous mice for *Tcte3 (Tcte3$^{-/-}$)* having two *neomycin* copies are represented by a mean of approximately 1 (no 1-6), while the heterozygous mice containing one *neo* copy (*Tcte3$^{+/-}$)* have a mean for quantity approximately 0.5.

No. of offspring	+/+	+/-	-/-
47	10	26	11

Table 3-7. Analysis of the genotype for the *Tcte3* locus of mice from F2 generation, genotyped by quantitative real-time PCR. A total of 47 animals were tested.

3.2.4 Generation of a Tcte3-GST fusion protein

Tcte3-GST fusion constructs generated as described in 2.2.14.1 were used to transform expression host bacterial BL21 cells and to produce the recombinant proteins. Isolated and purified proteins (2.2.14.3) were subjected to SDS-PAGE electrophoresis, blotted to PVDF membrane. The 62 kda Tcte3-GST fusion protein was detected by anti-His antibodies (Figure 3.33A). The purified Tcte3-GST fusion protein was used for the generation of a rabbit Tcte3 antiserum. In order to isolate the antibody of interest from the polyclonal serum, Strep-Tcte3

fusion proteins were generated (2.2.14.3). The Strep-Tcte3 fusion protein was blotted onto a PVDF membrane and incubated with rabbit α-Strep A, which detected a protein of 28 kDa (Figure 3.33B). The Strep-Tcte3 fusion proteins were used for the purification of Tcte3 polyclonal antibodies (2.2.14.3). The purified Tcte3 specific antibodies were checked by Western blot (Figure 3.33C) and immunohistochemical analyses (Figure 3.34).

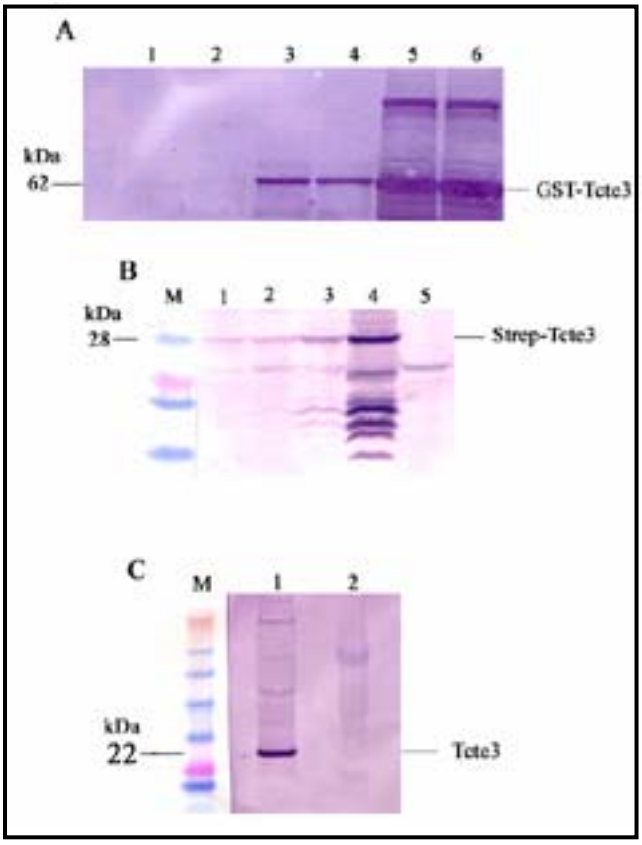

Figure 3.33. Generation of polyclonal antibodies against *Tcte3*. (A) Tcte3-GST fusion protein was induced by 10 ml of 100mM IPTG for 4 hrs. The induced protein was purified by affinity chromatography using GST-Bind Kit (2.2.14.1) and the corresponding proteins were tested by Western blot analysis by incubating the PVDF membrane with anti-His antibodies. (1,2) Fluid fractions after chromatography; (3,4) purified fusion protein; (5,6) cell debris fraction protein. (B) Strep-Tcte3 fusion protein was generated for the purification of Tcte3 specific antibodies (2.2.14.3) and was confirmed by immunoblotting with anti-Strep A, which recognized the 28 kDa Step-Tcte3 fusion protein. (1-4) Induction for 2 hrs, 3 hrs, 4 hrs and overnight, respectively, (5) uninduced protein. (C) Tcte3 polyclonal antibodies were purified through the sera obtained from immunized rabbits and were tested by Western blot analysis. A Tcte3-specific protein size of about 22 kDa was recognized in the testicular extract (1), while in heart protein (2) no signal was detected.

3.2.4.1 Immunostaining of mouse spermatozoa

Purified antibodies were used to localize Tcte3 protein in mouse sperm. The spermatozoa prepared from cauda epididymis were subjected to indirect immunofluorescence microscopy by incubating with Tcte3-specific and α-tubulin antibodies. Tcte3 protein was detected along the entire axoneme of sperm flagella supporting that Tcte3 is a part of the axonemal complex (Figure 3.34).

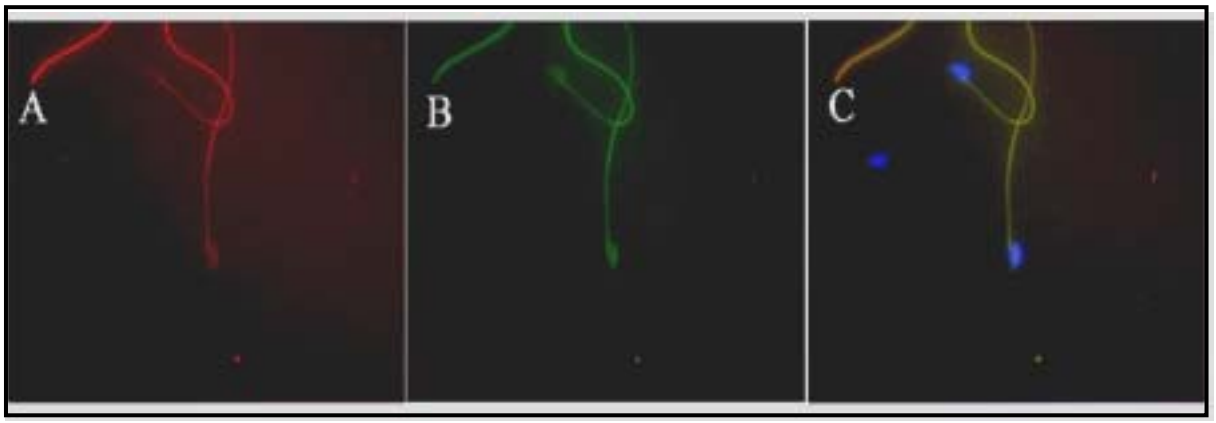

Figure 3.34. Mature spermatozoa isolated from mouse epididymes were incubated with purified Tcte3-specific and α-tubulin antibodies (A-C). Tcte3-specific antibodies staining was visualized by Cy3-conjugated anti-rabbit secondary antibodies (A; red colour) and tubulin was detected using FITC conjugated anti-mouse IgG (B; green colour). Nuclei were counterstained with DAPI (C; blue colour). The Tcte3 staining was detected along the entire axoneme of sperm flagella. No staining was observed in spermatozoa incubated with only secondary antibodies.

3.2.5 Characterization of *Tcte3* deficient mice

3.2.5.1 Transcriptional analysis

In order to assess the *Tcte3* transcript in the *Tcte3* mice, a Northern blot experiment was performed using testicular RNA from wildtype, heterozygous and homozygous animals of about 50 days of age. The filter was hybridized with the *Tcte3-A* cDNA probe (Figure 3.35A). To check the integrity of RNA, the filter was rehybridized with a *β-actin* cDNA probe. Northern blot analysis showed absence of *Tcte3* transcript in the *Tcte3*$^{-/-}$ animals (genotyped by real time PCR), indicating that, owing due to the integration of the *neomycin* cassette, the expression of *Tcte3* is hampered (Figure 3.35A). However, by RT-PCR analysis

using the testicular RNA from *Tcte3*$^{-/-}$ mice, a very faint transcript was detected owing to the *Tcte3* additional transcript presence (Figure 3.35B).

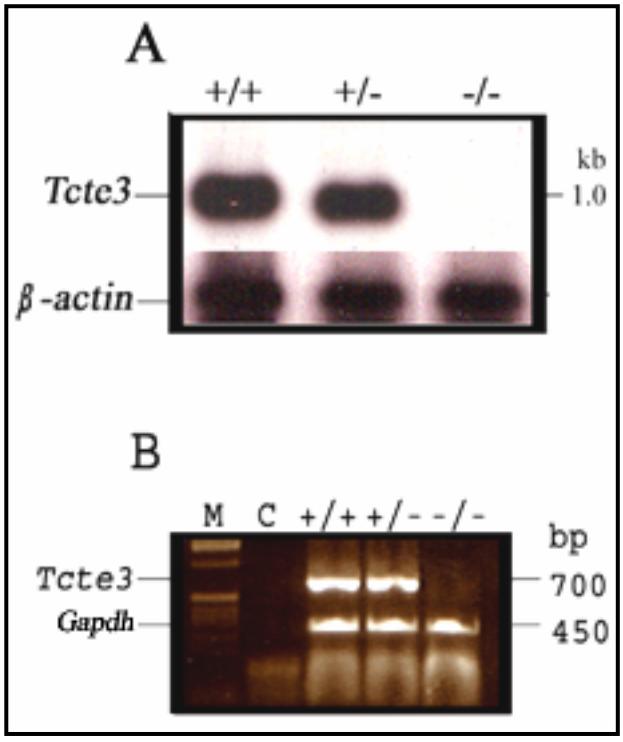

Figure 3.35. Transcriptional analyses of *Tcte3* deficient mice. (A) Northern blot analysis of testicular RNA from *Tcte3* wildtype, heterozygous and homozygous mice 50 days old. The *Tcte3* whole cDNA (700 bp) probe detected a specific transcript of about 1 kb. Variation of the loaded RNA was checked by hybridising the same blot with a *β-actin* cDNA probe. (B) RT-PCR analysis for *Tcte3* expression in testis. *Tcte3* specific product (700 bp) was detected both in the wildtype and heterozygous mice, while in *Tcte3*$^{-/-}$ mice, a very faint transcript of the same size was notified. Integrity of RNA was verified by *Gapdh* primers amplification (450 bp).

3.2.5.2 Translational analysis

Total testicular protein extracts from wildtype, heterozygous and mutant mice were prepared and subjected to SDS-PAGE electrophoresis. Western blot analyses were performed using affinity purified anti-Tcte3 antibodies, which detected a protein of 22 kDa size corresponding to the Tcte3 protein both in the wildtype and heterozygous mouse testis, while Tcte3 protein is absent in the testicular extract of the mutant mice (Figure 3.36).

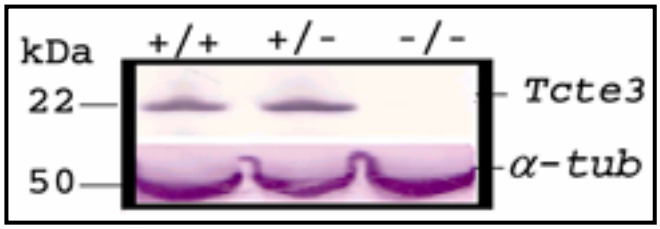

Figure 3.36. Western blot analysis of Tcte3 protein expression in Tcte3 knockout mice. Blot was incubated with anti-Tcte3 antibodies, which recognize a protein of 22 kDa in the total testicular extracts of wildtype and heterozygous mice but not in the mutant testis. No additional band corresponding to the Tcte3 protein was detected in testicular extract. Blot was incubated with α-tubulin antibodies to track the loaded protein in a quantitative manner.

3.2.5.3 Immunohistochemistry

Testes from wildtype and *Tcte3-A* deficient mice were fixed by immersion in Bouin's fixative and were embedded in paraffin wax. Five μm sections were incubated with Tcte3 specific antibodies for overnight and immunoreactivity was detected using alkaline phosphatase conjugated α-rabbit IgG secondary antibody. Specific staining of the Tcte3 was obtained in pachytene spermatocytes in the wildtype testis (Figure 3.37A) but none was detected in the testis of *Tcte3* homozygous null mice (Figure 3.37B).

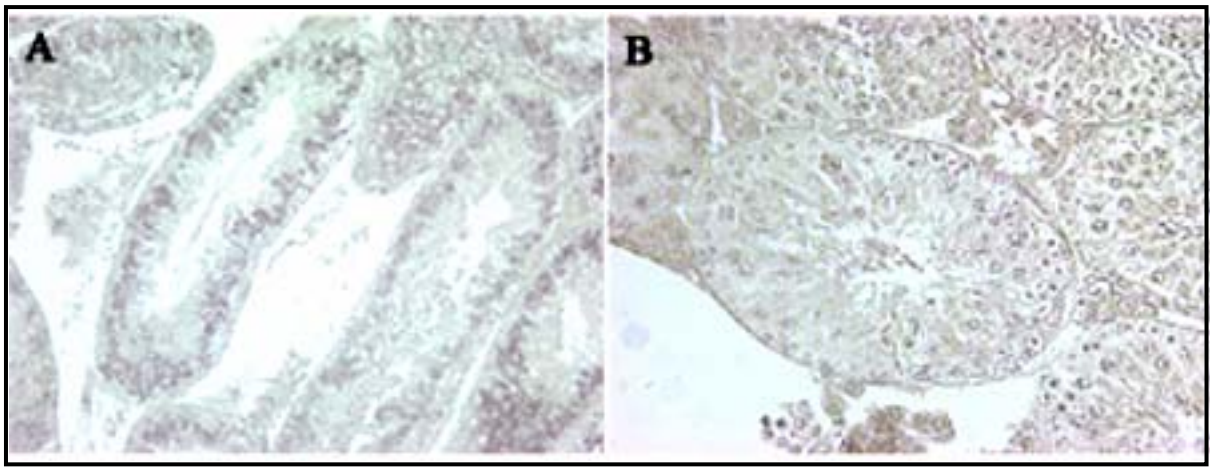

Figure 3.37. Immunohistological analysis of testes from *Tcte3-A* deficient and wildtype mice with Tcte3 specific antibodies. Wildtype testis (A) exhibit Tcte3 staining in the pachytene spermatocytes and later germ cell stages while no staining is observed in testes of *Tcte3-A* deficient mice (B).

3.2.5.4 *Tcte3-A* deficient male mice are infertile

Tcte3-A deficient mice were identified by quantitative PCR genotyping (3.2.5). *Tcte3* offspring derived from heterozygous parents, genotyped by quantitative real-time PCR displayed a normal Mendelian distribution (Table 3-7). Ten *Tcte3*$^{-/-}$ males at the age of 2 months were bred with *Tcte3* deficient and heterozygous females for 2-3 months. During this time, all females revealed vaginal plugs, but no pregnancies were recorded, indicating that *Tcte3*$^{-/-}$ male mice are infertile. However, breeding of *Tcte3*$^{-/-}$ females with wildtype males resulted in a normal amount of offspring and on genotyping PCR, all offspring were found to be heterozygous.

3.2.5.4.1 Sperm count and sperm motility analysis of *Tcte3* mutant males

In order to elucidate the causes of male infertility, the reproductive tracts of *Tcte3-A* deficient males were investigated. The total sperm number was determined in the cauda epididymes as well as in the uteri and oviducts of 4 females mated with the *Tcte3*$^{-/-}$ males (Table 3-8). Total sperm number in cauda epididymes of *Tcte3*$^{-/-}$ males was in the average of 1.6 ± 0.24 x (10^5) on C57BL/6J x 129/SvJ background, which is significantly reduced as compared to the wildtype; 1.9 ± 0.4 x (10^7). Number of spermatozoa in the oviducts and uteri of four females bred with *Tcte3*$^{-/-}$ males were 0.13± 0.7 x (10^1) and 1.5 ± 1.24 x (10^3), respectively (Table 3-8).

No. of sperm in	Genotype of male	
	+/+	-/-
Epididymis	1.9 ± 0.4 x (10^7)	1.6 ± 0.24 x (10^5)
Uterus	5.8 ± 1.5 x (10^3)	1.5 ± 1.24 x (10^3)
Oviduct	20 ± 2.9 x (10^1)	0.13 ± 0.7 x (10^1)

Table 3-8. Sperm analysis in wildtype and *Tcte3*$^{-/-}$ male mice. Data represent the mean ±SEM of the four individual measurements.

3.2.5.4.2 Sperm motility assay

Analysis of sperm motility for *Tcte3*$^{-/-}$ mice was done only on the C57BL/6J x 129/SvJ background due to the low number of 129/SvJ males (Table 3-5). The sperm motility of 2 wildtype males and five mutant males was measured at 1.5, 3.5 and 5.5 hrs incubation *in vitro*, using the Hamilton Thorne computer assisted sperm analyser. At 1.5 hrs, the proportion of motile spermatozoa of *Tcte3*$^{-/-}$ mice was reduced considerably (31%) as compared to wildtype mice (76%), (Table 3-9). A clear distinction (17.5%) was observed in the progressive movement in *Tcte3*$^{-/-}$ versus wildtype mice (54%), (Table 3-9). Similar observations were notified at 3.5 hrs and 5.5 hrs. At 3.5 hrs and 5.5 hrs, the difference in the motile spermatozoa of *Tcte3*$^{-/-}$ and wildtype mice was approximately 64% and 77% while in the degree of progressive spermatozoa the difference was 78% and 95%, respectively, as compared to the wildtype littermates (Table 3-9). The other parameters including, curvilinear velocity (VCL), average path velocity (VAP), Linearity (LIN), straight-line velocity (VSL), beat cross frequency (BCF), straightness (STR) and amplitude of the lateral head displacement (ALH) were also evaluated and statistically analysed (Figure 3.38). For the linearity (LIN), lateral head amplitude (ALH), curvilinear velocity (VCL) and straightness (STR), reduction was not significant at 1.5 h; LIN (3%), ALH (10%), VCL (0.01%), STR (1%). For other parameters like path velocity (VAP); beat frequency (BCF); and progressive velocity (VSL); a significant reduction of about 31%, 45% and 32% was observed (Figure 3.38) for *Tcte3*$^{-/-}$ spermatozoa in comparison to the wildtype ($P < 0.001$).

Genotype of male	Incubation time (hours)	Total no. of measured spermatozoa (%)	No. of motile spermatozoa (%)	No. of spermatozoa with progressive movement (%)
+/+	1.5	2895 (100)	2196 (76)	1575 (54)
	3.5	3069 (100)	2066 (67)	1356 (44)
	5.5	3681 (100)	2245 (61)	1520 (41)
-/-	1.5	4259 (100)	1326 (31)	748 (17.5)
	3.5	3974 (100)	1054 (26)	582 (14)
	5.5	4204 (100)	833 (19.8)	453 (10.7)

Table 3-9. Analysis of the sperm motility of *Tcte3*$^{-/-}$ and *Tcte3*$^{+/+}$ mice.

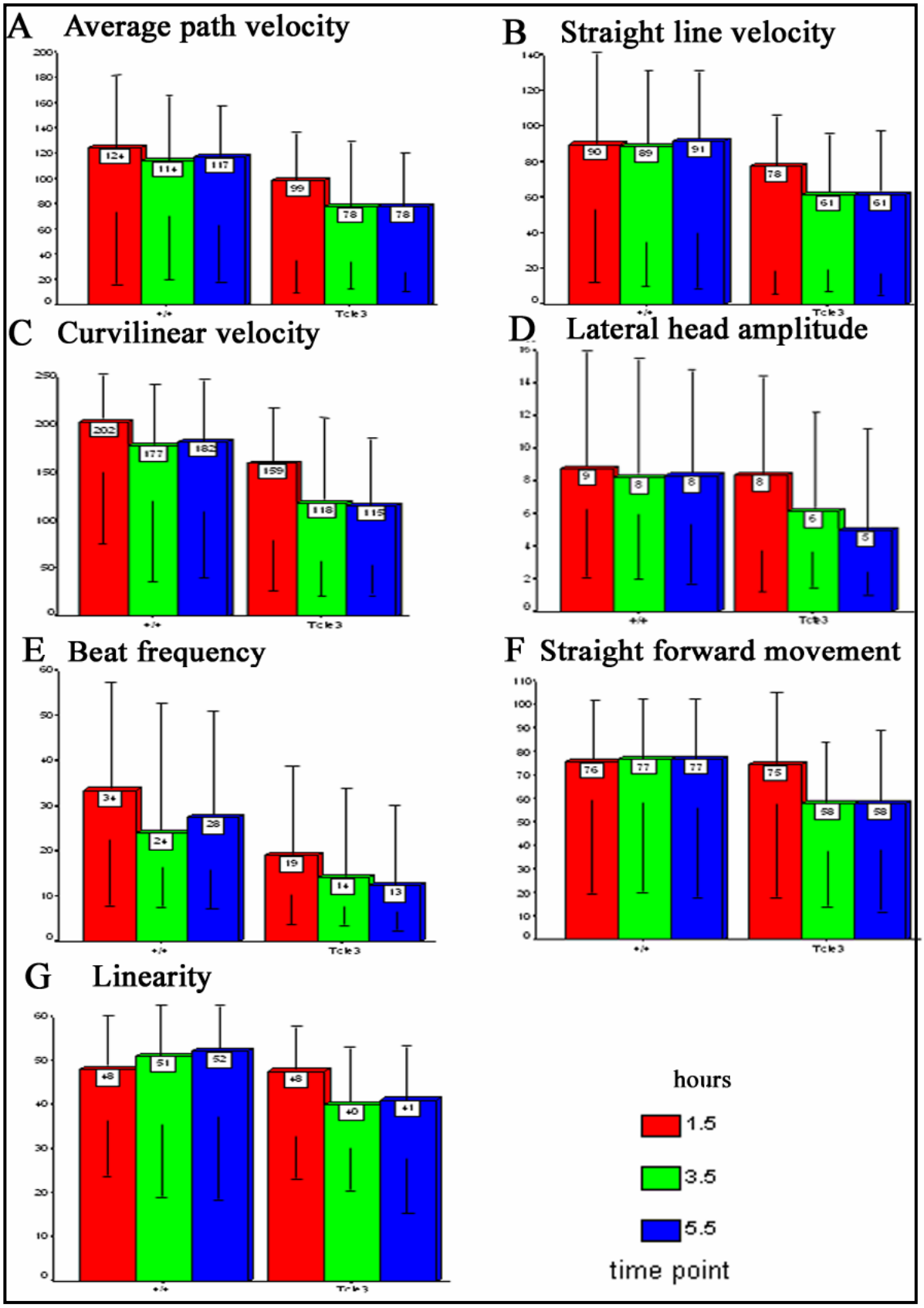

Figure 3.38. Computer-assisted analysis of sperm motility. The results of analyses of wildtype and Tcte3$^{-/-}$ spermatozoa are shown. Sperm velocities (μm/sec), forward movement (%), lateral

amplitude of the sperm head beat (μm) and beat frequency (Hz) were measured at 1.5, 3.5 and 5.5 hrs. For all parameters, the medians and percentiles are shown. The Tcte3 deficient spermatozoa exhibit significantly reduced path velocities, track speed, beat frequency and progressive velocities in comparison to wildtype spermatozoa (P < 0.001 by Mann-Whitney U-Test), while in case of straight forward movement and linearity, the differences were not significant. Median (25%-75%), Percentile (5-95%).

3.2.5.4.3 Testis histology

Given that the epididymal sperm count was significantly reduced (Table 3-8), the stage of spermatogenic arrest was examined by histology (Figure 3.39). Examination of the *Tcte3*$^{-/-}$ males revealed that testis development was affected in these mice. The testis in *Tcte3*$^{-/-}$ males was smaller (70.3 ± 10.1 mg) than in their wildtype littermates (90.2 ± 9.3 mg). Subsequent histological analysis indicated no abnormalities in the periphery of the seminiferous tubules of *Tcte3*$^{-/-}$ animals (Figure 3.39A), where spermatogonia and Sertoli cells are located. In contrast, spermatocytes were significantly reduced in number (30%), while postmeiotic stages spermatids and spermatozoa, were largely absent in mutant testis and epididymes (Figure 3.39A). In 50-60% round and elongated spermatids, a double tail formation was observed. Head abnormalities were also evident in sperms found in the epididymes (Figure 3.39 C and D). Type A spermatogonia with large spherical nuclei (subtype I) were located normally, at the base of epithelium. One or two dense nucleoli were also observed inside the nucleus. Chromatin appeared to be homogeneously stained in the nucleoplasm, avidly by the toluidine blue dye. These cells were identified as ‘dark spermatogonia’. Very few cells among the dark spermatogonia were in the dividing phase of cell cycle. The spermatogonia belonging to the second subtype (subtype II) containing round nuclei with a large number of heterochromatin clumps was also evident (Figure 3.39B). The third type of spermatogonia had the most characteristic features of reduced avidity for toluidine blue dye, thus termed as ‘pale spermatogonia’.

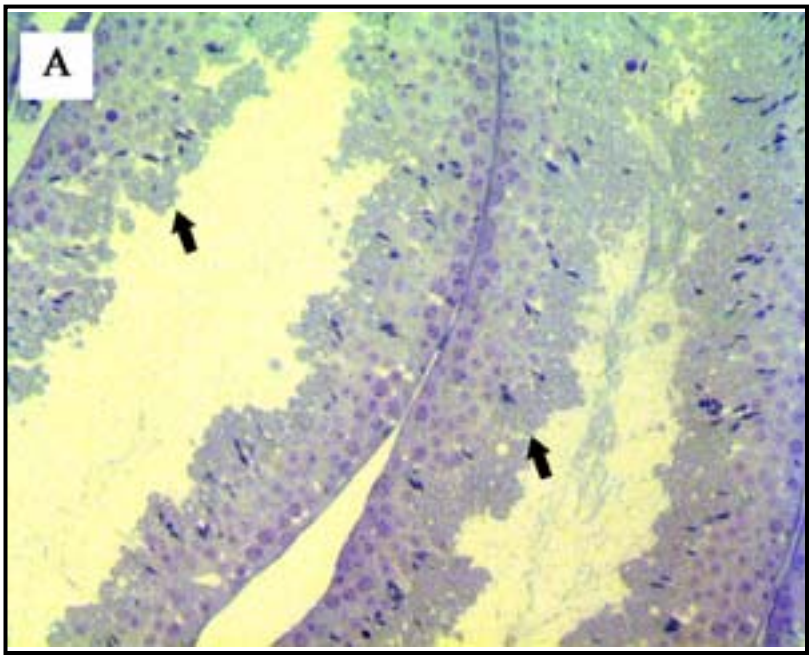
A

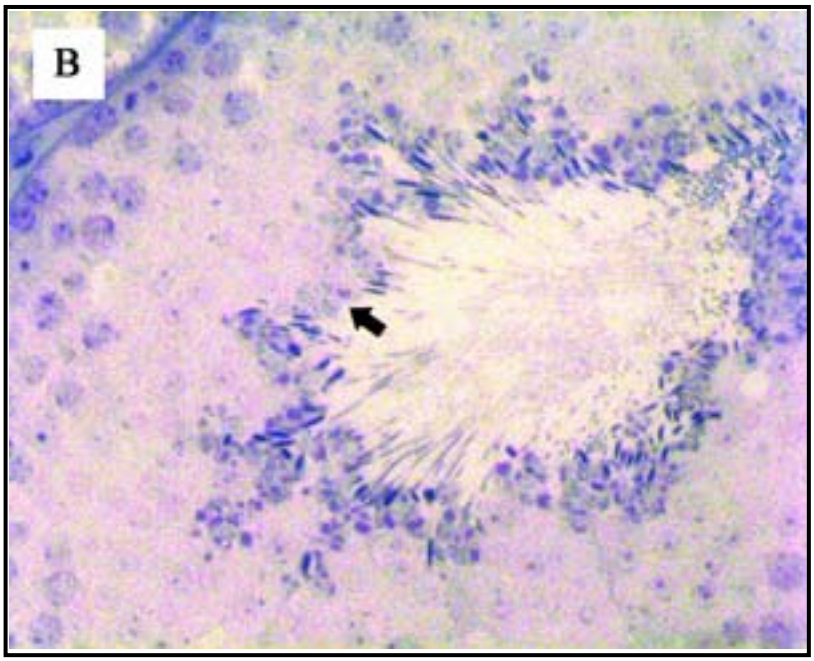
B

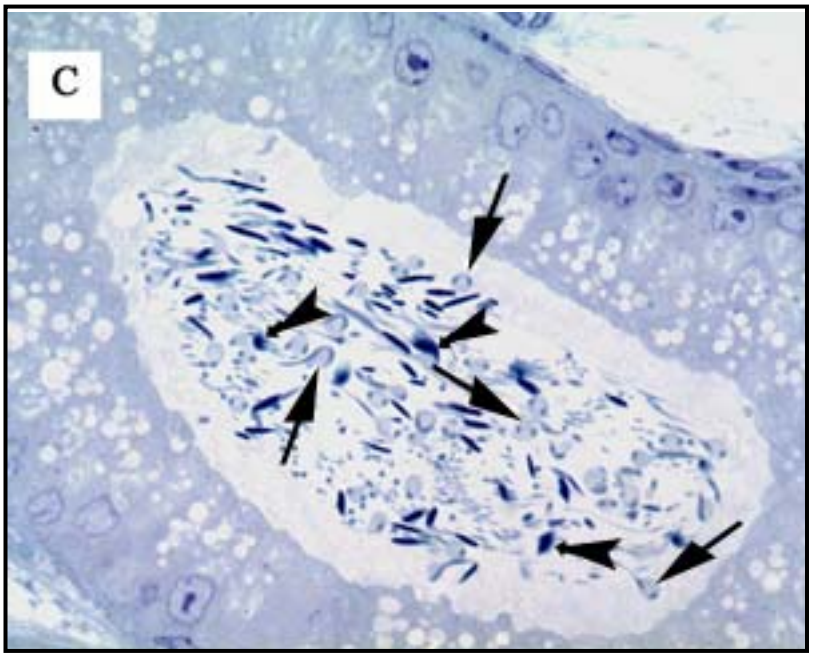

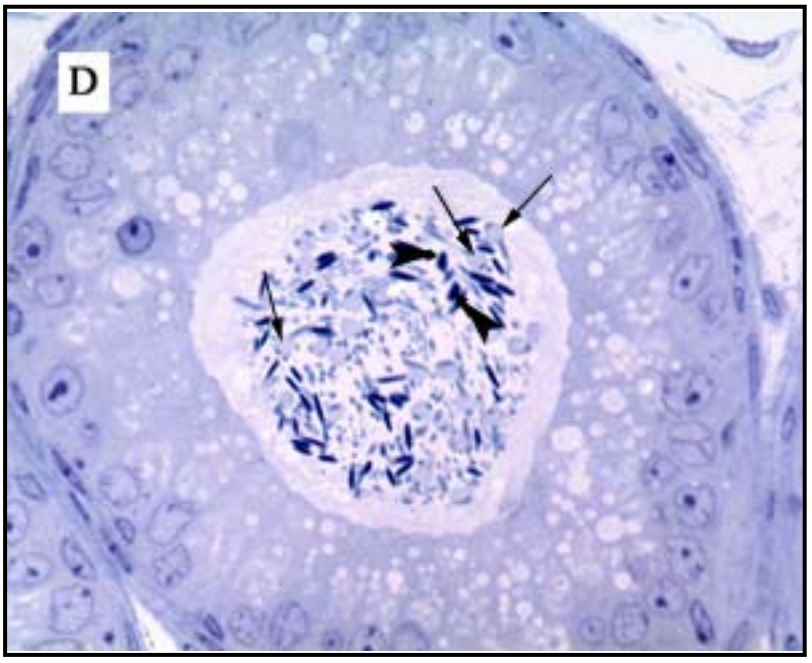

Figure 3.39. Light microscopy of epididymes and testis sections of *Tcte3*$^{-/-}$ mice. Thin sections of seminiferous tubule (A-B) and epididymes (C-D) from 2 months old *Tcte3*-A deficient mice were stained with toluidin blue. Spermatozoa stained dark blue with toluidine were undergoing apoptosis. Arrows show the double tail formation and the bend tail cross-section, while black arrowheads represent the malformed sperm heads, typically apoptotic cells. (A, B) Incomplete spermiation can be seen in the testis of the *Tcte3*$^{-/-}$ mouse.

3.2.5.4.4 Primary spermatocytes undergo apoptosis

Testicular degeneration found in *Tcte3*$^{-/-}$ mice suggested that spermatogenic cell apoptosis is enhanced in the *Tcte3*$^{-/-}$ testis. Therefore, terminal deoxynucleotidyltransferase-mediated dUTP nick end labelling (TUNEL) assay was performed with testicular sections of *Tcte3*$^{-/-}$ mice aged 3 months to assess the possible cell death rate. The regions in the *Tcte3*$^{-/-}$ seminiferous tubules where prophase I stages predominated were characterized by a high frequency (more than 50%) of cell death (Figure 3.40 C and D). At higher magnification, the majority of the labelled cells were pachytene and metaphase spermatocytes in most of the testicular tubules from *Tcte3*$^{-/-}$ mice (Figure 3.40B). In contrast, cell death was rare in the wildtype testis (Figure 3.40A).

Incidence of apoptosis was found different per seminiferous tubule in a varying degree of 10-60% (Figure 3.40 C and D). Quantification of apoptosis was carried out by counting the apoptotic germ cells that were clearly stained by the TUNEL assay (Table 3-10). A total of 25 randomly selected seminiferous tubule cross-sections were analysed from each of two mice. The rate of germ cell apoptosis was expressed as the number of apoptotic cells per tubule (Figure 3.41). This result suggests that germ cell development in the *Tcte3*$^{-/-}$ mice is already impaired before the appearance of round spermatids and that spermatid development could arise from the remaining viable cells.

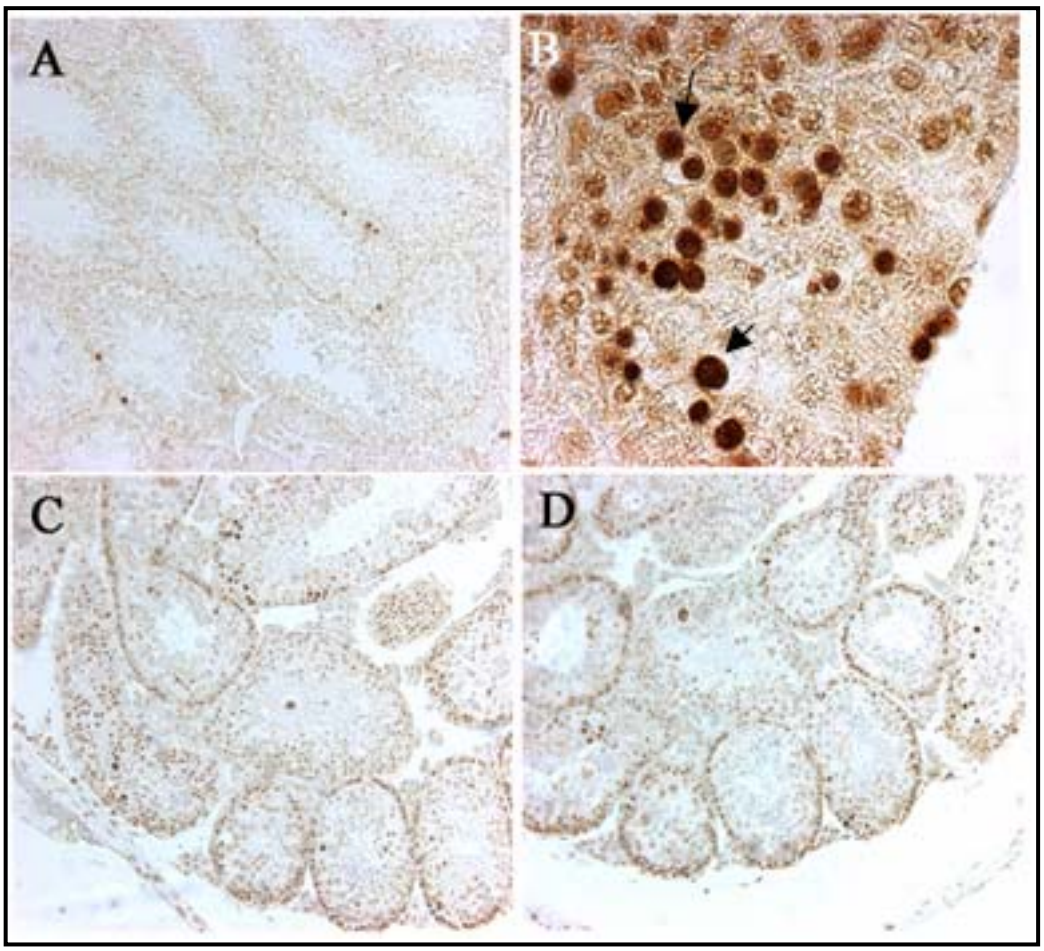

Figure 3.40. Apoptotic assay of *Tcte3*$^{-/-}$ testis (B-D). The TUNEL assay indicated that degenerating cells were undergoing apoptosis. (B) Many apoptotic bodies (black arrowheads) revealed by the deposition of dark brown reaction product. (C, D) Seminiferous tubules having numerous fully apoptotic cells or the cells (weakly stained) with the beginning of apoptotic incidence.

Genotype	% of seminiferous tubules with the no. of TUNEL positive germ cells	% or number of TUNEL positive cells per tubule
+/+	12	2.4 ± 0.91
-/-	73	27.2 ± 0.97

Table 3-10. TUNEL analysis was performed for *Tcte3*$^{-/-}$ testis sections. Values represent the mean ±SEM from two wildtype and two *Tcte3*$^{-/-}$ mice.

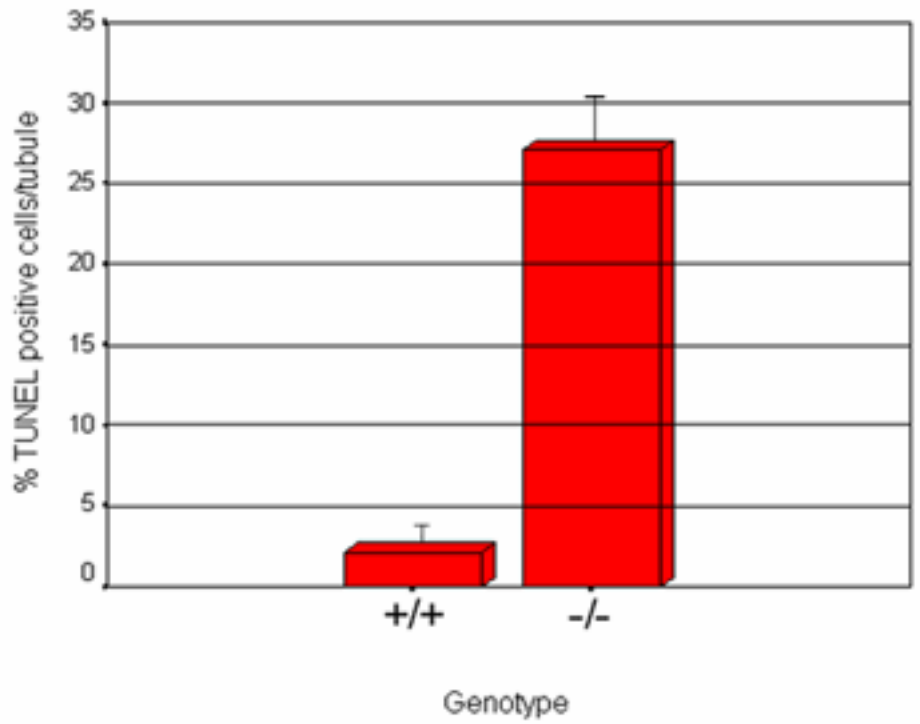

Figure 3.41. Quantification of the incidence of TUNEL-positive germ cells in wildtype and *Tcte3*$^{-/-}$ mice. A total of 25 randomly selected seminiferous tubule cross-sections were analysed from each of two mice. A sharp increase in the TUNEL-positive cells was observed in the *Tcte3-A* deficient mice. Percentage was calculated for seminiferous tubules having at least one TUNEL positive cell.

3.2.5.4.5 Electron Microscopy

Transmission electron microscopy (TEM) was used to further characterize the defective cells in the mutant testis (Figure 3.42). The Leydig cells seemed to be normal. In the cytoplasm of Sertoli cells and elongated spermatids large vacuoles were observed. TEM provided additional evidence that cell death in the *Tcte3*$^{-/-}$ testis was primarily occurring in the spermatocytes and occasionally in spermatids. Some spermatids exhibited a normal morphology with elongated nucleus, however, a greater number (25-30%) of degenerating spermatocytes and elongated spermatids with a lot of residual bodies were also observed in the *Tcte3*$^{-/-}$ testis (Figure 3.42B). Some putative spermatids, which were in the late stages of apoptosis, could not unequivocally be identified. Small clumps of heterochromatin could be distinguished in the nuclei of the cells in early stages of apoptosis. In the later stages of degeneration, the areas of heterochromatin became larger. Condensed chromatin and irregular pattern of organelles were seen in latest stages of apoptosis (Figure 3.42G). Axonemal tail sections of spermatozoa analysed by EM demonstrated the presence of normal 9+2 axonemes.

The arrangement of the inner and outer dynein arms, that generate the relative sliding movements between the outer doublet microtubules were detected normally (Figure 3.42C). Late spermatocytes and round spermatids exhibiting the degeneration, ranging from the nuclear condensation to the formation of abnormal sperm heads resulted in an abrupt arrest of spermatogenesis during the late meiotic prophase in *Tcte3*$^{-/-}$ males. Secondary spermatocyte and round spermatids, which had escaped from the degeneration, were occasionally harboured biflagellate pattern during the elongation step (Figure 3.42E, F and H).

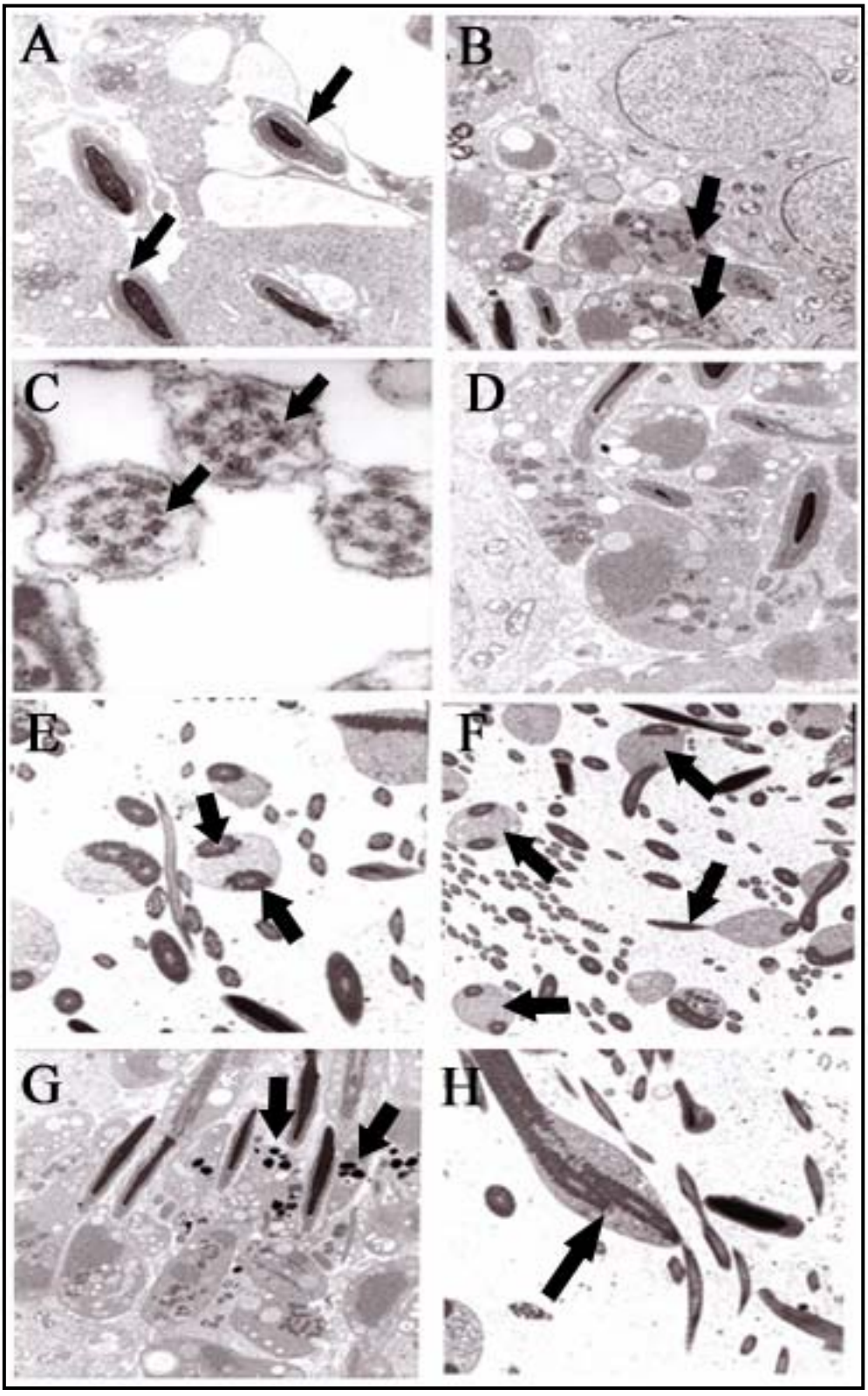

Figure 3.42. Morphological analysis of *Tcte3*$^{-/-}$ testis by electron microscopy. (A) High incidence of vacuolisation in the cytoplasm of elongated spermatids and Sertoli cells was observed (arrowheads). (B, G) Some spermatids with normal nucleus encompassing the acrosome, at the lower side, number of degenerating spermatids with residual bodies were detected. Arrowheads indicate spermatids undergoing apoptosis. (C) Axonemal cross sections revealed the presence of

normal outer dynein arms. (D) Degenerated elongated spermatids. (E, F and H) sperm exhibiting two flagella.

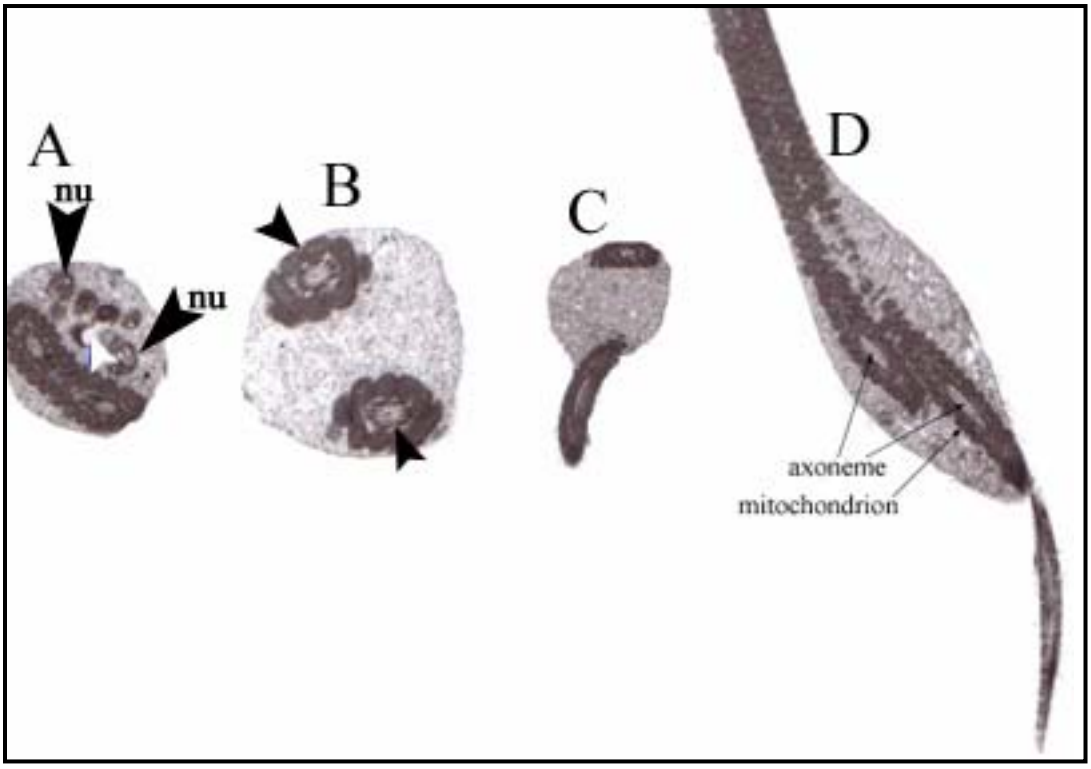

Figure 3.43. Detailed overview of biflagellation in *Tcte3*$^{-/-}$ spermatids. (A) *Tcte3*$^{-/-}$ spermatids with multiple nuclei were observed (indicated by black arrowheads). Some nuclei contained vacuoles (indicated by white arrowhead). Multi nucleation was evident in the spermatid with numerous nuclei sharing a common cytoplasm. (B-D) *Tcte3*$^{-/-}$ spermatids showing biflagellation.

4. DISCUSSION

Dyneins are complex, microtubule-dependent molecular motors, which can be classified into cytoplasmic and axonemal dyneins. The axonemal dyneins can be further divided into outer arm, inner arm I1, and inner arms I2/I3 motors (Witman et al., 1994). The flagellar dyneins generate motive force by causing interdoublet microtubule sliding that is ultimately converted to an axonemal bend (Warner et al., 1989). The outer arms provide most of the power for flagellar beating, whereas the heterogeneous inner arm system appears responsible for the initiation of a flagellar bend and for the shear amplitude of the propagated wave (Kamiya et al., 1989). Cytoplasmic dyneins exhibit a wide range of functions (for review: Karki and Holzbaur, 1999; King, 2000). The number of heavy chains (HCs), intermediate chains (ICs), light intermediate chains (LICs) and light chains (LCs) that each member of the diverse dynein groups contains, is summarized in the Table 4-1.

It is unclear whether each dynein light chain (LC) plays a specific role in a subset of dynein functions. Specifically, the observation that LC mutants do not exhibit as severe phenotype as dynein heavy chain mutants supports the non-equivalent phenotypes among LC mutants in *Chlamydomonas*. However, the presence of high homology among the LCs suggests that their functions in axonemal and cytoplasmic dyneins may be homologous.

Component	Cytoplasmic dynein	Outer arm dynein	Inner arm dynein I1	Inner arm dynein I2/3
HC	2	2-3	2	1
IC	2	2-3	3	-
LIC	+	-	-	-
LCs				
Ca2+ binding	-	+	-	-
LC1	-	+	-	-
Thioredoxin	-	+	-	-
LC8	+	+	+	-
Tctex1	+	+	+	-
LC2	+	+	+	-
LC7/roadblock	+	+	?	-
Actin	-	-	-	+
p28	-	-	-	+
Centrin	-	-	-	+

Table 4-1. Composition of cytoplasmic and flagellar dynein in *Chlamydomonas*. HC, heavy chain; IC, intermediate chain; LIC, light intermediate chain; LC, light chain; +, present; -, absent; ?, unknown.

However, despite the well-characterized data of dynein chains in *Chlamydomonas*, we know very little about the precise functions and protein interactions of the dynein light chains in mammals. Herein, we describe the functional analyses of two murine dynein light chain genes *Dnali1* and *Tcte3* by homologous recombination to uncover their putative roles in mammals.

4.1 Characterization of the murine *Dnali1* (Dynein, axonemal, light intermediate polypeptide 1) gene

4.1.1 Dnali1 is not uniquely an axonemal component

By RT-PCR experiment, *Dnali1* transcript was detected in almost every tissue including testis, ovary, brain, lung, trachea, kidney, colon, placenta, liver, epididymis and oviduct, with the exception of heart, spleen and pancreas. This result is in agreement with the EST Genbank database. However, by the Northern blot analysis, two hybridisation signals of 0.9 kb and 2.3 kb were detected only in the testis. Kastury et al. (1997) also detected two *DNALI1* transcripts in human, whereas in *Chlamydomonas reinharditii* only one p28 transcript was observed. The initiation of *Dnali1* expression was observed at day 15 during the postnatal development of testis, both by Northern and Western blot analyses. These findings altogether conclude that both *Dnali1* transcript and protein are present at the same time abundantly in the testis rather than in any other tissue. It could be suggested that *Dnali1* plays a crucial role in spermatogenesis. The immunohistochemical analysis revealed that Dnali1 is localized along the entire axoneme of sperm flagella, indicating a fundamental role in sperm motility. When testicular sections were incubated with α-Dnali1 specific antibodies, the putative localization of Dnali1 was found in the elongating spermatids, located closely to the lumen of the tubules, whereas round spermatids showed weaker labelling. Moreover, the finding of Dnali1 localization in the cilia of tracheal epithelium and brain lateral ventricles collectively suggest that Dnali1 is an integral component of axoneme.

Male infertility associated with the chronic respiratory disease Primary Ciliary Dyskinesia (PCD) or Kartagener Syndrome has been attributed to a genetic deficiency in the construction of dynein structures in the axoneme of sperm and respiratory cilia (Afzelius, 1976; McGrath et al., 2003), mostly in the structure of outer and inner dynein arms. For example, the gene responsible for the spontaneous classical mutation *inversus viscerum* (*iv*) is an axonemal dynein heavy chain named (*Dnahc11*) (Supp et al., 1997) and Dynein 2 light intermediate chain (*D2LIC*) (Amer et al., 2004) are required for the establishment of the left-right body axis in mouse embryo. Similarly, loss of function of axonemal dynein *Mdnah5* causes most of the classical features of PCD, including recurrent respiratory infections, situs inversus and ciliary immotility (Ibanez-Tallon et al., 2003). Similar axonemal abnormalities are observed in *Chlamydomonas reinhardtii* flagella lacking the *p28* gene product, suggesting that *Dnali1/DNALI1* may be candidate genes for disturbed ciliary motility in mammals.

DHPLC (Denaturing high performance liquid chromatography) analysis is considered to be very accurate, with a sensitivity and specificity thought to be higher than 96%. By this assay, the DNA of a total of 25 human patients affected with asthenozoospermia were screened for mutation in *DNALI1* gene. The variations detected by DHPLC have been verified by sequencing of the respective exons and flanking intronic sequences. However, variations discovered were polymorphisms (Table 3-4), with the exception of one splice-site mutation (IVS3 +2T>C) that was found to be absent in 50 control samples. It was not studied how this mutation contributes to the clinical manifestations characteristic of asthenozoospermia. The characterization of further mutations in *DNALI1* and the analysis of intronic mutations by studying their splicing behaviour may be of value in understanding the putative role of intronic mutations with respect to *DNALI1* function in asthenozoospermic patients.

Consistent with the previous findings, *Dnali1* deficient mice have been generated (3.1.4.7) to ascertain the involvement of *Dnali1* in the presentation of PCD. Our data establish that *Dnali1* gene does not seem to be a candidate for the primary cause of PCD like several other mouse lines with axonemal deficiencies, which have been proposed previously as models for PCD. However, these models present a very limited subset of the classical symptoms associated with the human disorder. For example, mice deficient in an inner arm dynein heavy chain gene (*Mdhc7*) displayed reduced sperm motility (Neesen et al., 2001) and *lrd* mice demonstrated randomisation of the left-right body axis (Supp et al., 1997).

Further identification and characterization of dynein genes in mammals is necessary to understand the implications of dyneins in possible cellular and developmental processes leading to PCD. Mouse model of *Dnali1* presented here harboured the similar phenotype related to the cytoplasmic dynein heavy chain *Dnchc1* knockout mouse (Harada et al., 1998).

In *Chlamydomonas* axoneme, association of p28 with the dynein heavy chain suggests that p28 is necessary for the stable assembly of a subset of inner dynein arms or for binding of these arms to the microtubule doublets (LeDizet and Piperno, 1995). In sea urchin, p28 light chain homologue (66% identical) plays a dynamic role in flagellar motility (Gingras et al., 1996). Similarly, a 29 kDa axonemal dynein light chain (p29) of *Paramecium* is found to be involved in the regulation of swimming speed (Barkalow et al., 1994). These findings imply the conventional role of this light chain in the axoneme as an axonemal dynein.

It is worth-mentioning at this point that Dnali1 may also be involved in the regulation of sperm motility. How this regulation is occurred and what are the possible mechanisms taking part in these events are still to be determined. Studies on dynein isoforms have shown that controlled phosphorylation/dephosphorylation of IC and LIC subunits is one mechanism for

regulating dynein activity, either by switching motor activity on and off (Habermacher and Sale, 1997; Yang and Sale, 2000). An important next step would be to determine whether Dnali1 is phosphorylated, and if it is, how the phosphorylation rate of this light chain might vary between the cell body and flagellar compartment. It is also important to understand whether the cytoplasmic and axonemal variants of dynein are regulated in a uniform cascade or some other factors are involved in the regulation.

Interestingly, several reports have shown that the light chains, which are known to be predominantly axonemal dynein components, are also parts of cytoplasmic dynein (Chuang et al., 2001). For example, rat homologue of p29 light chain is also reported to be involved in the regulation of cytoplasmic dynein in the rat liver and in mammalian cells (Wang and Satir, 1998). Similarly, the light chains like Tctex family members, LC7 and 8 kDa dynein light chain can be identified in both axonemal and cytoplasmic dynein variants. These findings partly suggest that ciliary and cytoplasmic dyneins may be regulated by similar mechanisms. Furthermore, light chains of both axonemal and cytoplasmic dyneins are found to be homogeneous.

Subsequent identification of human homologue *DNALI1* (Kastury et al., 1997) indicates the presence of this light chain also in the tissues not containing axonemal components, which is consistent to our findings in case of mouse *Dnali1*. These lines of evidence suggest that despite an axonemal component, Dnali1 may also be a part of cytoplasmic dynein.

Subcellular localization studies by Dnali1 specific antibodies revealed an interesting observation, which link with our previous finding that Dnali1 is also present in the cytoplasm of neuroblastoma cells. A punctuate staining pattern throughout the cytoplasm and intense localization surrounding the nucleus depict that Dnali1 may have some role in the cytoplasmic machinery. A similar expression pattern was observed when Dnali1-myc fusion protein was overexpressed in mouse neuroblastoma and fibroblast cell lines and immunoassayed with α-myc antibodies. Such a staining pattern indicates the putative co-localisation of Dnali1 with specific cell organelles. Further experiments, by incubating the mouse embryonic stem cells with organelle specific antibodies i.e. Golgi apparatus and γ-tubulin demonstrate that Dnali1 displays a typical Golgi localization at the light microscope level. On treating the cells with microtubule depolymerising agent, the Golgi apparatus becomes scattered in the cytoplasm, however the co-localization of Dnali1 and Golgi is not altered significantly, suggesting that Dnali1 interacts with the Golgi apparatus in a microtubule-independent manner. Previous reports suggest that both inhibition of cytoplasmic dynein function and depolymerisation of microtubules result in the formation of peripheral

Golgi stacklets (Vaisberg et al., 1996; Harada et al., 1998). Because it is unclear whether the Golgi fragmentation is due to an imbalance between plus end-directed motors and cytoplasmic dynein, resulting in the active movement of Golgi stacks towards the periphery (Minin, 1997). Even the induced depolymerisation by higher concentration of nocodazole does not alter the putative localization of Dnali1 and Golgi fragments, indicating the persistent co-localization. These lines of evidence imply the involvement of Dnali1 in vesicular trafficking and maintenance of the Golgi apparatus. It is not known whether the overlap between Dnali1 and Golgi apparatus is confined to a distinct cytoplasmic dynein, performing a different function in the same organelle or the organelle-specific membrane proteins, as yet unidentified are involved in the targeting of these complexes. Emerging evidence suggests that numerous biochemically and functionally distinct forms of cytoplasmic dyneins exist, probably performing specialised cellular tasks (Vaisberg et al., 1996; Criswell and Asai, 1998; King et al., 1998; Nurminsky et al., 1998).

It is unclear whether Dnali1 is also involved in targeting the Golgi apparatus to the centrosomes. The assembly of γ-tubuin onto centrosomes is mediated by cytoplasmic dynein in a microtubule-dependent manner (Young et al., 2000). Our observation by using both γ-tubulin and Dnali1 specific antibodies revealed the co-localisation of these proteins in cells, which were not treated with nocodazole. However, depolymerisation of microtubules, which resulted in alteration of centrosomal position with respect to the nucleus, no co-localization of Dnali1 was observed in the centrosomes. It might be concluded that Dnali1 localization with the centrosomes is microtubule-dependent.

The co-localization studies of Dnali1 with Golgi apparatus *in vitro* provide the assumption that Dnali1 may be involved in the organization of Golgi bodies. Although we cannot unequivocally exclude a role of Dnali1 in Golgi fragments, yet it is postulated that disruption of this protein in mammals would have a more profound effect than simply loss of inner dynein arms, as detected in *Chlamydomonas* mutant (LeDizet, 1995). An additional possibility is that this protein has acquired multiple functions in mammals both in the Golgi and in the cilia and flagella.

4.1.2 Dnali1 interacts with C-terminal part of Cytoplasmic dynein heavy chain

Previously, two p28 interacting proteins within the inner dynein arm isoform have been identified in *Chlamydomonas*. The p28 polypeptide directly binds to actin and to the N-terminal half of a dynein heavy chain (Ledizet and Piperno, 1995). The C-terminal part of p28

contains many short stretches (179-220 amino acids and 229-249 amino acids), with high homology to the α-helical domains (coiled-coil domains) found in the myosin heavy chains or in α-tropomyosin (LeDizet et al., 1995). Coiled-coil regions are known to play a basic role in mechanisms like dimerisation or interaction with other proteins, thus forming a rigid and extended spacer between protein domains. Moreover, α-helical domains are also important for a variety of signalling processes (Skiba et al., 1999). It is emphasized that these coiled-coils of Dnali1 are involved in the interaction with other proteins.

Our immunoprecipitation data reveal a physical interaction between Dnali1 and carboxy-terminal of cytoplasmic dynein heavy chain (*Dnchc1*), which is approximately a 500 kDa protein and contains several domains for protein-protein interaction (King et al., 2000; Asai et al., 2001). To date, several multiple cytoplasmic dynein heavy chains have been identified, at least two (CyDn and DLP4) in rat (Tanaka et al., 1995), two (DHC1A and DHC1B) in sea urchin (Gibbons et al, 1994), and three (DHC1, DHC2, and DHC3) in HeLa cells (Vaisberg et al., 1996). Conventional cytoplasmic dynein heavy chains (CyDn), DHC1A and DHC1, are homologs, while DLP4, DHC1B, and DHC2 are also homologs with each other. Although microtubule binding is the property of all dyneins, the region responsible for this is not highly conserved amongst dyneins of different origins, suggesting that only a few residues are actually required for the interaction. Diversification of dynein function appears to be regulated by the multiple proteins associated with the dynein heavy chains that provide motive force for the driving movement along the microtubules (Karcher et al., 2002). It is unclear at this stage whether there is a direct interaction between Dnali1 and cytoplasmic dynein heavy chain or some other proteins are also involved in this mechanism.

Dynein is a complex motor protein that is involved in multiple interactions. Comparisons between axonemal and cytoplasmic dyneins suggest a functional division of DHC into two regions. The two-third carboxy-terminal of DHC is highly conserved and comprises the motor domain. While the amino terminal forms a scaffold (part of the stalk) upon which most of the other subunits assemble to form the cargo-binding tail (Vallee et al., 1993). The molecular interactions within the dyneins are not well understood. Previous studies have shown that the central domain of the DHC amino terminus is responsible for interaction between the DHCs and with other dynein subunits. However, no study has been made yet to postulate the involvement of carboxy-terminal in the interaction with other proteins. Dnali1 protein interaction with the carboxy-terminal of DHC either directly or by controlling the interaction of dynein with other protein such as dynactin provides a target for investigations into the structure and assembly dynamics of the dynein.

Recent data indicate that dynein subunits are already assembled within the cytoplasm and that a cytoplasmic pool of ciliar or flagellar precursor proteins exists (Fowkes et al., 1998). Piperno et al. (1998) have found that p28 requires KHP1^{FLA10}, the heavy chain of an heterotrimeric kinesin II (Scholey, 1996), to reach the distal part of the flagella, where it binds to the outer doublet microtubules in a concentration gradient manner from distal to proximal part of the axoneme, supporting the evidence that transport of p28 within the axoneme is via a molecular motor. Later on, it has been reported that a cytoplasmic 17S complex of cytoplasmic dynein binds to p28 in substoichiometric amounts and requires KHP1^{FLA10} to be present in the flagella (Piperno and Mead, 1997). Moreover, cytoplasmic 17S complex and KHP1^{FLA10} are described to be parts of the same transport system (Kozminski et al., 1995; Cole et al., 1998). These findings implicate that a precursor of cytoplasmic dynein is required to carry the p28 from the tip of flagella to the site of incorporation by intraflagellar transport (IFT). IFT is a microtubule-based motility located between the flagellar membrane and axoneme, in which groups of protein particles are transported from the base to the tip of the flagellum (anterograde) by kinesin II and from the tip to the base (retrograde) by cytoplasmic dynein 1b (Piperno and Mead, 1996; Cole et al., 1998; Cole, 2003). However, still the question remains, how IFT participates in the axonemal assembly.

4.1.3 *Dnali1* targeted disruption results in embryonic lethality

To address the question, how the *Dnali1* gene contributes to the functional diversity within the cell, targeted disruption of the *Dnali1* gene was carried out. The first three exons of the *Dnali1* gene have been deleted by homologous recombination. Surprisingly, the resulting chimeras (>90% agouti coat colour) exhibited reduced testes weight and had severe problems in fertility during the first 3-4 months. However, one chimera successfully transmitted the mutant *Dnali1* allele to F1 progeny. On subsequent breedings, heterozygous animals appeared phenotypically normal and displayed no discernible abnormalities. However, no homozygous null *Dnali1* mice were identified among morphologically normal offspring. Finding of a great number of empty deciduae with resorbed embryos indicates that *Dnali1*$^{-/-}$ embryos seemed to develop and were able to hatch and be implanted. Indeed, during the later stages, *Dnali1*$^{-/-}$ embryos exhibited a severe defect in proliferation and undergo apoptotic death.

Our data that *Dnali1*$^{-/-}$ mice fail to propagate after the blastocyst stage and that localization of Dnali1 is in the Golgi apparatus reveal a striking similarity with that of *Dnchc1*$^{-/-}$ mice phenotype. *Dnchc1*$^{-/-}$ embryos die at the blastocyst stage due to a disrupted Golgi apparatus distributed throughout the cytoplasm (Harada et al., 1998). *Dnchc1*$^{-/-}$ blastocysts grown *in*

vitro show a highly vesiculated Golgi complex that is distributed throughout the cytoplasm. Interestingly, the finding of putative interaction between Dnali1 and Dnchc1 and the similar phenotype of prenatal embryonic lethality at blastocyst stage also suggests that Dnali1 light chain is an integral component of cytoplasmic dynein and is required for the proper function of cytoplasmic dynein in maintaining the proper position of Golgi bodies in the blastomeres.

RT-PCR analysis using RNA from blastocysts, ES-cells and embryos from E7.5 to E15.5 demonstrated the presence of *Dnali1* transcript at all stages. It is not studied whether *Dnali1* is also expressed in the preimplantative embryos. However, the phenotypic consequences of the targeted disruption of *Dnali1* reveal that the zygotic *Dnali1* expression may persist for the ICM/epiblast lineage, but it is not present until after implantation, presumably the maternal Dnali1 protein becomes diluted out through the rapid growth of embryo. Although most of the maternal gene products are destroyed at the 2 or 8-cell stage of development (Nothias et al., 1995; Schultz et al., 2003), some maternal proteins such as Sox-2 and Mtb are known to persist until the blastocyst stage (Avilion et al., 2003; Smith et al., 2004). Additionally, detectable amount of *Dnchc1* mRNA of maternal origin was also detected in the *Dnchc1*$^{-/-}$ blastocysts (Harada et al., 1998). Detection of maternal *Dnali1* gene transcript or products in *Dnali1* deficient embryo needs to be performed to clarify this point.

Immunostaining of embryos using Dnali1 specific antibodies at morula stage (E2.5) revealed the localization of Dnali1only in the cytoplasm. However, the blastocysts (E3.5) staining restricted the Dnali1 localization only in the ICM, supporting the result that in *Dnali1*$^{-/-}$ blastocysts there is no equivalent rapidly proliferating cell population, the only surviving cells being trophoblast giant cells.

Accumulating evidence indicates that *Dnali1*$^{-/-}$ blastocysts may also have abnormalities in the Golgi apparatus like that of *DnchcI*$^{-/-}$. The interpretation that Dnali1 may likely to play a role in the organization or function of the Golgi apparatus is supported both by the result of putative co-localization of Dnali1 in normal and drug-treated ES cells on the Golgi bodies and by the results of co-immunoprecipitation studies with Dnchc1. These results are compatible with the previous findings, which suggest that the isoforms of cytoplasmic dynein are involved in the Golgi activity. In mammals, D2LIC and DHC2 were found to localize to the Golgi apparatus and centrosomes of nonpolarized cells where they were thought to be involved in intracellular trafficking and Golgi organization. The D2LIC protein localization was also observed in the COS-7 cells where cilia are not likely to be present. (Grissom et al., 2002). In sum, the data provide strong support for the hypothesis that Dnali1 plays a role in Golgi organization.

Because the Golgi complex does behave as a potent organizer and a differentiating device of a stable subset of microtubules and its central localization requires cytoplasmic dynein (Burkhardt et al., 1997; Harada et al., 1998), it is evident that *Dnali1* deficient embryos lacking the proper function of dynein would have abnormalities in the Golgi positioning. It is well-established fact that cytoplasmic dynein is dispensable for the viability of organisms. For example, *ZW10* mutants, which fail to localize dynein to the kinetochore exhibit anaphase defects, and have led to the suggestion that an absence of kinetochore-associated dynein function may allow a bypass of the anaphase checkpoint (Starr et al., 1998). In *Drosophila,* cytoplasmic dynein (*Dhc64C*) is required for the nuclear attachment and migration of centrosomes during mitosis (Robinson et al., 1999). Similarly, knockout mice lacking Dynein 2 light intermediate chain (*D2LIC*) (Amer et al., 2004) and cytoplasmic dynein heavy chain (*Dnchc1*) function (Harada et al., 1998) die perinatally, due to the defects in protein maturation and mitotic abnormalities. Both D2LIC and Dnchc1 were reported to localize on the Golgi apparatus (Harada et al., 1998; Grissom et al., 2002). This is reminiscent with the Dnali1 localization/phenotype.

Alternatively, the absence or reduction of dynein function due to the lack of Dnali1 in the mitotic machinery may allow spindle or centrosomal microtubule bundles to interact inappropriately with neighbouring arrays. Dynein is also important for chromosome alignment and mitotic spindle assembly (Eshel et al., 1993; Li et al., 1993; Merdes et al, 1996). Dynein null mutants in budding yeast display defects in spindle elongation during anaphase B (Saunders et al., 1995). In *Drosophila*, hypomorphic mutations of the dynein heavy chain inhibit the spindle pole separation in early embryos (Robinson et al., 1999). Successful mitosis is reliant upon the formation of a bipolar spindle to properly segregate chromosomes into daughter cells. This spindle is composed of mainly microtubules with minus-ends, which are focused at two poles. These poles are formed among the centrosomes, with the help of a complex of proteins, mainly dynein, dynactin and nuclear protein associated with mitotic apparatus (NuMA) (Gaglio et al., 1997; Merdes et al., 2000). Dnali1 may be involved in making the complexes with NuMA and dynactin, causing transportation to reach NuMA into the cellular cortex and begin formation of esters. Possibly, in the Dnali1 deficient cells, mitotic progression halts without proper spindle formation and cells eventually undergo apoptotic cell death. The key part is to understand the complicated interactions of Dnali1 with other proteins of the mitotic machinery.

It is postulated that the axonemal function of Dnali1 may be inter-convertible upon cell’s need and shift more in the cytoplasm to take part in cargo-binding activities, when the axonemal

requirement is fulfilled. The hypothesis is supported by the multiple findings. The axonemal assignment of 11-13 dynein isoforms in sea urchins suggests an increase of dynein heavy chain expression in the cytoplasm when blastomeres were deciliated (Gibbons et al., 1994). Homologues of the human DHC3 isoforms also fulfill this definition of axonemal dynein (Vaisberg et al., 1996). This behaviour has led to an investigation of Dnali1 to distinguish these possibilities.

It is known that cytoplasmic dynein and dynactin have been implicated in the attachment of chromosomes to mitotic microtubules (Steuer et al., 1990). However, nothing is known about the isoforms of dynactin that associate with the cytoplasmic dynein family. Because cytoplasmic dynein seems to be linked to its cargo indirectly through dynactin, it would be important to understand the relation of *Dnali1* and cytoplasmic dynein regulation with respect to dynactin.

It is speculated that Dnali1 deficiency might have the ability to alter the function of dynein holoenzyme. Further investigations are needed to prove the role of Dnali1 in the cell proliferation and to study the possible mitotic defects occurring in the Dnali1 deficient blastocysts.

In sum, it is concluded that Dnali1 in mammals is essential for the autonomous cytoplasmic dynein function and global spatial organization of early development in the mouse embryo.

4.2 Characterization of the murine *Tcte3* (*t*-complex testis expressed 3) gene

4.2.1 *Tcte3* expression studies

Tcte3 belongs to a distinct subfamily of outer arm dynein light chains. In contrast to the inner dynein arms, which have more than seven different types, the outer dynein arms have a homogeneous molecular composition in the green alga *Chlamydomonas* (Kagami and Kamiya, 1992). By electron microscopy, each outer arm appears as two-headed structure composed of α- and β-DHC in mammals, while a three-headed structure composed of α-, β- and γ-DHC was detected in *Chlamydomonas, Paramecium and Tetrahymena* (Figure 4.1).

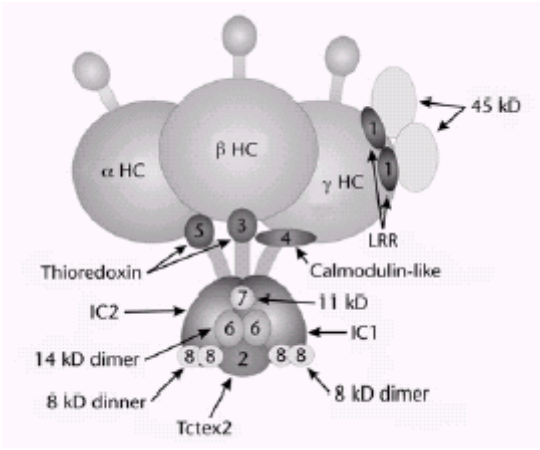

Figure 4.1. Polypeptide composition of dynein outer arm of *Chlamydomonas*. LRR, leucine rich repeats; Tctex2, LC2; thioredoxin, LC3 and LC5 and calmodulin-like, LC4 (adapted by Bernashski et al., 1999)

The murine *Tcte3* gene contains at least three alternatively spliced cDNAs in the testis (3.2), out of which two transcripts encode an identical protein of approximately 22 kDa. Strikingly, the smaller transcript is not detected to encode a protein (15 kDa) in the testis. It is postulated in previous studies that the 15 kDa protein might be a product of another similar gene (King et al., 1997; Bai et al., 2003). The evidence for this hypothesis comes from the result of Western blot analysis using Tcte3 specific antibodies, which detect a protein of 22 kDa size in the testis (3.2.4).

RT-PCR analysis using RNAs of different murine organs indicates the expression of *Tcte3* in brain, liver, lung, spleen, kidney and testis (Drenckhahn, 2000). However, subsequent Northern blot analysis revealed the *Tcte3* expression predominantly in the testis. Northern

blot analysis performed by using human RNAs of multiple tissues also detected the *TCTE3* transcript only in the testis (Neesen et al., 2002). The unique expression pattern and abundance of Tcte3 in the testis implies the role of this protein during spermatogenesis.

RT-PCR using the RNAs of mouse mutants for different spermatogenesis defects show that *Tcte3* expression is not only restricted to the germ cells, rather it is also expressed in the somatic cells (Drenckhahn, 2000). Several lines of evidence suggest that besides an axonemal component, mammalian *Tcte3* is also a part of cytoplasmic dynein (King et al., 1998; DiBella et al., 2001). Indeed, studies in mammalian cells and *Drosophila* have indicated that cytoplasmic dynein is abundant in the testis and appears to be involved in some aspects of spermatogenesis and male fertility (Collins and Vallee, 1989; Rasmusson et al., 1994; Gepner et al., 1996).

By Northern blot analysis, the expression of *Tcte3* was observed to begin at day 11 during the postnatal testis development while RT-PCR experiments demonstrated that *Tcte3* transcripts could be detected in 5 day old postnatal germ cells (Drenckhahn, 2000).

By immunohistochemical analysis, Tcte3 protein is first detected during the pachytene stage of the first meiotic division, but is present at a higher level in the later haploid spermatogenic stages. Immunolocalization experiments demonstrate that Tcte3 is distributed along the entire length of sperm tail. Previously, Tcte3 was described to be a peripheral sperm membrane protein, even Tcte3 was not found to have a signal sequence for transmembrane passage (Huw et al., 1995). Later on, studies in *Chlamydomonas* described that the Tcte3 homologue LC2 is not membrane-associated but is actually an integral component of the outer dynein arm complex (King et al., 1997).

4.2.2 Orthologous gene studies

Most of the Tctex family members have been identified on the proximal end of mouse chromosome 17 and mapped in a region of about 20-30 cM (Table 4-2), indicating to have profound effects on spermatogenesis. The accumulation of so many sperm function genes in this region of chromosome 17 is either by chance or by selection (Silver, 1993). The functions and sequence informations of most of the genes of this family are still to be determined. Homologues of many of these genes involved in sperm dysfunction are likely to be present on both arms of human chromosome 6 (Hamvas et al., 1996). Seven genes (*Tctex3*, *Tctex7*, *Tctex8*, *Tctex9*, *Tctex10*, *Tctex11* and *Tctex12*) have been identified by cDNA screening and chromosomal walking. They are expressed predominantly in the germ cells of the testis, and map to various regions of *t*-complex region (Table 4-2) (Yeom et al., 1992). Three genes are

more abundant at the pachytene stage; other three are at postmeiotic stages, while one gene (*Tctex10*) is expressed at all the stages of spermatogenesis (Ha et al., 1991). The molecular functions of these genes are still to be determined. However, the chromosomal location in a specific region and the prominent germ cell specific expression pattern implies that Tctex family genes may be important candidates for male sterility. *Tcte3* abundant expression in the testis as detected by Northern blot analysis both in mouse and human reveals that *Tcte3* plays an important role during the sperm maturation and function.

Subsequent identification of the multiple copies of Tctex family genes in the mouse genome has increased the complexity regarding their functional studies. Huw et al. (1995) suggested that multiple copies of *Tcte3* are present in the mouse genome in a tandem repeat array, which are apparently very similar to one another as no polymorphism was detected between them. In the present study, another similar *Tcte3* sequence was identified both at cDNA and genomic level (3.2.2.1) indicating that at least two copies of *Tcte3* gene are present in the mouse genome. There are four copies of the *Tctex1* gene clustered on mouse chromosome 17: two copies of each A and B gene (Neill and Artzt, 1995). The two distinct forms of *Tctex1* gene (A and B) have complete conservation at the level of coding sequence. However, at the genomic level *Tctex1A* and *Tctex1B* differ by the insertion (or deletion) of 11 kb of DNA. In humans, six *Tctex1*- like sequences were found on chromosomes 2, 4, 6, 17, 20 and X, respectively. The loci at 6q25 and Xp21 encode the proteins TCTEL1 (NP_006510) and TCTE1L or RP3 (NP_006511), respectively. The other four genomic loci do not appear to be expressed at a significant level, as these sequences could not be found in the protein or ESTs databanks. Similarly, *Tctex7* forms a small multigene family with four copies in the mouse genome (Yeom et al., 1992); two of them map to the *t* complex (*Tctex7*A and *Tctex7*B) (Table 4-2). It is not clear how many of the four copies actually encode the *Tctex7* message which is detected in the testis. *Tctex8* and *Tctex10* also appear to have at least two copies in the mouse genome (Yeom et al., 1992). Exclusion of the possibility that *Tcte3* exists in multiple copies requires the mapping and sequencing of the similar *Tcte3* genes. Absence of the sequence information and possible function of many genes of the Tctex family suggest that these genes may be very similar with one another and may be evolved by successive and recent duplication events.

Gene name	Mouse chromosome-17	Gene copy number	Reference
Tctex1	3.1 cM (NM_033368)	7	Lader et al., 1989 Ha et al., 1991
Tctex2 (Tcte3)	8.158 cM (NM_011560)	2	Present study Huw et al., 1995
Tctex3 **(Phf1, PHD finger protein 1)**	15.15 cM (NM_009343)	1	Ha et al., 1991 GNP core group, 2005
Tctex4	19.86 cM (AY172988)	ND	Bai X et al., 2003
Tctex5 **(PppIr11, Protein phosphatase 1, regulatory subunit)**	19.86 cM (NM_029632)	1	Ha et al., 1991 GNP core group, 2005
Tctex6	19.86 cM	1	Jones EP et al., 1999
Tctex7A **(Knsl2a, Kinesin-like 2a)**	18.38 cM	2	Himmelbauer et al., 1993 Yoem et al., 1992
Tctex7B (**Knsl2b, Kinesin-like 2b)**	15.15 cM	2	Himmelbauer et al., 1993 Yoem et al., 1992
Tctex8	18.37 cM	2-3	Yoem et al., 1992
Tctex9	18.36 cM	1	Yoem et al., 1992
Tctex10	18.35 cM	2	Yoem et al., 1992
Tctex11	18.34 cM	1	Yoem et al., 1992
Tctex12	15.15 cM	1	Yoem et al., 1992

Table 4-2. Members of the Tctex gene family mapped by chromosomal walking. The sequence information, which is not indicated is still lacking. ND, not determined.

4.2.3 Targeted disruption of *Tcte3* gene by homologous recombination

In order to elucidate the possible physiological roles of the *Tcte3* gene in mammals, the murine *Tcte3* gene disruption was carried out by homologous recombination. The exon 2 of *Tcte3* gene encompassing a region of about 7.7 kb was replaced by *neomycin* resistance gene. The targeting construct strategy (Figure 3.29) was designed to disrupt the *Tcte3* gene because of the multiple reasons. First: there is another gene present very close to the exon 1 of the *Tcte3* gene and deletion of *Tcte3* exon 1 may result in the functional disturbances of the other gene. Second: presence of CpG rich elements at the 5'-end of the *Tcte3* gene limit the possibility of homologous recombination (Rappold et al., 1987). Also, the targeted deletion of exon 2 was predicted for the inactivation of the putative conserved Tctex domain located at the carboxy-terminal of the encoded Tcte3 protein. Southern blot analysis performed on the DNA isolated from the heterozygous mice tail biopsies, using different restriction enzymes

and labelling with the multiple probes located at both ends of the targeting construct implied a significant difference of the hybridisation intensity between the wild type and mutant allele (Figure 3.29). Although, Southern blot analysis, Long-range PCR and sequence analysis of junctions clearly demonstrated the occurrence of correct homologous recombination events, yet we were unable to identify *Tcte3* deficient mice among the F2 offspring. The evidences that *Tcte3* gene could be present in a single copy as identified by Southern blot analysis, previously (Drenckhahn, 2000) and presence of no *Tcte3*$^{-/-}$ offspring among the *Tcte3* heterozygous animals imply that probably *Tcte3* gene disruption may result in the embryonic lethality. However, embryonic studies (genotyping) undertaken at E7.5 and E8.5 also revealed the same findings as detected in the adult mice. Moreover, the determination of normal litter size (8.6) of F2 progeny and high number of *Tcte3* heterozygous animals as compared to wildtype littermates (Table 3-5) suggested the possibility of the presence of another sequence with high homology to *Tcte3* gene in the mouse genome as reported by Huw et al. (1995). However, it is unclear whether these homologous sequences are located distantly apart or are present in a tandem array on the same chromosome. Later on, an additional *Tcte3* transcript (*Tcte3-B*) was found in the testis by sequence analysis of multiple RT-PCR clones containing highly conserved coding sequence with that of *Tcte3-A* (3.2.2.1). However, the expression of *Tcte3-B* seems to be quite low postulated by multiple facts. First, there was only one clone of *Tcte3-B* identified out of 35 clones sequenced, randomly. Secondly, the *Tcte3*$^{-/-}$ mice genotyped by real-time PCR analysis (3.2.3) and examined both by Northern blot and Western blot analyses revealed the indication of no product deriving from any other homologous gene. It may be hypothesized that *Tcte3-B* gene expression is time dependent and specifically initiated at some later or earlier stage during the postnatal progressive spermatogenesis in the mouse testis. Type A and B spermatogonia exhibit very little transcripts after the initiation of meiosis (Shima et al., 2004). The high level of overlap between spermatogonial genes and the pattern of expression suggests that many unique spermatogonial genes are downregulated as germ cells enter meiosis. For example human *dlk1* (delta-like homolg 1), a gene, which is highly expressed in type A and B spermatogonia, loses its total expression by 20 days at the appearance of haploid germ cells (Shima et al., 2004). It is also not clear at the moment, whether more sequences related to *Tcte3* transcripts are present in the mouse genome, which are either not expressing at a substantial level or are pseudogenes. Intriguingly, the *Tcte3-A* mice identified by real-time PCR exhibited the fertility defects supporting the notion that the defects in this dynein chain function may be the underlying cause of the resulting phenotype. The support for this result comes from the

previous studies, which indicate that Tctex family genes loss of function is not dispensable for the viability of organisms rather effect the male fertility. *Chlamydomonas* mutants lacking *Tctex2b* (close homologue of murine *Tcte3*; 63% similar) swim more slowly than wildtype (DiBella et al., 2004). In *Drosophila*, a homozygous mutant of *dtctex1* is viable, although males are sterile due to defects in sperm motility (Caggese et al., 2001).

4.2.4 Dysfunction of murine *Tcte3* gene contributes to male infertility

Because *Tcte3* function is hypothesized in the testis both by expression analyses and the previous studies (Rappold et al., 1992; Huw et al., 1995), present study put more emphasis on the critical role of *Tcte3* in the spermatogenesis. Interestingly, *Tcte3*$^{-/-}$ male mice exhibited fertility disturbances and were unable to show normal reproduction capabilities. The total sperm count in the cauda epididymis of *Tcte3*$^{-/-}$ male mice as well as in uteri and oviducts of females inseminated by *Tcte3*$^{-/-}$ male mice was determined and a significant difference in the number of sperms (3.2.5.4.1) between wildtype and *Tcte3*$^{-/-}$ male mice was observed (Table 3-9). Additionally, *Tcte3* deficient mice sperms exhibited a highly reduced motility as compared to that of wildtype littermates (in total path velocity, progressive velocity, beat frequency and track speed). These findings are reminiscent with the earlier studies, which indicate that Tcte3-related protein (LC2) undergoes phosphorylation at the activation of sperm motility in a cAMP-dependent manner (Inaba et al., 1999). Phosphorylation of Tcte3 related proteins in salmonid fish and sea urchin dyneins has been correlated with the activation of sperm motility (Inuba et al., 1999). Thus, Tcte3 in mammals is suggested to play a dual role to be an essential protein for outer arm dynein assembly during spermatogenesis as well as a component of signal cascade that regulates the sperm motility (Ogawa and Inaba, 2003). In addition, Tcte3 may also be involved in facilitating interactions with the axonemal kinases that modify the activity of the sperm during motility, increasing the probability that *Tcte3* deficient sperms may have defects in the phosphorylation of dynein subunits leading to the reduction in motility. More studies are needed to understand the possible mechanisms by which the *Tcte3* influences the sperm assembly and function regarding the activation of sperm motility. However, presence of reduced number of sperms in the *Tcte3*$^{-/-}$ seminiferous tubules hypothesizes the involvement of some indirect mechanism.

4.2.5 Apoptosis as a consequence of meiotic abnormalities

The morphological studies of testes of *Tcte3*$^{-/-}$ mice indicate that the pachytene spermatocytes and metaphase cells were the most susceptible cells for undergoing apoptosis in *Tcte3*$^{-/-}$ mice. However, the increase in the number of pachytene spermatocytes and metaphase cells in some tubules and decrease in or even absence of cells at later maturation steps in some tubules suggested the existence of a partial arrest during the first meiotic division. An overall reduction in the number of spermatids may be a cause of the fertility impairment in *Tcte3*$^{-/-}$ male mice. The mechanism by which a decrease in spermatid number occurs is not clear. Although it seems that the reduction is caused by cellular degeneration of this differentiated cell type, we conclude that the spermatid decrease is more likely due to the interruption of spermatogenesis rather than to spermatid degeneration.

Several studies have demonstrated the existence of germ cell apoptosis during normal spermatogenesis (Kerr et al., 1992; Brinkworth et al., 1995; Billig et al., 1995). Spontaneous germ cell loss occurs during the mitotic divisions of spermatogonia, the meiotic division of spermatocytes, and spermiogenesis. In general, the fertility disturbances and the abnormal spermatogenesis observed in mammals are produced by the loss of specific gene function regulating spermatogenesis (Huckins, 1978; De Rooij and Lok, 1987). In particular, the prophase of the first meiotic division and the number of primary spermatocytes entering meiosis seem to be regulated by apoptosis (Stephan et al., 1996). During meiosis, DNA damage is detected at specific checkpoints, providing the cell with a control mechanism that may result in cell cycle arrest and ultimately, in genomic instability and cell death. Among genes whose targeted disruption causes meiotic arrest in mice are BAX, PMS2, CREM, MLH-1, ATM, and HSP70-2 (Odorisio et al., 1988; Rubin et al., 1993; King et al., 1995; Dix et al., 1996; Corsi, 1997; Paulovich et al., 1997; Reventos et al., 1997; Braune, 1998). All of these proteins have been localized in germ cells undergoing meiosis in normal mice.

Our hypothesis that *Tcte3* gene may have some role in the meiotic division received a considerable support from the observation that Tcte3 protein might interact with CREB/CREM (cAMP-responsive element modulator) protein family member (Stelzer and Don, 2002). Male mice deficient for CREM are sterile, as their developing spermatids fail to differentiate into sperm and postmeiotic gene expression in the testis declines dramatically (Blendy et al., 1996). High number of cell death in *Tcte3*$^{-/-}$ spermatocytes suggests the existence of a coordinated role of *Tcte3* gene in the meiotic divisions correlating that the deficiency of this protein may be responsible for the meiotic defects in spermatogenesis

leading to apoptosis. The developmental spermatocyte arrest in *Tcte3*$^{-/-}$ testis is incomplete, as some *Tcte3* deficient germ cells are able to proceed through the normal differentiation pathway to become functional spermatozoa. Further studies will be necessary to elucidate the precise mechanism of this action.

4.2.6 *Tcte3* deficient spermatozoa exhibit multiple morphological abnormalities

In mouse testis, Tcte3 localization is observed in the spermatocytes and in the entire sperm tails, predominantly. Although, a great number of the *Tcte3*$^{-/-}$ spermatocytes exhibit disturbances in the meiotic divisions (undergoing apoptosis), yet some retain the ability to perform spermiogenesis, as detected in the epididymis sections. It is unknown whether some other compensatory mechanisms exist in mice lacking Tcte3 protein.

Spermatogenic progression in the *Tcte3*$^{-/-}$ mice is characterized by the presence of giant nuclei, multiple nuclei in the spermatids, vacuolisation in the cytoplasm of elongated spermatids and abnormal number of flagella, which can be visualized both by the light and electron microscopy in the *Tcte3*$^{-/-}$ epididymis/testis. However, no biflagellated sperm was observed in the uteri of the female mice bred with the *Tcte3*$^{-/-}$ males. One reason for this finding could be the presence of significantly low number of spermatozoa in the uterine contents and oviduct (Table 3-8) due to the high rate of apoptosis during spermiogenesis in *Tcte3*$^{-/-}$ testis, which diminished the sperm morphology assay in the ejaculate.

A role of *Tcte3* must be taken into account in the development of major elongating spermatid structures, as described in context with meiotic drive mechanism in *t*-mice. *Tcte3* gene is considered to be a candidate for one of the 3-4 distorter products that interact with a cell-specific responder and thus results in meiotic drive in *t*-mice. The *t* complex is a region of mouse chromosome 17 containing several genes that affect male fertility (Table 4-2).

The functional diversity, possibly association with Golgi apparatus due to a part of cytoplasmic dynein and putative abundant localization of Tcte3 protein specifically in the testis and sperm flagella reveal the involvement of this protein in the multiple events during spermiogenesis. Multiple microtubule (MT) anomalies arise due to the meiotic deficiencies (MDD) in the spermatids such as a failure of Golgi partitioning and displacement prior to the nuclear envelope breakdown, failure of centrosomes duplication or separation, formation of a monopolar MT spindle and of a unilateral MT manchette (Figure 4.2). The anomalies of MT assembly mediated events result in the abnormal giant sperm heads and axonemal assembly defects (Kemphues et al., 1982) as detected in the *Tcte3*$^{-/-}$ mice. These anomalies could furnish the key for locating the affected factor and could raise the possibility that polyploid

spermatids in the *Tcte3*$^{-/-}$ mice could be due to the failure of meiotic spindle function, as seen in the *Drosophila* mutants (Hackstein et al., 2000). *Drosophila Twine* mutants exhibit absence of meiotic divisions but retain the ability to perform spermiogenesis, although no mature spermatozoa are formed (Courtot et al., 1992; Maines and Wasserman, 1999).

The phenotypes of *Tcte3*$^{-/-}$ spermatozoa including high percentage of polyploidy in the spermatids, multi-tail deformities, presence of vacuoles in the cytoplasm of elongated spermatids and high rate of spermatocytes undergoing apoptosis suggest that *Tcte3* may be involved in coordinating meiosis and spermatid differentiation. This implies that the targeted disruption of *Tcte3* may result in the discrepancies of meiotic progression during spermatogenesis. The possible defects by meiotic abnormalities are summarized in the Figure 4.2. The hypothesis is based on the *Tcte3* gene expression in pachytene spermatocytes and possible involvement of *Tcte3* gene in the meiotic progression. It postulates that the *Tcte3* deficient pachytene spermatocytes may have defects in the portioning or positioning of Golgi apparatus. Spermatocytes at the pachytene stage display microtubule (MT) bundles in close association with the Golgi apparatus (Moreno and Schatten, 2000). In primary spermatocytes, the Golgi complex begins its partition at the mid-pachytene I stage and then separates into two bodies, which move around the nucleus to be located at opposite nuclear poles. Later on, the Golgi bodies are present in the plane at opposite sides of the metaphase plate (Oke and Suarez-Quian, 1992). Meiotic deficiencies in *Tcte3*$^{-/-}$ cells may result in the blockage of Golgi displacement during spermatogenesis or may disable the assembly of bipolar meiotic spindle thus leading to apoptosis (Figure 4.2 G). It may be possible that some spermatocytes escape the pachytene checkpoint. However, the *Tcte3*$^{-/-}$ spermatocytes, which fail to build a bipolar meiotic spindle and which are unable to progress in metaphase may again enter in the apoptotic pathway. (Figure 4.2 H). The meiotic deficient germ cells are able to reconstitute a nucleus and perform spermiogenesis events giving rise to giant round spermatids and spermatozoa with two to three flagella as observed in the *Tcte3* deficient mice epididymis section. Further investigations of the *Tcte3*$^{-/-}$ mice might help in understanding the informational networks and in proving the predictions that support the *Tcte3* deficient mice phenotypic modularity.

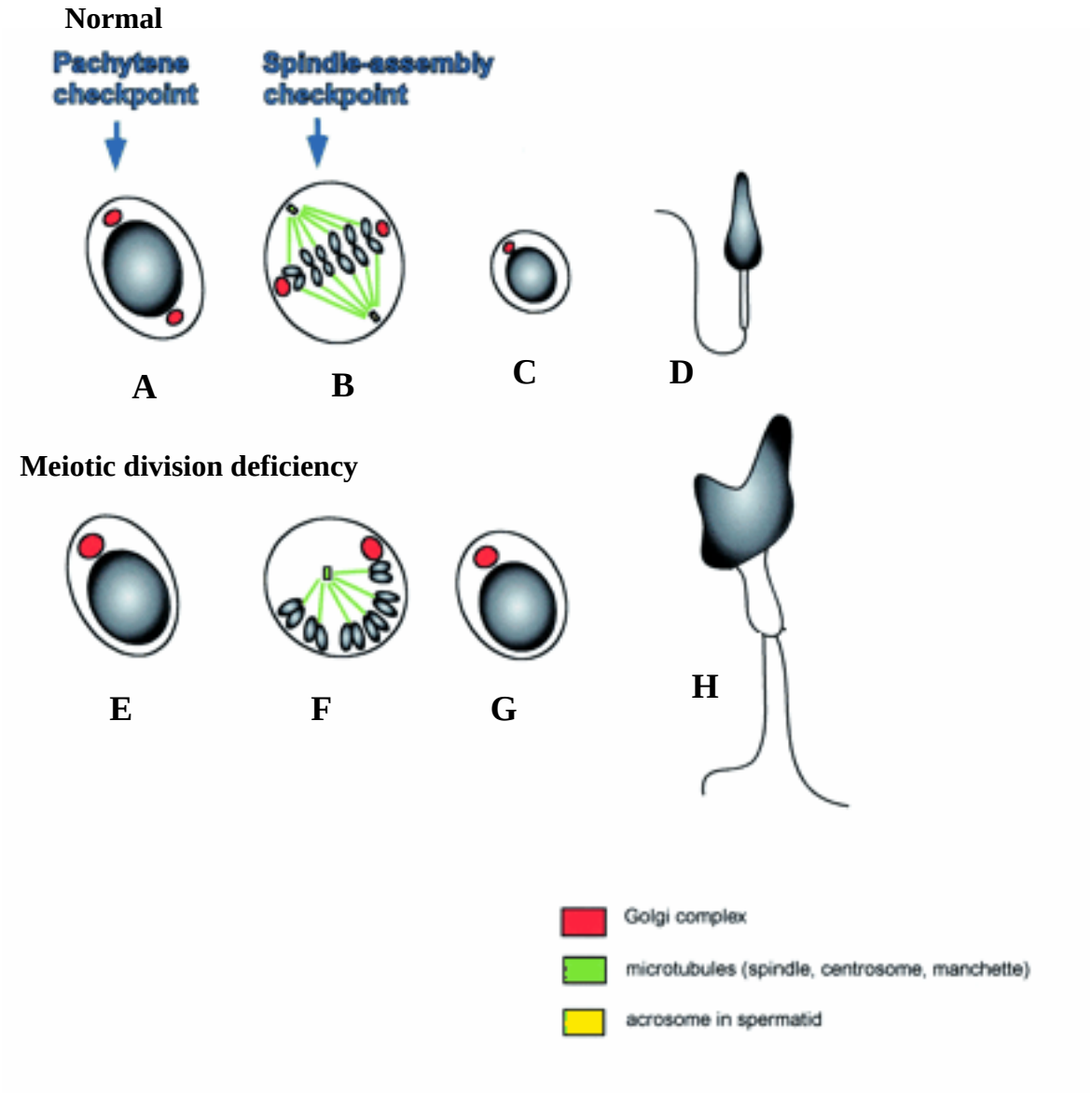

Figure 4.2. Possible meiotic and post-meiotic anomalies of *Tcte3* deficient spermatozoa. (A–D) Normal spermatogenesis events. (E) Failure of organelle partition in late pachytene spermatocytes I, as seen for the Golgi complex (red). Nevertheless, the spermatocytes escape the pachytene checkpoint. (F) The nuclear envelope breakdown has occurred and the chromosomes have condensed and are arranged in pre-metaphase. The spermatocytes fail to build a bipolar meiotic spindle (green: microtubules and centrosomes) and never progress in metaphase. (G and H) The meiotic deficient germ cells are able to reconstitute a nucleus and to perform spermiogenesis events giving rise to giant round spermatids and abnormal flagella (adapted by Escalier, 2002).

Tcte3$^{-/-}$ mouse sperms show the defects resembling with the human male infertility cases of oligoasthenoteratozoospermia syndrome. The human infertile patients reveal multiple defects including polyploidy (2-4), macrocephaly, multiflagellation (2-5 flagella), nuclear and cytoplasmic vacuolisation, disorganization of mitochondrial helix sheath, acrosomal

abnormality and chromatin packaging defect (Benzacken et al., 2001; Devillard et al, 2002; Lewis-Jones et al., 2003). The *Tcte3*$^{-/-}$ mice may be useful in understanding the genetic basis of the oligoasthenoteratozoospermia syndrome

5. SUMMARY

In the present study, the function of two murine genes, *Dnali1* and *Tcte3* were investigated. Murine *Dnali1* gene is a homologue of *Chlamydomonas* p28 and belongs to the family of inner arm dynein light chains. The immunolocalization studies indicate that Dnali1 is localized along the entire length of sperm flagella and tracheal cilia. Moreover, Dnali1 is also detected in cilia of brain lateral ventricle lining, suggesting that Dnali1 is an integral component of axoneme. However, the expression of Dnali1 and its human orthologue *DNALI1* in tissues, which lack the axonemal structures, supports a putative role of this dynein light chain in the cytoplasmic dynein complex. The results of the co-localisation studies of Dnali1 and Dnchc1 in the mouse Neuroblastoma and ES cells sustain this assumption. Moreover, yeast-two-hybrid assay and co-immunoprecipitation studies demonstrated that Dnali1 might be interacting with the carboxy-terminal of cytoplasmic dynein heavy chain. Targeted disruption of *Dnali1* gene was carried out by homologous recombination. On subsequent breedings, the heterozygous animals were found to be fertile and had no apparent abnormalities. However, no *Dnali1*$^{-/-}$ offspring were obtained by heterozygous breedings, indicating that *Dnali1* gene deficiency leads to prenatal embryonic lethality. The *Dnali1* deficient embryos die shortly after implantation. To further characterize the reason for embryonic lethality, *in vitro* culture experiments were performed. It was revealed that putative *Dnali1* null mutants exhibited lack of a distinguishable ICM-like structure, although the trophectoderm layer differentiated into giant cells. Subsequently, it was observed that Dnali1 was associated with the Golgi apparatus even in the ES cells treated with depolymerising drug, indicating that the Dnali1 interacts with the Golgi apparatus in a microtubule-independent manner. Thus, it can be speculated that Dnali1 function is necessary for the organization of the Golgi apparatus and is required for the proper function of this organelle presumably as a putative component of the cytoplasmic dynein complex machinery.

The *Tcte3* gene encodes a member of outer arm dynein light chain family and is part of both axonemal and cytoplasmic dynein complexes. To elucidate the function of *Tcte3* gene and its role in spermatogenesis, an attempt was made to inactivate the entire gene. No *Tcte3* deficient mice were identified among offspring derived from the F1 intercrosses by conventional genotyping approach. On genomic and cDNA analyses, it was revealed that more than one copy of *Tcte3* gene is present in the mouse genome. However, the other copies seem to be either not expressing at a substantial level or are pseudogenes. Therefore, quantitative real-time PCR analysis was performed, which demonstrated the presence of *Tcte3*$^{-/-}$ mice in

normal Mendelian ratios among the F2 progeny. Following Northern and Western blot analyses confirmed the real-time PCR result. Mice lacking *Tcte3* displayed male infertility due to multiple defects in spermatogenesis and due to a high incidence of cell death at the spermatocyte and spermatid stages.

6. REFERENCES

Afzelius B.A., Eliasson R. (1979). Flagellar mutants in man: on the heterogeneity of the immotile-cilia syndrome. *J. Ultrastruct. Res.* **69:** 43-52.

Afzelius B.A. (1976). A human syndrome caused by immotile cilia. *Science* **193**: 317 - 319.

Altmann, M. (2000). Ein Gen für ein neues Ubiquitin-konjugierendes Enzyme. Genomische Organisation, Expression und function. Institute für Humangenetik, Göttingen.

Ausubel F.M., Brent R., Kingston R. E., Moore D.D., Seidman J.G., Smith J.A., and Struhl K. (1994). Current Protocols in Molecular Biology, (John Wiley & Sons Inc., USA).

Avilion A.A., Nicolis S.K., Pevny L.H., Perez L., Vivian N. and Lovell-Badge R. (2003). Multipotent cell lineages in early mouse development depend on SOX2 function. *Genes Dev.* **17:** 126 - 140.

Bai X., Xu X., Zhang F., Shu H.B., Chan E.D. (2003). The protein of a new gene, Tctex4, interacts with protein kinase CK2beta subunit and is highly expressed in mouse testis. *Biochem. Biophys. Res. Commun.* **307**: 86 - 91.

Barkalow K., Hamasaki T., Satir P. (1994). Regulation of 22 S dynein by a 29-kDa light chain. *J. Cell Biol*. **126**: 727 - 35.

Beaudouin J., Gerlich D., Daigle N., Eils R. and Ellenberg J. (2002). Nuclear envelope breakdown proceeds by microtubule-induced tearing of the lamina. *Cell* **108:** 83 - 96.

Bernashski S. E., Patel-King R. S. and King S. M. (1999). Light chain 1 from the Chlamydomonas outer dynein arm is a leucine-rich repeat protein associated with the motor domain of the gamma heavy chain. *Biochemistry* **38:** 7253–7264.

Billig H., Furuta I., Rivier C., Tapanainen J., Parvinen N., Hsueh A.J. (1995). Apoptosis in testis germ cells: developmental changes in gonadotropin dependence and localization to selective tubule stages. *Endocrinology* **136**: 5 – 12.

Blendy J.A., Kaestner K.H., Weinbauer G.F., Neischlag E., Schutz G. (1996). Severe impairment of spermatogenesis in mice lacking the CREM gene. *Nature* **380**: 162 - 5.

Braun R.E. (1988). Every sperm is sacred– or is it? *Nat. Genet.* **18:** 202 – 204.

Breckle R. (2000). Klonierung und Charakterisierung des Gens der axonemalen leichten Dyneinkette mp28. Institute für Humangenetik, Göttingen.

Brigitte Benzacken, Frédérique Monier Gavelle, Brigitte Martin-Pont, Olivier Dupuy, Nicole Lièvre, Jean-Noël Hugues and Jean-Philippe Wolf (2001). Familial sperm polyploidy induced by genetic spermatogenesis failure: Case report. *Human Rep.* **16:** 2646 - 2651.

Brinkworth M.H., Weinbauer G.F., Schlatt S., Nieschlag E. (1995). Identification of male germ cells undergoing apoptosis in adult rats. *J. Reprod. Fertil.* **105**: 25 – 33.

Burkhardt, J.K., Echeverri, C.J., Nilsson, T., and Vallee, R.B. (1997). Overexpression of the dynamitin (p50) subunit of the dynactin complex disrupts dynein-dependent maintenance of membrane organelle distribution. *J. Cell Biol.* **139:** 469 – 484.

Caggese C., Moschetti R., Ragone G., Barsanti P., and Caizzi R. (2001). *dtxtex-1*, the *Drosophila melanogaster* homolog of a putative murine t-complex distorter encoding a dynein light chain, is required for production of functional sperm. *Mol. Genet. Genomics* **265:** 436 - 444.

Chuang J., Milner T. and Sung C. H., (2001). Subunit heterogeneity of cytoplasmic dynein: Differential expression of 14 kDa dynein light chains in Rat hippocampus. *J. Neuro Sci.* **21:** 5501 - 5512.

Cole D.G. (2003). The intraflagellar transport machinery of *Chlamydomonas reinhardtii*. *Traffic* **4:** 435 - 442.

Cole D.G., Diener D.R., Himelblau A.L., Beech P.L., Fuster J.C. and Rosenbaum J.L. (1998). *Chlamydomonas* kinesin-II-dependent intraflagellar transport (IFT): IFT particles contain proteins required for ciliary assembly in Caenorhabditis elegans sensory neurons. *J. Cell Biol.* **141:** 993 - 1008.

Collins, C.A. and Vallee, R.B. (1989). Preperation of microtubules from rat liver and testis: cytoplasmic dynein is a major microtubule-associated protein. *Cell Motil. Cyto.* **14**: 491 -500.

Courtot C., Frankhauser C., Simanis V. and Lehner C. (1992). The *Drosophila cdc25* homolog *twine* is required for meiosis. *Development* **116:** 405 - 416.

Criswell P. S. and Asai D. J. (1998). Evidence for four cytoplasmic dynein heavy chain isoforms in rat testis. *Mol. Biol. Cell* **9:** 237 - 247.

De-Rooij D.G., Lok D. (1987). Regulation of the density of spermatogonia in the seminiferous epithelium of the Chinese hamster. II. Differentiating spermatogonia. *Anat. Rec.* **217**: 131–136.

Devillard F., Metzler-Guillemain C., Pelletier R., DeRobertis C., Bergues U., Hennebicq S., Guichaoua M., Sele B. and Rousseaux S. (2002) Polyploidy in large-headed sperm: FISH study of three cases. *Hum. Reprod.* **17:** 1292 – 1298.

DiBella L.M., and King S.M. (2001). Dynein motors of the *Chlamydomonas* flagellum. *Int. Rev. Cytol.* **210:** 227 - 268.

DiBella L. M., Smith E. F., Patel-King R. S., Wakabayashi and King S. M.. (2004). A Novel Tctex2-related Light Chain Is Required for Stability of Inner Dynein Arm I1 and Motor Function in the Chlamydomonas Flagellum. *J. Biol. Chem.* **20**: 21666 - 21676.

Dix DJ, Allen JW, Collins BW, Mori C, Nakamura N, Poorman-Allen P, Goulding EH, Eddy EM. (1996) Targeted gene disruption of Hsp70–2 results in failed meiosis, germ cell apoptosis and male infertility. *Proc Natl Acad Sci USA* **93**: 3264 – 897.

Dreckhahn (2000). Moleculare Analyse des hmanen tctex2-Gens und Untersuchungen zu Mutationen in diesem Gen bei Männern mit Fertilitätsstörungen. Dissertation, Institute für Humangenetik.

Escalier D. (2002). Genetic approach to male meiotic division deficiency: the human macronuclear spermatozoa. *Mol. Hum. Reprod*. **8:** 1 – 7.

Eshel D., L.A. Urrestarazu, S. Vissers, J.-C. Jauniaux, J.C. van Vliet-Reedijk, R.J. Planta and I.R. Gibbons. (1993). Cytoplasmic dynein is required for normal nuclear segregation in yeast. *Proc. Natl. Acad. Sci. USA.* **90**: 11172 – 11176.

Fowkers M.E., Mitchell D.R. (1998). The role of pre-assembles cytoplasmic complexes in assembly of flagellar dynein subunits. *Mol. Biol. Cell* **9:** 2337 - 2347.

Gaglio T., Dionne M.A., Compton D.A. (1997). Mitotic spindle poles are organized by structural and motor proteins in addition to centrosomes. *J. Cell Biol.* **138:**1055 - 1066.

Gepner J., Li M.-G., Ludmann S., Kortas, Boylan C., K. Iyadurai S.J.P., McGrail M., and Hays T.S. (1996). Cytoplasmic dynein function is essential in *Drosophila melanogaster*. *Genetics* **142:** 865 - 878.

Gibbons B.H., Asai D.J., Tang W.-J.Y., Hays T.S., and Gibbons I.R. (1994). Phylogeny and expression of axonemal and cytoplasmic dynein genes in sea urchins. *Mol. Biol. Cell* **5:** 57 -70.

Gibbons, I.R. (1995). Dynein family of motor proteins: present status and future questions. *Cell Motil. Cytoskeleton.* **32:** 136 - 144.

Gil Stelzer and Jeremy Don. (2002). *Atce1*: A Novel Mouse Cyclic Adenosine 3',5'-Monophosphate-Responsive Element-Binding Protein-Like Gene Exclusively Expressed in Postmeiotic Spermatids. *Endocrinology* **143:** 1578 - 1588.

Gingras D., White D., Garin J., Multigner L., Job D., Cosson J., Huitorel P., Zingg H., Dumas F., Gagnon C. (1996). Purification, cloning, and sequence analysis of a Mr = 30,000 protein from sea urchin axonemes that is important for sperm motility. Relationship of the protein to a dynein light chain. *J. Biol. Chem*. **271**: 12807 - 13.

Grissom P.M., Vaisberg E.A., and McIntosh J.R. (2002). Identification of a novel light intermediate chain (D2LIC) for mammalian cytoplasmic dynein 2. *Mol. Biol. Cell* **13:** 817 – 829.

Habermacher G., and Sale W.S. (1997). Regulation of flagellar dynein by phosphorylation of a 138-kD inner arm dynein intermediate chain. *J. Cell Biol.* **136:** 167 - 176.

Hackstein J.H., Hochstenbach R. and Pearson P.L. (2000). Towards an understanding of the genetics of human male infertility: lessons from flies. *Trends Genet.* **16:** 565 – 572.

Hamvas R., Z. Trachtulec J. Forejt R.W. Williams K. Arzt K. Fischer-Lindahl and L.M. Silver (1996). Encyclopedia of the mouse genome V. Mouse chromosome 17. *Mamm. Genome* **6:** 281 - 299.

Harada A., Takei Y., Kanai Y., Tanaka Y., Nonaka S., and Hirokawa N. (1998). Golgi vesiculation and lysosome dispersion in cells lacking cytoplasmic dynein. *J. Cell Biol*. **141:** 51 – 59.

Himmelbauer H., Artzt K., Barlow D., Fischer-Lindahl L., Lyon M., Klein J., Silver L.M. (1993). Encyclopedia of the mouse genome III. Ocbtober 1993. Mouse chromosome 17. *Mamm. Genome* **4**: 230 - 52.

Huckins C. (1978). The morphology and kinetics of spermatogonial degeneration in normal adult rats: an analysis using a simplified classification of the germinal epithelium. *Anat. Rec.* **180**: 905 – 926.

Hupe M. (2003). Identifizierung von Interaktiospartnern der leichten Dyneinkette MP28. Institute für Humangenetik, Göttingen.

Huw L., Goldsborough A.S., Willison K. and Artzt K. (1995). Tctex2: a sperm tail surface protein mapping to the t complex. *Dev. Biol.* **170:** 183 - 194.

Ibanez-Tallon I. Heintz N. and Omran H. (2003). To beat or not to beat: roles of cilia in development and disease. *Hum. Mol. Genet.* **1**: 27 - 35.

Inaba, K., Kagami, O., and Ogawa, K. (1999). Tctex2-related outer arm dynein light chain is phosphorylated at activation of sperm motility. *Biochem. Biophys. Res. Commun.* **256:** 177 - 183.

James E., Shima, Derek J. McLean, John R. McCarrey and Michael D. Griswold. (2004). The Murine Testicular Transcriptome: Characterizing Gene Expression in the Testis during the Progression of Spermatogenesis. *Biol. Reprod*. **71**: 319 – 330.

Kagami O., and R. Kamiya. (1992). Translocation and rotation of microtubules caused by multiple species of *Chlamydomonas* inner-arm dynein. *J. Cell Sci.* **103:** 653 - 664.

Kamiya R., E. Kurimoto, H. Sakakibara, and T. Okagaki. (1989). A genetic approach to the function of inner and outer arm dynein. *In* Cell Movement, Vol. 1. The Dynein ATPases. F.D. Warner, P. Satir, and I.R. Gibbons, editors. *Alan R. Liss, Inc., New York.* 209 - 218.

Karcher R.L., Deacon S.W., and Gelfand V.I. (2002). Motor-cargo interactions: the key to transport specificity. *Trends Cell Biol*. **12:** 21 – 27.

Karki S., and Holzbaur E.L.F. (1999). Cytoplasmic dynein and dynactin in cell division and intracellular transport. *Curr. Opin. Cell Biol*. **11:** 45 - 53.

Kemphues K.J., Kaufman T.C., Raff R.A. and Raff E.C. (1982) The testis-specific beta-tubulin subunit in *Drosophila melanogaster* has multiple functions in spermatogenesis. *Cell* **31**: 655 – 670.

Kerr J.B. (1992) Spontaneous degeneration of germ cells in normal rat testis: assessment of cell types and frequency during the spermatogenic cycle. *J. Reprod. Fertil.* **95**: 825 – 830.

King K.L., Cidlowski J.A. (1995) Cell cycle and apoptosis: common pathways to life and death. *J. Cell Biochem*. **58**: 175 – 180.

King R. S. and Pfister, K. K. (1998) Cytoplasmic dynein contains a family of differentially expressed light chains. *Biochemistry* **37**: 15033 - 15041.

King S.M. (2000). The dynein microtubule motor. *Biochim. Biophys. Acta* **1496:** 60 - 75.

King S.M. (2000). AAA domains and organization of the dynein motor unit. *J. Cell Sci*. **113:** 2521 - 2526.

King S.M., Wilkerson, C.G., and Witman, G.B. (1991). The M_r 78,000 intermediate chain of *Chlamydomonas* outer arm dynein interacts with α-tubulin in situ. *J. Biol. Chem.* **266:** 8401 - 8407.

Kozminski K.G., Beech P.L., and Rosenbaum J.L. (1995). The *Chlamydomonas* kinesin-like protein *FLA10* is involved in motility associated with the flagellar membrane. *J. Cell Biol.* **131:** 1517 - 1527.

Kumar Kastury, Wayne E. Taylor, Roquing Shen, Stefan Arver, Matthew Gutierrez, Charles E. Fisher, Paul J. Coucke, Peter Van Hauwe, Guy Van Camp and Shalender Bhasin (1997). Complementary Deoxyribonucleic Acid Cloning and Characterization of a Putative Human Axonemal Dynein Light Chain Gene. *J. Clin. Endo. Met.* **9:** 3047 - 3053.

Lader E., Ha H. S., Neil M., Artzt K., Bennett D. (1989). tctex-1: a candidate gene family for a mouse *t* complex sterility locus. *Cell* **58**: 969 - 79.

Laird P.W., Zijderveld A., Linders K., Rudnicki M.A., Jaenisch R., Berns A. (1991). Simplified mammalian DNA isolation procedure. *Nucleic Acids Res.* **19**: 4293.

LeDizet M., and Piperno G. (1995). The light chain p28 associates with a subset of inner dynein arm heavy chains in *Chlamydomonas* axonemes. *Mol. Biol. Cell.* **6:** 697 - 711.

LeDizet M., and Piperno G. (1995). *a. ida4*-1, *ida4*-2 and *ida4*-3 are intron splicing mutations affecting the locus encoding p28, a light chain of *Chlamydomonas* axonemal inner dynein arms. *Mol. Biol. Cell.* **6:** 713 - 723.

Lewis-Jones I., Aziz N., Seshadri S., Douglas A., Howard P. (2003). Sperm chromosomal abnormalities are linked to sperm morphologic deformities. *Fertility and Sterility* **79:** 212 -215.

Li Y.Y., Yeh E., Hays T., and Bloom K. (1993). Disruption of mitotic spindle cott. orientation in a yeast dynein mutant. *Proc. Natl. Acad. Sci. USA.* **90**: 10096 – 10100.

Maines J.Z. and Wasserman S.A. (1999). Post-transcriptional regulation of the meiotic Cdc25 protein Twine by the Dazl orthologue Boule. *Nat. Cell Biol.* **1:** 171 – 174.

Maines J. and Wasserman S. (1998). Regulation and execution of meiosis in Drosophila males. *Curr. Top. Dev.* **37:** 301 – 332.

Mansour S.L., Thomas K.R., Capecchi M.R. (1988). Disruption of the proto-oncogene int-2 in mouse embryo-derived stem cells: a general strategy for targeting mutations to non-selectable genes. *Nature* **336:** 348 - 352.

McGrath J., Somlo S., Makova S., Tian X. and Brueckner M. (2003). Two populations of node monocilia initiate left-right asymmetry in the mouse. *Cell* **114:** 61 - 73.

Merdes A.K. Ramyar J.D., Vechio and Cleveland D.W. (1996). A complex of NuMa and cytoplasmic dynein is essential for mitotic spindle assembly. *Cell* **87:** 447 – 458.

Merdes A.R. Heald Samejima K., Earnshaw W.C. and Clevelanc D.W. (2000). Formation of spindle poles by dynein/dynactin-dependent transport of NuMA. *J. Cell Biol.* **149:** 851 –861.

Michael J.O'Neill and Karen Artzt. (1995). Identification of a germ-cell specific transcriptional repressor in the promoter of Tctex1. *Development* **121:** 561 - 568.

Minin A.A. (1997). Dispersal of Golgi apparatus in nocodazole-treated fibroblasts is a kinesin-driven process. *J. Cell Sci.* **110:** 2495 - 2505.

Mitchell D.R. (1994). Cell and molecular biology of flagellar dyneins. In: *International Reviews of Cytology, ed. K.W. Jeon, and J. Jarvik, San Diego:* Academic Press 141 - 175.

Mitchell D.R. (2000). *Chlamydomonas* flagella. *J. Phycol* **36:** 261 - 273.

Moreno R.D. and Schatten G. (2000) Microtubule configurations and post-translational alpha-tubulin modifications during mammalian spermatogenesis. *Cell Motil. Cytoskeleton* **46:** 235 – 246.

Neesen J., Drenckhahn J-D., Tiede S., Burfeind P., Grzmil M., Konietzko C., Kreutzberger J., Laccone F., Omran H. (2002). Identification of the human ortholog of the t-complex-encoded protein TCTE3 and evaluation as a candidate gene for primary ciliary dyskinesia. *Cytogenetic and Genome Research* **98**: 38 - 44.

Neesen J., Koehler M.R., Kirschner R., Steinlein C., Kreutzberger J., Engel W., Schmid M. (1997) Identification of dynein heavy chain genes expressed in human and mouse testis; chromosomal localization of an axonemal dynein gene. *Gene* **200:** 193 - 202.

Neesen J., Kirschner R., Ochs M., Schmiedl A., Habermann B., Mueller C., Holstein A. F., Nuesslein T., Adham I., and Engel W. (2001) Disruption of an inner arm dynein heavy chain gene results in asthenozoospermia and reduced ciliary beat frequency. *Hum. Mol. Genet*. **10**: 1117 - 1128.

Nothias J., Majumder S., Kaneko K.J. and Depamphilis M.L. (1995). Regulation of gene expression at the beginning of mammalian development. *J. Biol. Chem.* **270:** 22077 - 22080.

Nurminsky D. I., Nurminskaya M. V., Benevolenskaya E. V., Shevelyov Y. Y., Hartl D. L. and Gvozdev V. A. (1998). Cytoplasmic dynein intermediate-chain isoforms with different

targeting properties created by tissue-specific alternative splicing. *Mol. Cell. Biol.* **18:** 6816 - 6825.

Odorisio T, Rodriguez TA, Evans EP, Clarke AR, Burgoyne PS 1988 The meiotic checkpoint monitoring synapsis eliminates spermatocytes via p53- independent apoptosis. *Nat. Genet.* **18:** 257 – 261.

Ogawa K. and Inaba K. (2003). Sperm motility-activating complex formed by t-complex distorters. *Biochem. Biophys. Res. Commun.* **310:** 1155 - 1159.

Oke B.O. and Suarez-Quian C.A. (1992). Partitioning of the Golgi apparatus in rat primary and secondary spermatocytes during meiosis. *Anat. Rec.* **233:** 245 – 256.

Patel-King R.S., S.E. Benashski, A. Harrison and S.M. King (1997). A *Chlamydomonas* homologue of the putative murine *t* complex distorter *Tctex-2* is an outer arm dynein light chain. *J. Cell Biol.* **137:** 1081 - 1090.

Paulovich A.G., Toczyski D.P., Hartwell L.H. (1997). When checkpoints fail. *Cell* **88:** 315 – 321.

Pazour G. J., Koutoulis A., Benashski S. E., Dickert B. L., Sheng H., Patel-King R. S., King S. M., and Witman G. B. (1999) LC2, the Chlamydomonas Homologue of the t Complex-encoded Protein Tctex2 is essential for Outer Dynein Arm Assembly. *Mol. Biol. Cell* **10**: 3507 - 3520.

Piperno G., K. Mead, and S. Henderson (1996). Inner dynein arms but not outer dynein arms require the activity of kinesin homologue protein KHP1Fla10 to reach the distal part of the flagella in *Chlamydomonas. J. Cell Biol.* **133**: 371 - 379.

Piperno G., Z. Ramanis E.F. Smith, and W. S. Sale. (1990). Three distinct inner dynein arms in *Chlamydomonas* flagella: molecular composition and location in the axoneme. *J. Cell Biol.* **110:** 379 - 389.

Porter M.E., Bower R., Knott J.A., Byrd P., and Dentler W. (1999). Cytoplasmic dynein heavy chain 1b is required for flagellar assembly in *Chlamydomonas*. *Mol. Biol. Cell* **10:** 693 - 712.

Porter M. E. and Johnson K. A. (1989). Dynein structure and function. *Annu. Rev. Cell Biol.* **5:** 119 - 151.

Ramila S. Patel-King, Sharon E. Benashski, Alistair Harrison, and Stephen M. King (1997). A *Chlamydomonas* Homologue of the putative Murine *t* Complex distorter Tctex-2 is an outer arm dynein light chain. *J.Cell Biol*. **137**: 1081 - 1090.

Rana A., J.P.M. Barbera, T. A. Rodriguez, D. Lynch, E. Hirst, J. C. Smith, and R. S. P. Beddington (2004). Targeted deletion of the novel cytoplasmic dynein mD2LIC disrupts the embryonic organiser, formation of the body axes and specification of ventral cell fates *Development* **131:** 4999 - 5007.

Rappold G.A., L. Stubbs, S. Labeit, R.B. Crkvenjakov and H. Lehrach (1987). Identification of a testis-specific gene from the mouse *t*-complex next to a CpG-rich island. *EMBO J.* **6:** 1975 - 1980.

Rappold G. A., Trowsdale J., Lichter P., (1992). Assignment of the human homologue of the mouse t-complex gene TCTE3 to human chromosome 6q27. *Genomics* **13:** 1337-9.

Rasmusson K., Serr M., Gepner J., Gibbons I., and Hays T.S. (1994). A family of dynein genes in *Drosophila melanogaster*. *Mol. Biol. Cell* **5:** 45 - 55.

Reventos J., Munell F. (1997). Transgenic animal models in reproductive endocrine research. *Eur. J. Endocrinol.* **136:** 566 – 580.

Robinson J.T., Wojcik E.J., Sanders M.A., McGrail M., and Hays T.S. (1999). Cytoplasmic dynein is required for the nuclear attachment and migration of centrosomes during mitosis in *Drosophila*. *J. Cell Biol.* **146:** 597 - 608.

Rubin L.L., Philpott K.L., Brooks S.F. (1993) The cell cycle and cell death. *Curr. Biol.* **3:** 391 –394.

Salina D., Bodoor K., Eckley D., M. Schroer T. A., Rattner J. B., and Burke B. (2002). Cytoplasmic dynein as a facilitator of nuclear envelope breakdown. *Cell* **108:** 97 – 107.

Sallam M. (2001). Expression and function of mouse pelota gene. Institute für Humangenetik, Göttingen.

Sambrook J., Fritsch E. F., Maniatis T. (1989). Molecular cloning: a laboratory manual (2nd edition). *Cold Spring Habour, New York, USA.*

Sanger F., Nicklen S. and Coulsen A.R. (1977). DNA sequencing with chain-terminating inhibitors. *Proc. Natl. Acad. Sci. USA* **74:** 5463 – 5467.

Sassone-Corsi P. (1997). Transcriptional checkpoints determining the fate of male germ cells. *Cell* **88:** 163 – 166.

Saunders W.S., Koshland D., Eshel D., Gibbons I.R., and Hoyt M.A. (1995). *Saccharomyces cerevisiae* kinesin- and dynein-related proteins required for anaphase chromosome segregation. *J. Cell Biol*. **128:** 617 - 624.

Scholey J.M. (1996). Kinesin-II, a membrane traffic motor in axons, axonemes, and spindles. *J. Cell Biol.* **133:** 1 - 4.

Shirneshan K. (2005). UnterSuchungen zur Expression, Funktion und Regulation ausgewählter Gene der insulinfamilie. Institute für Humangenetik, Göttingen.

Silflow C.D., Lefebvre P.A. (2001). Assembly and motility of eukaryotic cilia and flagella. Lessons from *Chlamydomonas reinhardtii*. *Plant Physiol.* **127:** 1500 - 1507.

Skiba N.P., Yang C.S., Huang T, Bae H, Hamm H.E. (1999). The alpha-helical domain of Galphat determines specific interaction with regulator of G protein signaling. *J. Biol. Chem*. **274**: 8770 - 8.

Smith E.D., Xu Y., Tomson B.N. (2004) More than blood, a novel gene required for mammalian postimplantation development. *Mol. Cell. Biol.* **24:** 1168 – 1173.

Starr D.A., B.C. Williams, T.S. Hays, and M.L. Goldberg. (1998). ZW10 helps recruit dynactin and dynein to the kinetochore. *J. Cell Biol*. **142:** 763 – 774.

Stephan H, Polzar B, Rauch F, Zanotti S, Ulke C, Mannherz HG (1996). Distribution of deoxyribonuclease I (DNase I) and p53 in rat testis and their correlation with apoptosis. *Histochem. Cell Biol.* **106:** 383–393.

Steuer E., Worderman L., Schroer T. A. and Sheetz M. P. (1990). Localization of cytoplasmic dynein to mitotic spindles and kinetochores. *Nature* **345:** 266 - 268.

Supp D.M., Witte D. P., Potter S. S. and Brueckner M. (1997). Mutation of an axonemal dynein affects left-right asymmetry in inversus viscerum mice. *Nature* **389:** 963 – 966.

Tanaka Y., Zhang Z., Hirokawa N. (1995). Identification and molecular evolution of new dynein-like protein sequences in rat brain. *J. Cell Sci*. **108**: 1883 - 1893.

Tiede S. (2001). Molekulare Analyse des tctex2-Gens und Evaluation als Kandidaten-Gen für die Primäre Ziliäre Dyskinesie. Diplomarbeit, Institute für Humangenetik.

Tybulewicz V.L., Crawford C.E., Jackson P.K., Bronson R.T., Mulligan R.C. (1991). Neonatal Lethality and Lymphopenia in Mice with a Homozygous Disruption of the c-abl Proto-Oncogene. *Cell* **65**: 1153 - 1163.

Vaisberg E.A., Grissom P.M., and McIntosh J.R. (1996). Mammalian cells express three distinct dynein heavy chains that are localized to different cytoplasmic organelles. *J. Cell Biol*. **133:** 831 – 842.

Vallee R. B. (1993). Molecular analysis of the microtubule motor dynein. *Proc. Natl. Acad. Sci. U. S. A.* **90:** 8769 - 8772.

Wang H., Statir P. (1998). The 29 kDa light chain that regulates axonemal dynein activity binds to cytoplasmic dyneins. *Cell Mot. Cyto*. **39:** 1 - 8.

Warner F.D., P. Satir and I.R. Gibbons. (1989). Cell Movement, Vol. 1. The dynein ATPases. *Alan R. Liss, Inc., New York.*

Witman G.B. (1992). Axonemal dyneins. *Curr. Opin. Cell Biol.* **4:** 74 - 79.

Witman G.B., Wilkerson C.G., King S.M., in: Hyams J.S.and Lloyd C.W. (Eds.), (1994). The biochemistry, genetics and molecular biology of flagellar dyneins. *Microtubules, Wiley-Liss, New York* 229 - 249.

Wojcik E., Basto R., Serr M., Scaerou F., Karess R., and Hays T. (2001). Kinetochore dynein: its dynamics and role in the transport of the Rough deal checkpoint protein. *Nat. Cell Biol.* **3:** 1001 – 1007.

Yang P., and Sale W.S. (1998). The M_r 140,000 intermediate chain of *Chlamydomonas* flagellar inner arm dynein is a WD-repeat protein implicated in dynein arm anchoring. *Mol. Biol. Cell* **9:** 3335 - 3349.

Yang P., and Sale W.S. (2000). Casein kinase I is anchored on axonemal doublet microtubules and regulates flagellar dynein phosphorylation and activity. *J. Biol. Chem.* **275:** 18905 - 18912.

Yoem Y. L., Abr K., Bennett D., Artzt K. (1992). Testis-/embryo-expresses genes are clustured in the mouse H-2K rgion. *Proc. Natl. Acad. Sci. USA* **89:** 773 - 7.

Young A., Dictenberg J.B., Purohit A., Tuft R., and Doxsey S.J. (2000). Cytoplasmic dynein-mediated assembly of pericentrin and γ-tubulin onto centrosomes. *Mol. Biol. Cell* **11:** 2047 – 2056.

Zeng F. and Schultz R. M. (2003). Gene Expression in Mouse Oocytes and Preimplantation Embryos: Use of Suppression Subtractive Hybridization to Identify Oocyte- and Embryo-Specific Genes. *Biol. Reprod*, **68:** 31 - 39.

ACKNOWLEDGEMENTS

First of all, I would like to express my gratitude to PD Dr. Jürgen Neesen, who initiated these projects and provided me with excellent scientific guidance, instructive ideas and intensive theoretical discussions over the period of my Ph.D study.

Further, special acknowledgement is due to Prof. Wolfgang Engel who provided supreme lab facilities without which this work could not have succeeded. I am especially indebted to Prof. Engel for an extensive review of the complete manuscript of this thesis. Without his comments, many of the results and much of the discussion wouldn't have been presented as pointed and structured.

I am much indebted to PD Dr. Adham, who most patiently shared his competence and enthusiasm with me and certainly provided a valuable stimulus to me.

I would like to thank Dr. S. Hoyer-Fender for being my co-referee in this study and to Prof. Dr. Rolf Daniel and to Prof. Andreas Schwienhorst for being my dissertation examiners.

I have much pleasure and delight in acknowledging all of my colleagues in the Institute of Human Genetics, including Nadine, Philip, Andre, Arvind, Kristina, Christian, Stephanie, Angela, Bymba, Khulan, Katty, Lina, Prakasha and Pandian for providing friendly atmosphere.

My sincere gratitude goes to Dr. Asif Abdul Rahman who provided stimulating suggestions throughout this research and his 'open door' for all kind of problems.

Special thanks to my loving wife Firdous for her care, patience and encouragement. Thank you for giving me two cute babies Dayyan and Hamdan.

Last but not least I thank my parents, brothers and sisters for their extensive financial and moral support throughout my studies.

Many thanks.